PHONON MEAN FREE PATH - THERMAL CONDUCTIVITY RELATION OF $Al_xGa_{1-x}N$, AND β-Ga_2O_3 SEMICONDUCTORS

by

Pegah Ghanizadeh

B.S., Aerospace Engineering, Urmia University of Technology, 2019

Submitted to the Institute for Graduate Studies in
Science and Engineering in partial fulfillment of
the requirements for the degree of
Master of Science

Graduate Program in Mechanical Engineering

Boğaziçi University

2023

ACKNOWLEDGEMENTS

The successful completion of this thesis would not have been possible without the kind assistance and support of the people around me. I would like to express my sincere gratitude to certain individuals, among the kind people around me, for their invaluable support in completing this thesis.

I would like to express my deepest appreciation to my supervisor Dr. Nazli Donmezer. I am very thankful for her guidance, expertise, and constant encouragement. Her mentorship has shaped this thesis and elevated its quality. I am sincerely grateful to my committee for dedicating their time and expertise to review my work, provide valuable guidance, and offer constructive criticism. Their contribution has been invaluable, and I truly appreciate their support.

I would also like to thank my dear friends and colleagues Sahand, Kaveh, Amir, Onurcan, Emine, Ilke, and Taher for their unwavering support. Their encouragement, understanding, and presence have been invaluable and motivating during challenging times.

I am grateful for the support and endless love of my dear father, Sirous, my beloved mother, Nasrin, and my wonderful sister, Nasim. Their support has been foundational to my success.

ABSTRACT

PHONON MEAN FREE PATH - THERMAL CONDUCTIVITY RELATION OF $Al_xGa_{1-x}N$, AND β-Ga_2O_3 SEMICONDUCTORS

Ultrawide-bandgap (UWBG) semiconductors like $Al_xGa_{1-x}N$ and β-Ga_2O_3 emerge as a promising option for advancing next-generation high-power electronic devices. *AlGaN* preserves significant attention due to its unique capability of tuning the bandgap from 3.4 (eV) to 6 eV, enabling a nonlinear increase in the critical breakdown field. β-Ga_2O_3, with a wide bandgap of 4.8 eV , surpasses GaN and has cost-effective substrates, making it appealing for high-power electronics. However, field-effect transistors (FET) and Schottky-barrier diodes based on $Al_xGa_{1-x}N$ and β-Ga_2O_3 have shown superior performance to GaN, indicating their potential for overcoming this challenge. The pressing issue of local heat build-up and narrowing thermal pathways in such high-performance small scales devices is a significant challenge.To optimize the performance and ensure reliable operation, efficient dissipation of heat generated in the device is essential. This can be done by understanding the thermal transport of these systems at a short-length scale, in this case, lattice vibrations (i.e., phonons). One of the critical properties that characterize this behaviour is the phonon mean free path (MFP). This research offers a detailed analysis of phonon mean free path accumulation spectra in β-Ga_2O_3, and $Al_xGa_{1-x}N$ alloys with different Al fractions at different lattice temperatures by utilizing ab-initio and lattice dynamics calculations based on density functional theory (DFT) along with the Boltzmann transport equation (BTE). Our results indicated that the normalized cumulative thermal conductivity of alloys is notably reduced compared to that observed in pure systems. This effect is particularly pronounced for larger mean free paths (MFPs).

ÖZET

$Al_xGa_{1-x}N$ VE β-Ga_2O_3 YARIİLETKENLERİNİN FONON ORTALAMA SERBEST YOLU - ISIL İLETKENLİK İLİŞKİSİ

$Al_xGa_{1-x}N$ ve β-Ga_2O_3 gibi ultra geniş bant aralıklı (UWBG) yarı iletkenler, yeni nesil yüksek güçlü elektronik cihazların geliştirilmesi için umut verici bir seçenek olarak ortaya çıkmaktadır. AlGaN, bant aralığını 3,4 (eV) ila 6 eV arasında ayarlama ve kritik kırılma alanında doğrusal olmayan bir artış sağlama konusundaki benzersiz kabiliyeti nedeniyle büyük ilgi görmektedir.β-Ga_2O_3, 4,8 eV'lik geniş bant aralığıyla GaN'i geride bırakır ve uygun maliyetli alt katmanlara sahiptir, bu da onu yüksek güçlü elektronikler için cazip hale getirir. Bununla birlikte, $Al_xGa_{1-x}N$ ve β-Ga_2O_3 bazlı alan etkili transistörler (FET) ve Schottky bariyerli diyotlar, GaN'den daha üstün performans göstererek bu zorluğun üstesinden gelme potansiyellerini ortaya koymuştur. Bu tür yüksek performanslı küçük ölçekli cihazlarda yerel ısı birikimi ve termal yolların daraltılması önemli bir sorundur. Performansı optimize etmek ve güvenilir çalışmayı sağlamak için cihazda üretilen ısının verimli bir şekilde dağıtılması esastır. Bu, sistemlerin kısa uzunluk ölçeğindeki termal taşınımını, bu durumda kafes titreşimlerini (yani fononları) anlayarak yapılabilir. Bu davranışı karakterize eden kritik özelliklerden biri de fonon ortalama serbest yoludur (MFP). Bu araştırma, ab-initio ve kafes dinamiği hesaplamalarını kullanarak farklı kafes sıcaklıklarında farklı Al fraksiyonlarına sahip β-Ga_2O_3 ve $Al_xGa_{1-x}N$ alaşımlarında fonon ortalama serbest yol birikim spektrumlarının ayrıntılı bir analizini sunmaktadır. Sonuçlarımız, alaşımların normalleştirilmiş kümülatif termal iletkenliğinin saf sistemlerde gözlemlenene kıyasla önemli ölçüde azaldığını göstermiştir. Bu etki özellikle daha büyük ortalama serbest yollar (MFP'ler) için belirgindir.

TABLE OF CONTENTS

LIST OF FIGURES

LIST OF TABLES

LIST OF SYMBOLS

c	Specific heat
C	Spring constant
k	Thermal conductivity
k_b	Boltzmann constant
L	Characteristic length
n	Phonon equilibrium occupation number
N	Number of unit cells in sample
r	Spatial variable
T	Temperature in K
u	Displacement
U	Particle energy
v	Phonon group velocity
V_0	Volume of unit cell
Γ	Inverse phonon lifetime
Λ	Mean Free Path
q	Wavevector
Φ	Crystal energy
Ψ	Wave function
ω	Frequency
$\hbar$	Reduced Planck constant
τ	Relaxation time

LIST OF ACRONYMS/ABBREVIATIONS

2D	Two dimensional
2DEG	Two dimensional electron gas
3D	Three dimensional
ALD	Atomic Layer Deposition
ALE	Atomic Layer Epitaxy
AlGaN	Aluminum Gallium Nitride
AlN	Aluminum Nitride
BB-FDTR	Broadband Frequency Domain Thermoreflectance
BTE	Boltzmann Transport Equation
DFT	Density Functional Theory
DOS	Density of States
DUV	Deep Ultraviolet
FC2	Second Order Force Constants
FC3	Third Order Force Constants
FDTR	Frequency Domain Thermoreflectance
FET	Fin Field Effect Transistor
FOM	Figure of Merit
GaN	Gallium Nitride
HCP	Hexagonal Closed Pack
HEMT	High Electron Mobility Transistor
HVPE	Hydride Vapor Phase Epitaxy
Kn	Knudsen Number
LED	Light Emitting Diode
MFP	Mean Free Path
MD	Molecular Dynamics
MODFET	Modulation Doped Field Effect Transistor
MOCVD	Metal Organic Chemical Vapor Deposition
MOSFET	Metal Oxide Semiconductor Field Effect Transistor

MOVPE	Metal Oxide Vapor Phase Epitaxy
PAW	Projector Augmented Wave
RF	Radio Frequency
SCF	Self Consistent Field
TDTR	Time Domain Thermoreflectance
TTI	Thermoreflectance Imaging
UWBG	Ultra Wide Band Gap
UV	Ultraviolet
VASP	Vienna Ab-initio Simulation Package
WBG	Wide Band Gap

1. INTRODUCTION

1.1. Emerging Materials for FETs

The global pursuit for a reliable energy supply and the need to decrease greenhouse gas emissions has increased demand for alternative energy sources and cutting-edge technologies for efficient energy utilization. Among these technologies, power electronics stand out as a means of converting and managing electrical power for energy generation, transmission, and storage.Semiconductor switching devices are integral components of power electronic systems, playing a fundamental role in controlling the flow of electrical current. While silicon-based devices have dominated the industry for several decades, their performance is now constrained by the limits of silicon material properties. Researchers have begun exploring the potential of wide-bandgap semiconductors, such as SiC and GaN, to overcome these limitations and develop more efficient power electronic devices. These materials offer significant advantages over traditional silicon-based devices, including higher voltage capacity, faster switching speeds, and lower on-state resistance [1].

As the demand for high-performance electronic and optoelectronic devices continues to surge, developing advanced materials with exceptional properties becomes increasingly crucial. Ultra-wide bandgap (UWBG) semiconductor materials have emerged as highly promising candidates for various applications due to their unique properties. With bandgaps electronic higher than 3.4 eV, these materials exhibit exceptional properties such as high breakdown voltage, high thermal conductivity, and high radiation hardness. Compared to traditional semiconductors such as Si and GaAs, UWBG materials offer higher power handling capabilities, faster switching speeds, and improved efficiency, making them the next generation of materials for advanced electronic and optoelectronic devices [2]. Figure 1.1 depicts the potential of WBG and UWBG materials in revolutionizing the field of power electronics and optoelectronics by replacing traditional silicon-based devices.

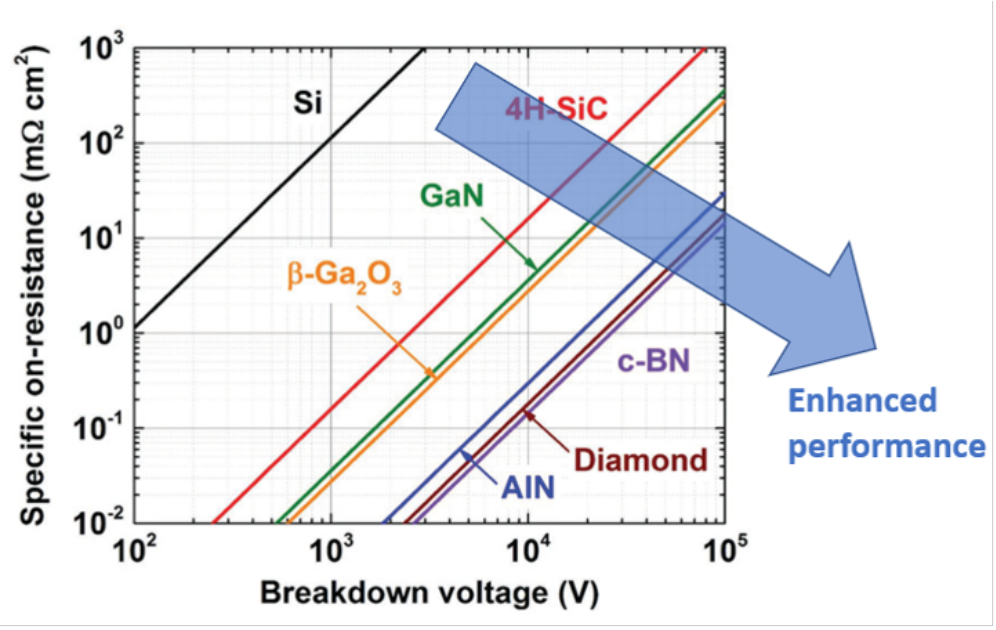

Figure 1.1. Relationship between specific on-resistance and breakdown voltage of WBG and UWBG materials, indicating their potential for power switches [3].

The exceptional properties of UWBG materials make them highly desirable for various applications, particularly those that require high power, high frequency, and high-temperature operation. For example, high electron mobility transistors (HEMTs) made from UWBG materials have shown superior performance in wireless communications and power amplifiers compared to traditional silicon-based devices. UWBG-based LEDs offer higher brightness, efficiency, and longer lifetimes than conventional LEDs. Additionally, UWBG lasers possess the potential for high-power and high-speed operation, making them suitable for optical communication systems, manufacturing, and medical applications [4, 5].

Moreover, these materials are also being explored for their potential in photovoltaic cells, sensors, and high-temperature electronics. Finally, the high-temperature stability and durability of UWBG materials make them ideal for use in extreme environments such as aerospace and defense applications [6]. Figure 1.2 depicts several applications, highlighting the versatility and potential impact of UWBG materials in various industries.

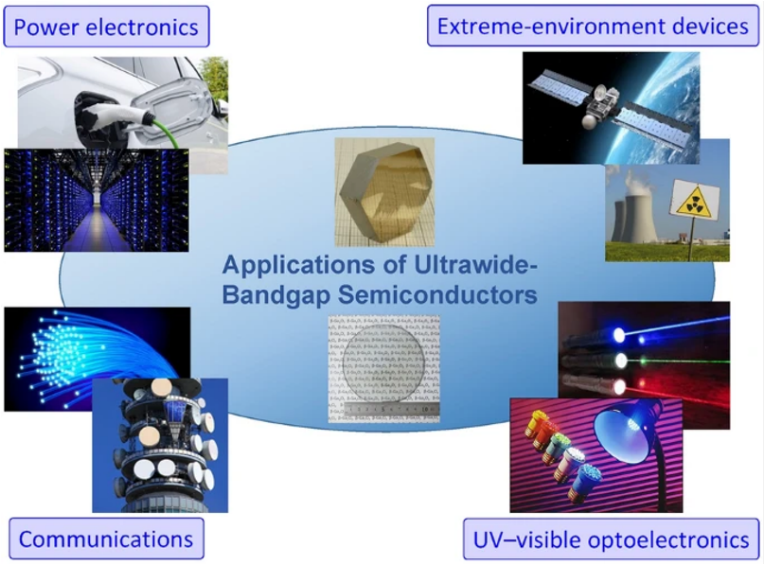

Figure 1.2. Applications of Ultra-wide bandgap (UWBG) semiconductor materials [6].

Aluminum gallium nitride ($Al_xGa_{1-x}N$), and β-form gallium oxide ($\beta - Ga_2O_3$) are two examples of UWBG semiconductor materials that have unique properties and potential for various applications. High Al-including $AlGaN$ and $\beta - Ga_2O_3$, with their UWBG characteristics, are expected to create new opportunities in fields such as deep ultraviolet (DUV) optoelectronics, quantum information, and extreme-environment applications [3]. Furthermore, replacing conventional power electronics materials such as silicon with alternative materials like GaN and $\beta - Ga_2O_3$, which offer superior performance and environmental benefits such as reducing CO_2 emissions and saving energy, has been attracting attention [7, 8]. This section will briefly introduce the distinctive properties of $AlGaN$ and β-form gallium oxide ($\beta - Ga_2O_3$).

1.1.1. Aluminum Gallium Nitride *(AlGaN)*

Aluminum Gallium Nitride $AlGaN$ is a semiconductor material with a hexagonal and cubic crystal structure that belongs to the ultra-wide bandgap (UWBG) materials. It is commonly represented as $Al_xGa_{1-x}N$, where x refers to the fraction of aluminum in the material. The unit cell structure $Al_xGa_{1-x}N$ for ($x = 0.25$, $x = 0.5$, $x = 0.75$) is depicted in Figure 1.3. $AlGaN$ possesses the remarkable characteristic of having a

broad range of bandgap energies that can be adjusted by varying the aluminum composition x in the material, allowing for tunability of the bandgap energy from 3.4 eV for Gallium Nitride *GaN* to over 6 eV for Aluminum Nitride *AlN*. This unique property makes *AlGaN* a highly attractive material for a variety of applications, including UV emitters, solar-blind photodetectors, and electronic devices that require heterostructures with tailored bandgap energies. *AlGaN* is classified as a group III-V material, and it is commonly grown using various techniques such as molecular beam epitaxy (MBE), metalorganic chemical vapor deposition (MOCVD), and reactive sputtering. In some cases, *AlGaN* is also grown using the hydride vapor phase epitaxy (HVPE) and organometallic vapor phase epitaxy (VPE) techniques [9–11]. These methods allow for the controlled deposition of *AlGaN*, which is a crucial factor for producing high-quality materials used in various electronic and optoelectronic devices.

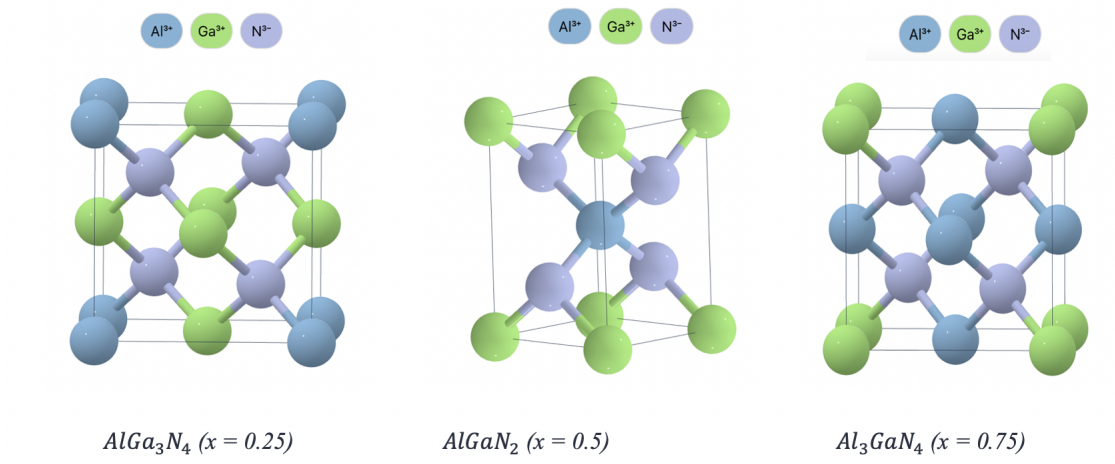

Figure 1.3. The unit cell structure of ($Al_xGa_{1-x}N$) for (x = 0.25, x = 0.5, x = 0.75).

With its unique properties, such as high thermal stability, high breakdown voltage, and a direct bandgap, *AlGaN* is increasingly being used in a wide range of electronic and optoelectronic applications [4]. For instance, *AlGaN*-based HEMTs and MODFETs are used in high-frequency applications such as amplifiers and switches due to their excellent power-handling capabilities [12, 13]. *AlGaN* also shows great promise in the development of UV LEDs, offering high efficiency and long lifetimes. Figure 1.4 provides a basic schematic illustration of AlGaN/GaN HEMTs.

One key advantage of *AlGaN* is its versatile doping, encompassing spontaneous, piezoelectric polarization, and impurity doping. This enables the creation of 2D electron gases (2DEGs) and 3D electron slabs [14–16]. Additionally, *AlGaN*'s direct bandgap promotes efficient electron transitions without phonon interference, enhancing external quantum efficiency (EQE) in devices like edge/surface-emitting lasers and UV/DUV LEDs [17–19] (see Figure 1.4). Ongoing research aims to optimize crystal structures and material quality, especially in polarization-induced doping and 2DEG formation, potentially unlocking new applications in power electronics, sensing, and communication technologies.

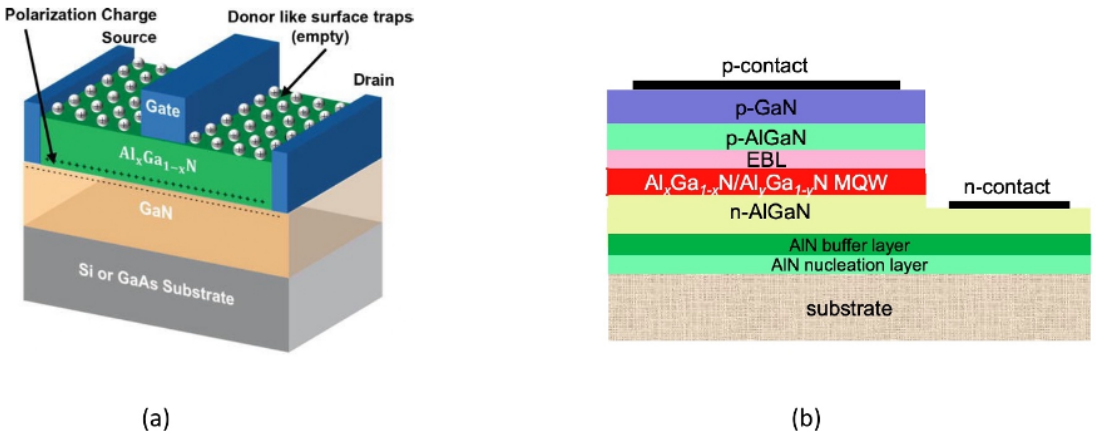

Figure 1.4. (a) Schematic of AlGaN/GaN HEMTs [20]. (b) Schematic of AlGaN based DUV LED [21].

1.1.2. β-form gallium oxide (β-form Ga_2O_3)

Ga_2O_3 is classified as a TCO (transparent conductive oxide), and it can take on multiple polymorphs, including α, β, γ, δ, and ε. $\beta - Ga_2O_3$ has been identified as the Ga_2O_3 polymorph with the most stable crystal structure [22]. Due to its physically and chemically metastable state, $\beta - Ga_2O_3$ has a significant advantage in being able to endure high electric fields when operating at high temperatures [23]. The unit cell representation of $\beta - Ga_2O_3$ is illustrated in Figure 1.5, providing a visual insight into its distinctive crystal lattice.

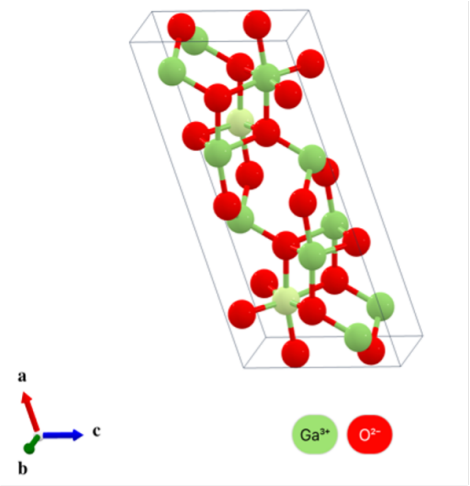

Figure 1.5. Unit cell of β-form Ga_2O_3.

Beta gallium oxide ($\beta - Ga_2O_3$) is a promising semiconductor material with a wide bandgap of 4.9 eV [24] , high breakdown voltage [25], and high thermal conductivity, making it suitable for use in high-power [26] and high-frequency [27] electronic devices, power electronics applications, and as transparent conductive oxide in touchscreens and flat panel displays. Furthermore, beta gallium oxide has a high sensitivity to UV radiation, making it an attractive material for UV photodetectors in environmental monitoring, biochemical sensing, and defense systems [28]. Figure 1.6 displays an instance of MSM solar-blind UV photodetector [29], and (Ga_2O_3)-based DUV LEDs [23]. The unique combination of properties of beta gallium oxide offers significant opportunities for various applications in multiple fields.

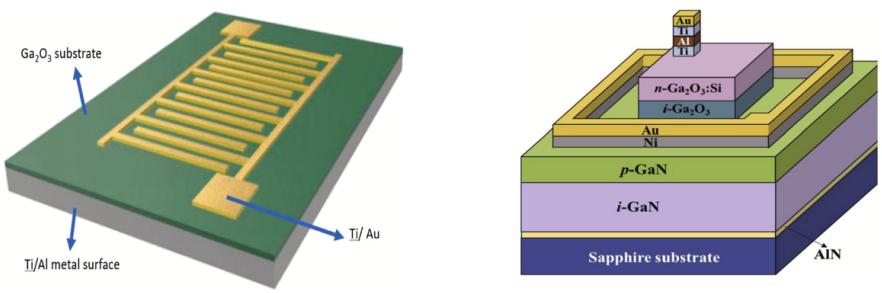

Figure 1.6. (a) Schematic of (Ga_2O_3) Solar-blind UV Photodetector [29]. (b) Diagram depicting the structure of a deep ultraviolet LED of (Ga_2O_3) [23].

1.2. Thermal Issues and Size Effects

Thermal management stands as an indispensable pillar in the realm of micro and nanoscale devices, especially those that harness the unique attributes of wide bandgap (WBG) and ultra-wide bandgap (UWBG) materials to fuel their operations. The delicate balance between operational efficiency and thermal stability becomes increasingly vital in this context. Figure 1.7 serves as an illustrative example for high electron mobility transistors (HEMTs), showcasing the intricate interplay between thermal management and device functionality. The pronounced diminishment in thermal conductivity resulting from confinement within these structures amplifies the challenges associated with heat management, introducing the potential for adverse consequences, such as substrate deterioration and operational failures. This underscores the critical importance of effectively dissipating the heat generated within these devices.

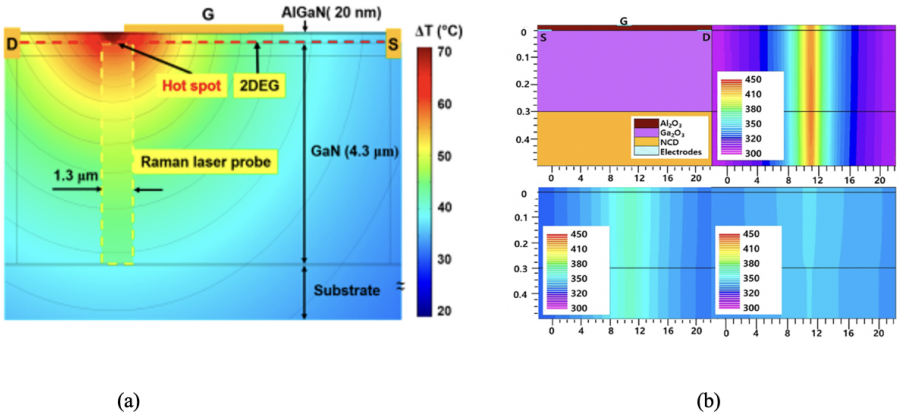

Figure 1.7. Cross-sectional schematics illustrating the localized heating of the structure of (a) $AlGaN$ HEMT [30] (b) and $\beta - Ga_2O_3$ MOSFET [31].

The intricacies of heat dissipation intensify as phonons, the carriers of thermal energy, find themselves constrained within the confines of these diminutive structures. Their movement becomes restricted, posing formidable hurdles to efficient heat transfer. Moreover, the concentration of heat in localized hotspots further constrains phonon mobility, exacerbating the size effects that govern thermal transport in such nanoscale domains. Consequently, these confined structures, including thin films, nanowires,

and hotspots, deviate significantly in terms of thermal conductivity from their bulk material counterparts. To facilitate precise modeling of device heating and thermal behavior, it becomes imperative to conduct meticulous investigations for the accurate determination of the thermal conductivity of these intricate structures. This entails a comprehensive exploration into the transport properties of these microscopic energy carriers, uncovering the nuanced dynamics that underpin the thermal management of micro and nanoscale devices.

1.2.1. Phonons

In solid materials, heat transfer occurs primarily through the movement of electrons. However, in semiconductors, due to electron mobility constraints, heat conduction primarily occurs via lattice vibrations, also known as phonons. Lattice thermal conductivity refers to the transfer of vibrations within the lattice structure as atoms become excited and pass this energy to neighboring atoms. These excitations are measured in discrete units called phonons. The thermal properties of semiconductor materials are significantly influenced by the quantized behavior of phonons, which can be described by their wavevector and frequency amplitude. The phonon dispersion relation is the term used to describe this relationship. The energy of the phonons is quantified in discrete steps as $E = \hbar\omega$, where $\hbar$ is the reduced Planck's constant. Therefore, in semiconductors, heat transfer is mainly the movement of Phonon particles that resist the thermal gradient [32, 33]. The correlation between phonon wavevector, k, and phonon frequency $\omega(k)$ in a chain composed of two atoms is expressed as

$$\omega(k) = \sqrt{\left(C\frac{(M+m)}{Mm} \pm C\sqrt{\frac{(M+m)^2}{M^2m^2} - \frac{4}{Mm}\sin^2\frac{ka}{2}}\right)}, \tag{1.1}$$

where C represents the spring constant and $\omega(k)$ denotes the frequency associated with wavevector k. M and m indicate the masses of the two atoms in the chain [34]. The eigenvalue problem posed by Equation (1.1) gives rise to the curve depicted in Figure. 1.8, which exhibits two distinct types of solutions: optical and acoustic. These solutions correspond to the optical and acoustic phonon modes and arise due to the $\pm$ term present in Equation (1.1). In the acoustic mode, neighboring atoms oscillate in

phase and the same direction as the considered atom. At the Gamma point, located at the center of the Brillouin zone, the frequency of the acoustic mode is zero. On the other hand, in the optical mode, neighboring atoms move in opposite directions, and the frequency of this mode has a non-zero value at the Gamma point.

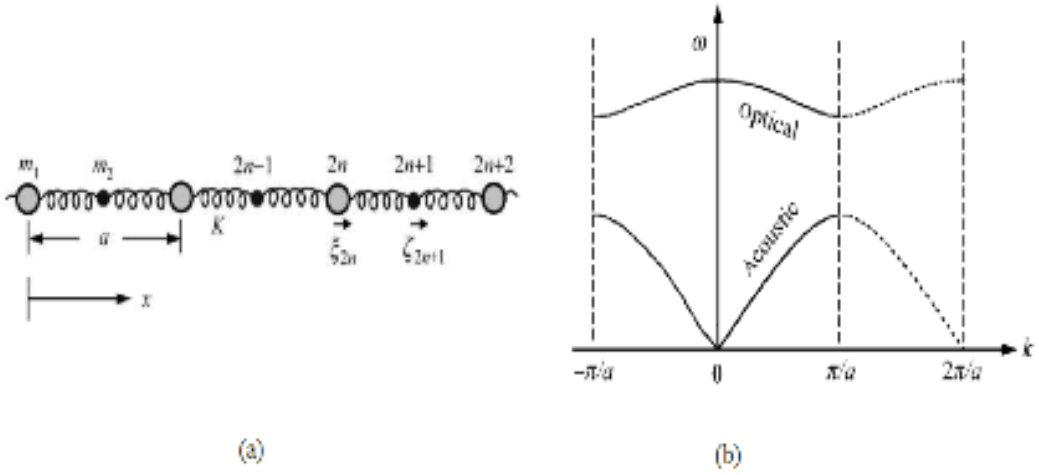

Figure 1.8. (a) Linear diatomic chain and (b) its corresponding phonon dispersion relation [34].

The phonon dispersion relations in two-dimensional (2D) and three-dimensional (3D) materials exhibit a heightened level of complexity compared to their one-dimensional counterparts. In these multidimensional materials, the dispersion relations comprise a multitude of optical and acoustic phonon branches, which collectively describe the intricate behavior of phonons across the crystal lattice. A noteworthy example of this complexity is illustrated in Figure 1.9, where the phonon dispersion of GaN, as investigated by Albar et al., is visually represented. To facilitate a comprehensive understanding of these dispersion relations, specific notations such as A, Γ, M, and K are employed, aiding in the interpretation of crystallographic directions and their corresponding phonon behaviors.

In the context of phonon dispersion analysis, the irreducible Brillouin zone assumes a pivotal role. This zone, representing the primitive cell of the real space lattice (i.e., the arrangement of atoms in the crystal), serves as a fundamental reference for displaying lattice directions in the phonon dispersion diagram. The Brillouin zone

encapsulates the essential symmetries and reciprocal space features that underpin the vibrational properties of the material, allowing researchers to gain valuable insights into how phonons propagate and interact within the crystal lattice. Consequently, the phonon dispersion relations in 2D and 3D materials, as elucidated through figures like Figure 1.9 and with reference to the irreducible Brillouin zone, contribute significantly to our comprehension of the dynamic behavior of lattice vibrations in complex materials.

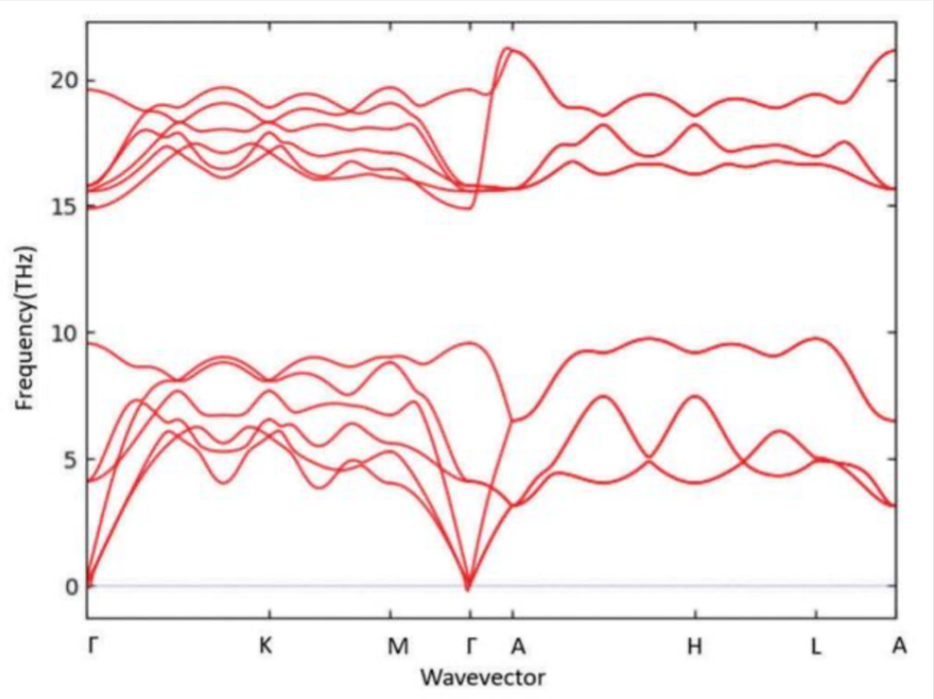

Figure 1.9. Phonon dispersion of wurtzite GaN [35].

1.2.2. Phonon Scattering

Phonon scattering, encompassing interactions such as phonon-phonon, phonon-boundary, and phonon-defect (like impurities, dislocations, or vacancies) scattering, plays a paramount role in governing the energy transport characteristics of insulators and semiconductors. Phonon-phonon interactions arise due to the anharmonic terms present in the expansion of crystal potential energy. This anharmonicity, in turn, occurs because atoms deviate significantly from their equilibrium positions. The principle of energy conservation necessitates the involvement of a minimum of three phonons in the

scattering process. While there are phonon-phonon interactions involving more than three phonons, the probability of three-phonon interactions is considerably higher, especially at room temperature [34, 36].

There are two types of phonon-phonon scattering mechanisms: normal- and Umklapp scattering. In normal scattering, two phonons collide and combine into a single phonon that conserves the crystal momentum and does not affect the lattice thermal conductivity. This type of scattering occurs only at low temperatures when the phonons are sparsely distributed in the lattice. On the other hand, Umklapp scattering happens when two colliding phonons merge into a phonon with a wave vector that extends beyond the first Brillouin zone into the second zone, and the resulting vector can be described as a vector in the opposite direction within the first Brillouin zone. The crystal momentum is not preserved in this case due to the translation between Brillouin zones, and this affects the lattice thermal conductivity.

Umklapp scattering intensifies with rising temperature and plays a substantial role in degrading lattice thermal conductivity at high temperatures [34, 36]. This is tied to the conservation of energy in three-phonon scattering, which is expressed as

$$\omega_{\mathbf{q}s} \pm \omega_{\mathbf{q}'s} = \omega_{\mathbf{q}''s}, \tag{1.2}$$

where the symbol $\omega_{\mathbf{q}s}$ represents the frequency of the phonon associated with the wavevector $\mathbf{q}$ and mode s. The fundamental principle governing the preservation of momentum within the context of three-phonon interactions can be articulated as

$$\mathbf{q} \pm \mathbf{q}' = \mathbf{q}'' + \mathbf{G}, \tag{1.3}$$

in normal processes, where $\mathbf{G}$ represents the reciprocal lattice vector, its value is zero. However, in umklapp processes, $\mathbf{G}$ takes a non-zero value.

In three-phonon interactions, there are two potential processes: fission, where one phonon transforms into two new phonons (indicated by a minus sign in equations (1.2) and (1.3)), and fusion, where two phonons merge to form a new phonon (indicated by a plus sign in equations (1.2) and (1.3)), visually represented in Figure 1.10.

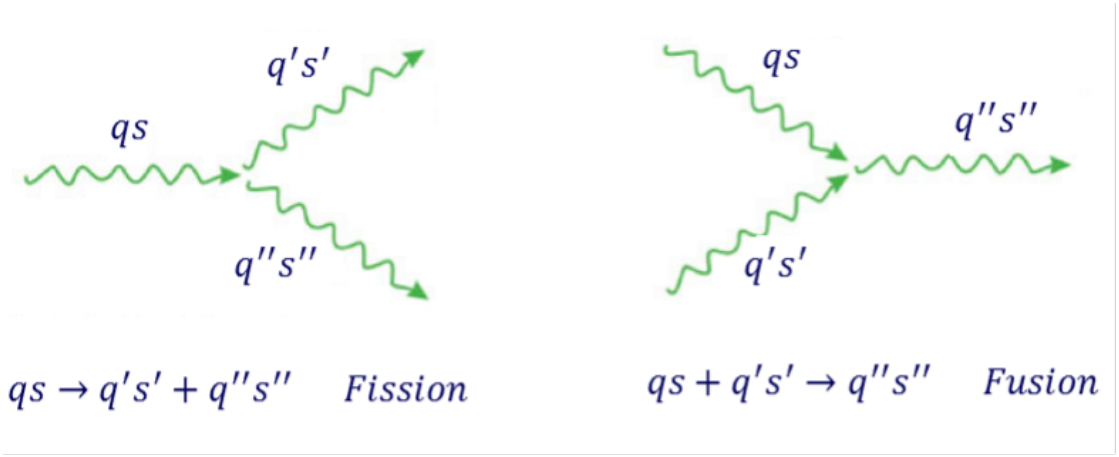

Figure 1.10. Three phonon interactions.

1.2.3. Mean Free Path

The Phonon Mean Free Path (MFP) is a crucial metric in studying thermal transport and phonon behavior within materials. It quantifies the average distance a phonon can move through a material before interacting with another phonon or energy carrier, providing essential insights into heat conduction and thermal properties [37]. In the realm of small-dimensional structures, such as thin films or devices subject to localized heating, the trajectory of phonons along their MFP is frequently interrupted due to a fascinating phenomenon referred to as the size effect. This phenomenon is a testament to the intricate interplay between phonon behavior and the spatial constraints imposed by the nanoscale dimensions of these structures, leading to distinctive thermal transport characteristics that diverge from bulk materials.

The Knudsen number *(Kn)*, is defined as the ratio of phonon *MFP* (Λ) to the characteristic device length *(L)*, and can be written as

$$Kn = \frac{\Lambda}{L}, \tag{1.4}$$

it is used to determine whether size effects exist. When $(Kn) > 1$, the characteristic length is smaller than the MFP of phonons, and size effects are expected to dominate. Figure 1.11 shows that when thin film lengths restrict phonon pathways, conductivity can be reduced due to trapped phonons. Phonons with longer MFPs may also be restricted in small/thin structures, potentially leading to heating and degradation [38].

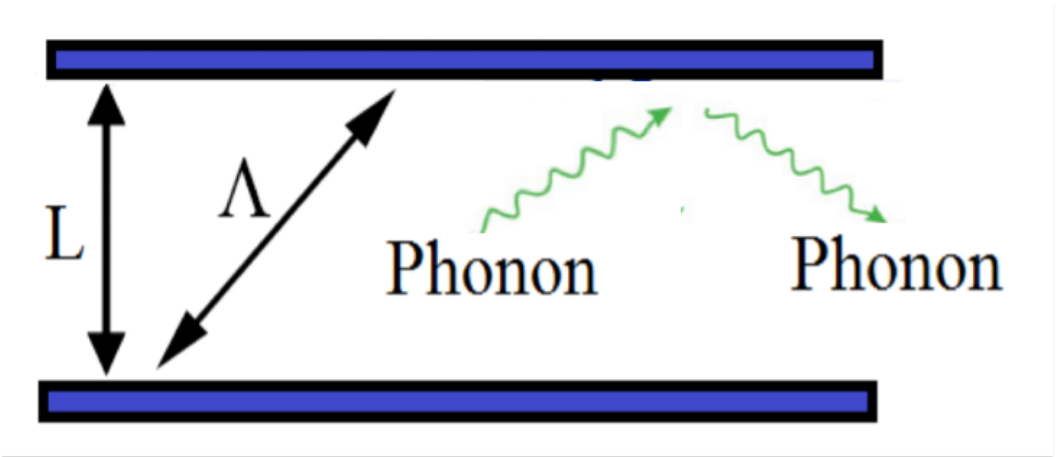

Figure 1.11. Phonon boundary scattering.

Localized heating can also impede phonon travel. Thus, entrapment of phonons should also be considered in devices subjected to localized heating and small heating spots. To accurately model thermal transport, it is necessary to consider phonon mean free path *MFP* and relaxation time.

1.3. Characterization of Thermal Size Effects

When it comes to designing and implementing devices at the nano and micro scale, understanding thermal transport is crucial. Thermal transport in materials at the nano and micro scale exhibits distinct behavior compared to bulk materials, owing to thermal size effects. As a result, a robust body of research has emerged, encompassing both experimental and theoretical approaches. These efforts are aimed at unraveling the intricate thermal dynamics of thin materials and micro-scale devices when subjected to localized heating. In essence, this section serves as a comprehensive summary of these endeavors, focusing on augmenting our comprehension of thermal transport at small scales, which, in turn, serves to streamline the development of more efficient micro and nano-scale devices. What's even more intriguing is that the knowledge gleaned from this research holds the promise of ushering in a new era of cutting-edge technologies characterized by superior heat management and enhanced energy efficiency. This potential has far-reaching implications across many industries, prominently including electronics, aerospace, and renewable energy.

1.4. Phonon Mean Free Path and Accumulation Spectra

Accumulation spectra is a well-established technique for investigating the thermal transport properties of materials. Often referred to as the thermal conductivity accumulation function or the mean free path accumulation, this approach provides insight into the relationship between the accumulated thermal conductivity and the mean free path of phonons, which are the primary carriers of heat in most materials. Understanding phonon behavior is critical for predicting thermal conductivity, making the thermal accumulation spectrum a valuable tool for researchers and engineers seeking to optimize the thermal performance of micro and nano-scale devices. In the presence of size effects, the thermal conductivity can differ significantly from the bulk thermal conductivity. This is because phonons can be scattered by various defects, interfaces, or boundaries. The thermal accumulation spectrum helps to determine how much of the bulk conductivity is covered by the sample and provides insights into the thermal transport mechanisms of the material. In addition, the accumulation spectrum is utilized when the presence of size effects is unknown. If the MFP range provided in the spectrum is exceeded, a loss of bulk thermal conductivity can be expected. Materials' thermal conductivity generally increases along the covered length until the entire spectrum is reached. This demonstrates the significance of the accumulation spectrum in analyzing the thermal behavior of micro and nano-scale samples. This section discusses a few experimental and theoretical attempts to construct accumulation spectra.

In literature, several experimental accumulation spectra have been obtained for different materials using the transient thermoreflectance (TTR) method. Tran Dat et al. [39] extended this experimental approach to investigate the phonon MFP and thermal conductivity of $AlGaN$ thin films with varying Al composition. As seen in Figure 1.12, they obtained thermal conductivity accumulation data for the thin films as a function of device layer thickness and analyzed the phonon MFP and thermal conductivity relation using a modified Callaway model [39]. The accumulation spectra provide valuable insight into the phonon scattering mechanisms and thermal transport properties of various materials, This aids micro and nano device design and optimization.

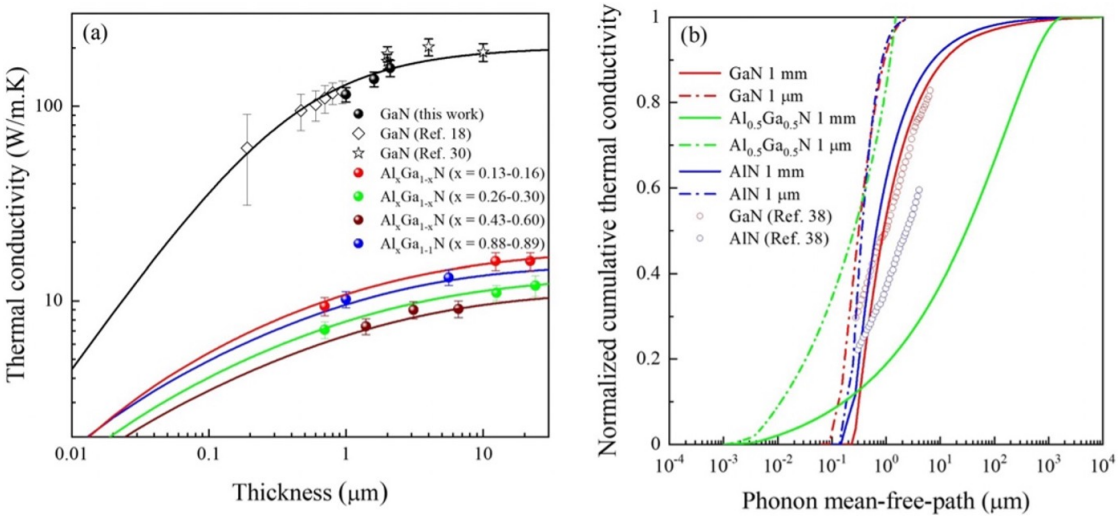

Figure 1.12. (a) Thickness depends on the thermal conductivity of GaN and $Al_xGa_{1-x}N$, (b) Experimentally obtained accumulation spectra [39].

Accumulation functions of the β-form Ga_2O_3, are built via TDTR in literature as a function of device layer thickness, as seen in Figure 2.1. In addition to $AlGaN$, Szwejkowski et al. [38] investigated the thermal conductivity of $\beta - Ga_2O_3$ films grown via open-atmosphere annealing of GaN. Their TDTR measurements showed that the thermal conductivity of the films decreased with decreasing film thickness, indicating a significant size effect. The phonon MFP in the films was estimated using the accumulation function approach.

It was found that phonon scattering at the surface and grain boundaries contributed significantly to the size effect in thermal conductivity. The results of their study highlight the importance of considering size effects when designing micro- and nanoscale devices based on β-form Ga_2O_3 films. Other studies, such as those by Freedman et al. and Beechem et al., also used TDTR to construct accumulation functions for various materials, including AlN, $\beta - Ga_2O_3$ and GaN layers, providing further insights into thermal conductivity accumulation and phonon transport properties [38, 40–42].

One way to theoretically build thermal accumulation spectra is through the use of first-principles calculations, which can be incorporated into phonon scattering rates

using a phonon Boltzmann Transport Equation (BTE) solver such as ShengBTE or an in-house code. As a result, calculating the phonon distribution to thermal conductivity enables the determination of accumulated conductivity assigned to each MFP value [43, 44].

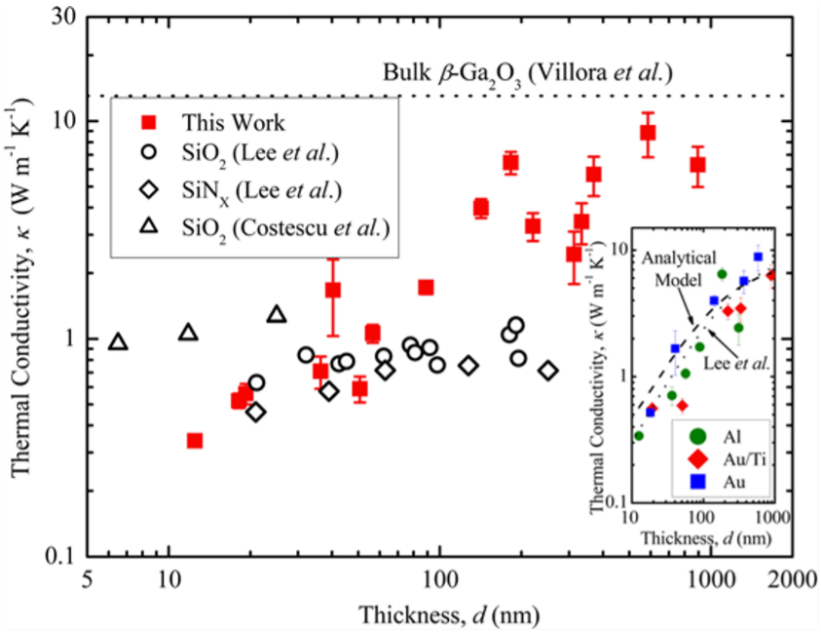

Figure 1.13. Thermal conductivity comparison of $\beta - Ga_2O_3$ films to other thin film dielectrics as a function of film thickness [38].

First-principles calculations are an essential tool in determining phonon frequency data, which is critical to understanding the behavior of crystalline materials. Phonon dispersion relations are derived from these calculations, which provide information about the way in which phonons propagate through a crystal lattice. In order to fully define the crystal energy, it is necessary also to determine the harmonic and anharmonic force constants [45]. These constants are crucial in providing a comprehensive understanding of phonon interactions by shedding light on both the mean free path that a phonon can travel and its relaxation time [46]. In some works, iteration-related methods such as Monte-Carlo simulations have been employed, while harmonic approximation is used in others [47]. The harmonic approximation is an extension of the spring analogy, where each bond between atoms is treated as a spring, and the atomic vibrations are modeled as the oscillation of these springs. This approximation is valid

when the atomic vibrations are small compared to the bond length, and it allows for the calculation of phonon modes and their lifetimes. These lifetimes can then be used to calculate the phonon scattering rates and the resulting thermal conductivity. Imaginary springs, also known as virtual springs, are a useful theoretical construct used in materials science and solid-state physics to model the forces between atoms in a crystal lattice when it is perturbed, such as when atoms are displaced from their equilibrium positions. These springs are used to represent the effective force constants or stiffness of the lattice, which describe how the atoms interact with each other in response to the perturbation. Imaginary springs are typically used in computational methods, such as molecular dynamics or lattice dynamics simulations, to calculate the vibrational properties of materials, including phonon frequencies and dispersion relations.

Subsequently, the lattice's crystal ground energy (Φ) is estimated using

$$\begin{aligned}\Phi = \Phi_0 &+ \sum_{lk}\sum_{\alpha} \Phi_\alpha\left(lk\right) u_\alpha\left(lk\right) \\ &+ \frac{1}{2}\sum_{ll'kk'}\sum_{\alpha\beta} \Phi_{\alpha\beta}\left(lk, l'k'\right) u_\alpha\left(lk\right) u_\beta\left(l'k'\right) \\ &+ \frac{1}{3!}\sum_{ll'l''kk'k'}\sum_{\alpha\beta\gamma} \Phi_{\alpha\beta\gamma}\left(lk, l'k', l''k''\right) u_\alpha\left(lk\right) u_\beta\left(l'k'\right) u_\gamma\left(l''k''\right),\end{aligned} \tag{1.5}$$

in accordance with the spring analogy, the terms denoted as $\Phi_{\alpha\beta}$ corresponds to second-order force constants (FC2s), while the terms $\Phi_{\alpha\beta\gamma}$ represents third-order force constants (FC3s). Here, α, β, and γ denote Cartesian coordinates, and u(lk) represents the displacement of atom number k in unit cell number l.

The harmonic approximation, which only considers second-order force constants (FC2) obtained via phonon dispersion relations, has limitations in accurately modeling phonon interactions in crystalline materials. Researchers have employed various methods to overcome this limitation, such as the Gruneisen parameter or fitting bulk conductivity to previously tabulated conductivity values. However, these approaches heavily rely on approximations and fitting parameters, which may not accurately represent the phonon interactions in all materials. Therefore, it is crucial to consider higher-order force constants and develop more accurate models to better understand

phonon interactions in crystalline materials. For instance, ab initio calculations can provide an accurate estimate of these force constants and provide a more comprehensive understanding of the vibrational properties of materials. This approach can be especially useful in predicting the thermal properties of materials that are difficult to measure experimentally. By developing more accurate models, researchers can improve our understanding of phonon interactions in crystalline materials and facilitate the design of materials with tailored thermal properties.

Expanding on the limitations of the harmonic approximation, this study aims to incorporate third-order force constants (FC3) into the thermal conductivity calculations of $AlGaN$ alloys and the β-form Ga_2O_3. FC3s are the coefficients that appear in the further expansion of the crystal ground energy approximation, as seen in Equation 1.3 [35]. By including FC3s, the hope is to achieve more accurate results for thermal conductivity without having to rely on potentially problematic approximations or fitting parameters, as has been done in previous studies. This approach has the potential to provide a more comprehensive understanding of phonon interactions in crystalline materials and enable more accurate predictions of thermal transport properties.

1.4.1. Experimental Studies

Experimental studies on the thermal properties of wide and ultra-wide bandgap materials, such as $AlGaN$ alloys and β-form Ga_2O_3, can be classified into two groups based on the methods used to measure thermal size effects. The first group measures the thermal conductivities of thin films, while the second group directly measures the temperature of devices with localized heating. Experimental methods used for the first group include time-domain thermoreflectance (TDTR) [48], frequency-domain thermoreflectance (FDTR) [49], broad-band frequency-domain thermoreflectance (BB-FDTR) [40], Raman spectroscopy, and laser-based thermal conductivity measurements. TDTR is a powerful technique for measuring the thermal conductivity of thin films, while Raman spectroscopy can be used to determine the phonon dispersion relations and the lifetime of phonons. Laser-based thermal conductivity measurements can be

used to measure the thermal conductivity of bulk samples. The second group of methods includes techniques such as optical spectroscopy, thermoreflectance imaging (TTI), and micro-Raman spectroscopy [50, 51]. These techniques directly measure the sample temperature and are useful for studying localized heating and temperature gradients in devices. By utilizing a combination of experimental techniques from both groups, researchers can gain a comprehensive understanding of the phonon mean free path and thermal conductivity of these materials.

TDTR and Raman spectroscopy are one of the experimental methods used to study phonon mean free path and thermal conductivity in $AlGaN$ alloys and β-form gallium oxide. TDTR is a non-destructive, contactless technique that can measure the thermal conductivity of thin films with high spatial resolution. However, it is limited by the thickness of the film and its thermal boundary resistance, which can lead to an underestimation of the thermal conductivity [48]. On the other hand, Raman spectroscopy provides information on the phonon dispersion relation. It can be used to determine the phonon lifetime, a critical parameter in determining thermal conductivity [52]. However, Raman spectroscopy is less sensitive than TDTR, and applying it to thin films with thicknesses below a few hundred nanometers is difficult. Laser-based thermal conductivity measurements are useful for measuring the thermal conductivity of bulk samples . Optical spectroscopy and micro-Raman spectroscopy are useful for directly measuring sample temperature and studying localized heating, but their spatial resolution is typically lower than TDTR.

Recent studies explored $AlGaN$ alloy thermal properties with diverse techniques. M. Kuball used Raman spectroscopy to study the thermal conductivity of $AlGaN$ thin films with different Al compositions [53], while N. Killat et al., used the same technique to investigate the effect of dislocations on thermal transport in AlGaN epilayers [54]. The 3ω method was used by Liu et al., to explore the thermal conductivity of AlN films [55]. L. Mitterhuber et al. used a combination of time-domain thermoreflectance (TDRT) and Raman spectroscopy to study the thermal transport in $AlGaN/GaN$ heterostructures [42].

One important property that determines the performance of $\beta - Ga_2O_3$-based devices is its thermal conductivity. To design and optimize such devices, the thermal conductivity of $\beta - Ga_2O_3$ must be accurately measured. In recent years, various experimental techniques have been used to measure the thermal conductivity of $\beta - Ga_2O_3$, including time-domain thermoreflectance (TDTR), laser flash analysis (LFA), and Raman spectroscopy. Reported values for the thermal conductivity of $\beta - Ga_2O_3$ using these methods range from approximately 10 $Wm^{-1}K^{-1}$ to 29 $Wm^{-1}K^{-1}$ at room temperature, depending on the measurement technique and sample preparation methods. Z. Guo et al., based on the TDTR method, measured the thermal conductivity of thin film $\beta - Ga_2O_3$ samples and reported a value of approximately 27 $Wm^{-1}K^{-1}$ at room temperature [56], while 13 $Wm^{-1}K^{-1}$ reported based on Laser-flash methods [57]. 3ω method was used by M. Handwerg to measure the thermal conductivity of single-crystal $\beta - Ga_2O_3$ samples and reported values ranging from 10 $Wm^{-1}K^{-1}$ to 27 $Wm^{-1}K^{-1}$ at room temperature [58]. Z. Galazka et al. determined the thermal conductivity of $\beta - Ga_2O_3$ thin films and reported a value of 21 $Wm^{-1}K^{-1}$ at room temperature [59]. These experimental studies provide important information for developing and optimizing electronic and optoelectronic devices based on $\beta - Ga_2O_3$.

In conclusion, various experimental methods are available for studying phonon mean free path and thermal conductivity relation in wide and ultra-wide bandgap materials such as $AlGaN$ alloys and $\beta - Ga_2O_3$. TDTR and Raman spectroscopy are the most commonly used techniques, but other methods such as 3ω, FDTR, BB-FDTR, and TTI have also been utilized [56–60]. These experimental methods have provided valuable insights into the phonon transport behavior of these materials, which can inform the development of more efficient thermal management strategies for electronic devices. However, there are still some limitations and challenges associated with experimental studies, such as the difficulty of measuring the thermal conductivity of thin films with high accuracy and the lack of sensitivity in some techniques for small changes in thermal conductivity. These limitations can lead to discrepancies between experimental results and theoretical predictions, making it challenging to design and optimize thermal management strategies for electronic devices.

Therefore, theoretical studies are often used in conjunction with experimental studies to provide a more complete understanding of phonon transport in these materials. Theoretical models can help to explain experimental observations and provide insights into the underlying physics of phonon transport. Additionally, theoretical predictions can guide experimental design and interpretation and provide predictions for materials properties that are difficult or impossible to measure experimentally.

1.4.2. Theoretical Studies

Theoretical studies have played a crucial role in understanding phonon transport and thermal conductivity in wide and ultra-wide bandgap materials. These studies can be classified into two main groups. The first group directly measures the temperature of devices where localized heating is present, using finite element and/or finite volume analysis to predict the temperature profile of samples and devices. This approach frequently employs the solution of Fourier's Equation [61]. However, when size effects, such as those observed in these materials, are present, the material's thermal conductivity is compromised, and traditional approaches may not be applicable. Therefore, the second group of theoretical studies focuses on measuring the thermal conductivities of thin films, employing the phonon Boltzmann Transport Equation (BTE) to model phonons and their contribution to bulk thermal conductivity [62, 63].

The thermal conductivity of *GaN* films has been explored in previous theoretical studies, particularly by Zou et al., based on the Callaway-Klemens approach [64, 65]. These studies have revealed that impurities and dislocations have a notable impact, leading to a significant reduction in the thermal conductivity of *GaN* films. The thermal conductivity of $Al_xGa_{1-x}N$ is not extensively studied, and only limited studies are available for Al molar fractions below 0.44 [66, 67]. Furthermore, there is a lack of studies examining the influence of layer thickness and phonon mean free path-thermal conductivity relations for $Al_xGa_{1-x}N$ with various Al concentrations. A study by Jinlong et al. utilized the first-principles calculations within the virtual crystal approximation to investigate the phonon transport in *AlGaN* alloys. They found that alloying

AlN with GaN can enhance the anharmonicity of the lattice, which decreases thermal conductivity. Another study by Liu et al. used the molecular dynamics simulation method to explore the phonon transport properties of $AlGaN/GaN$ heterostructures. They found that the thermal conductivity of the $AlGaN$ layer was significantly lower than that of the GaN layer, which was attributed to the phonon scattering at the $AlGaN/GaN$ interface. Furthermore, a study by Li et al. employed a combination of density functional theory and Monte Carlo simulations to investigate the phonon transport in $AlGaN/GaN$ superlattices. They found that the superlattice structure can effectively scatter phonons and reduce the material's thermal conductivity [39,55,68,69]. These theoretical studies provide insights into the underlying mechanisms of phonon transport in $AlGaN$ alloys and may guide the development of new thermal management strategies for the electronic devices.

There have been theoretical studies on the thermal transport properties of beta gallium oxide $\beta - Ga_2O_3$ as well. Katre et al. used a combination of first-principles calculations and Boltzmann transport equation (BTE) to calculate the thermal conductivity of $\beta - Ga_2O_3$. They also identified the contribution of phonon-phonon scattering and anharmonicity to the thermal conductivity, indicating that the dominant mechanism of phonon-phonon scattering in $\beta - Ga_2O_3$ was the three-phonon Umklapp process [70].

In a study by Zhang et al. the authors investigated the phonon thermal conductivity of $\beta - Ga_2O_3$ using first-principles calculations and an iterative solution of the phonon Boltzmann transport equation. They found that the phonon thermal conductivity of $\beta - Ga_2O_3$ is anisotropic and is influenced by both the phonon mean free path and the phonon group velocity [71]. Munshi et al. also used first-principles calculations to study the impact of defects on thermal conductivity in $\beta - Ga_2O_3$. They employed density functional theory (DFT) and BTE calculations to evaluate the thermal conductivity tensor and found that the presence of defects They also found that the thermal conductivity anisotropy was sensitive to the material's nature and concentration of defects [72].

Overall, these studies have provided valuable insights into the thermal conductivity of $\beta - Ga_2O_3$ and have implications for developing high-performance thermal management materials. To overcome these challenges, future research could focus on refining the accuracy and efficiency of first-principles calculations, exploring the role of various factors such as alloying, defects, and interfaces on phonon transport, and developing new experimental techniques to validate and refine theoretical predictions. Developing new materials with optimized thermal transport properties could also be explored through computational modeling and experimental synthesis. By addressing these challenges, a more comprehensive and accurate understanding of phonon transport in wide and ultra-wide bandgap materials can be achieved, with important implications for designing and optimizing materials for various applications, including thermal management in electronic devices.

1.5. Motivation and Problem Definition

As explored in previous sections, UWBG materials such as $AlGaN$ and $\beta - Ga_2O_3$ are commonly used in high-power electronic devices. However, they face challenges with localized heating in thin films or small-scale forms, causing non-continuum thermal transport. This can lead to unexpected heating, performance degradation, reduced device lifetimes, and economic and environmental disadvantages. To enhance performance in electronic devices, a thorough understanding and optimization of the thermal properties of UWBG materials are crucial. This includes focusing on the phonon mean free path (MFP), which plays a significant role in thermal conductivity by determining the distance phonons can travel before encountering collisions. In non-continuum thermal transport, interrupted phonon MFPs hinder efficient thermal energy conduction.

The accumulation spectra is a vital parameter for predicting thermal conductivity in confined structures. It provides valuable insight into the relationship between phonon mean free path (MFP) and thermal conductivity, optimizing the thermal management of UWBG materials in high-power electronic devices. Obtaining accumulation spectra for UWBG materials through experiments can be resource-intensive and

time-consuming. Therefore, a reliable theoretical approach is necessary to complement these efforts. However, most theoretical methods rely on approximations and fitting parameters, which may limit their accuracy and reliability in predicting accumulation spectra. Molecular dynamics simulations and other theoretical approaches can be time-consuming and lack a continuous accumulation spectrum due to repeated calculations at different length scales. These challenges in experimental and theoretical studies highlight the need for further research to develop robust and efficient methods for obtaining accurate and reliable accumulation spectra of phonon MFP in UWBG materials. Bridging this gap will enhance our understanding of thermal transport behavior in UWBG materials and optimize their thermal management in high-power electronic devices. The main motivation of this thesis is to calculate the phonon accumulation spectra for ultra-wide bandgap materials, particularly $AlGaN$ alloys with varying Al composition and $\beta-Ga_2O_3$, using ab-initio calculations and third-order force constants. The obtained data on phonon MFP - thermal conductivity relations for AlGaN alloys can be used to better understand the boundaries of thermal size effects and run more accurate thermal transport models for devices that exhibit size effects. Ultimately, the findings of this work may improve estimates of the thermal performance of UWBG $AlGaN$ alloys used in new-generation devices, which can enhance their lifetime and predict thermal responses at small scales.

1.6. Outline of the Thesis

The following chapters of this thesis aim to construct accumulation spectra of $AlGaN$ alloys and $\beta - Ga_2O_3$. This objective is pursued through ab-initio calculations and thermal calculations via VASP and Phono3py software, respectively. The second chapter, following the introduction, provides a detailed explanation of the methodology adopted in this study. The introduction defines some fundamental terms associated with this research, including phonon, MFP, and relaxation time. Chapter 2 provides the relevant equations, outlines the software's logical evolution, and introduces essential concepts such as force constants and phonon group velocity to establish a comprehensive foundation for the subsequent discussions.

Chapter 3 will outline the key findings of this study, including the accumulation spectra of thermal conductivity and bulk thermal conductivity outcomes for these materials at different temperatures. It will also feature a thorough comparison of the study's results with those obtained from previous experimental and theoretical studies in the literature. Moreover, the accumulation results will also be compared with each other to examine the variation in the materials' accumulation spectrum. The chapter will conclude with a discussion of any discrepancies in the literature and among the materials.

Chapter 4 will focus on the implications of this study's outcomes in the field of materials science and engineering, specifically on the design and development of devices that incorporate $AlGaN$ alloys and $\beta - Ga_2O_3$. Deductions derived from Chapters 3, including the effect of using third-order force constants on the thermal accumulation-MFP spectrum and considerations of anharmonicity in materials, will be thoroughly examined. Additionally, the chapter will explore future work possibilities, such as investigating the effect of impurities and defects on the thermal properties of these materials and provide recommendations for improving the methodology in future

2. METHOD

The primary objective of this study is to investigate the thermal properties of $AlGaN$ alloys and $\beta - Ga_2O_3$, including their thermal conductivities and accumulation spectra by utilizing a combination of ab-initio calculations and thermal calculations using Phono3py.

The computational workflow of this study, as depicted in Figure 2.1, consists of two main steps. In the first step, the unit cells of the materials are processed using VASP, which includes geometric relaxation to establish the proper initial conditions. The relaxed unit cell is then fed into Phono3py, where it is multiplied to create a supercell, ensuring proper replication of the unit cell. Next, small displacements are introduced to the supercell structure, and SCF calculations are performed on each displacement. Then phono3py scans all folders, evaluating the forces exerted on the structure by considering the displacement values. This procedure enables the determination of second and third-order force constants.

In the second step, the force constants are incorporated into the dynamical matrix in Phono3py and used to calculate the phonon dispersion and inverse relaxation times. These properties can then be used to derive the thermal properties of the materials, including the group velocity, mean free path, and accumulated thermal conductivity.

The obtained results will be analyzed to better understand the thermal properties of $AlGaN$ alloys and $\beta - Ga_2O_3$. Specifically, we aim to identify the mechanisms that govern thermal transport in these materials and the factors that affect their thermal conductivity. Additionally, the insights gained from this study may have practical applications in developing new materials for various technological applications, such as electronics, and energy conversion. These applications could potentially lead to more energy-efficient electronic devices, improved thermoelectric materials for waste heat recovery, and enhanced materials for renewable energy technologies.

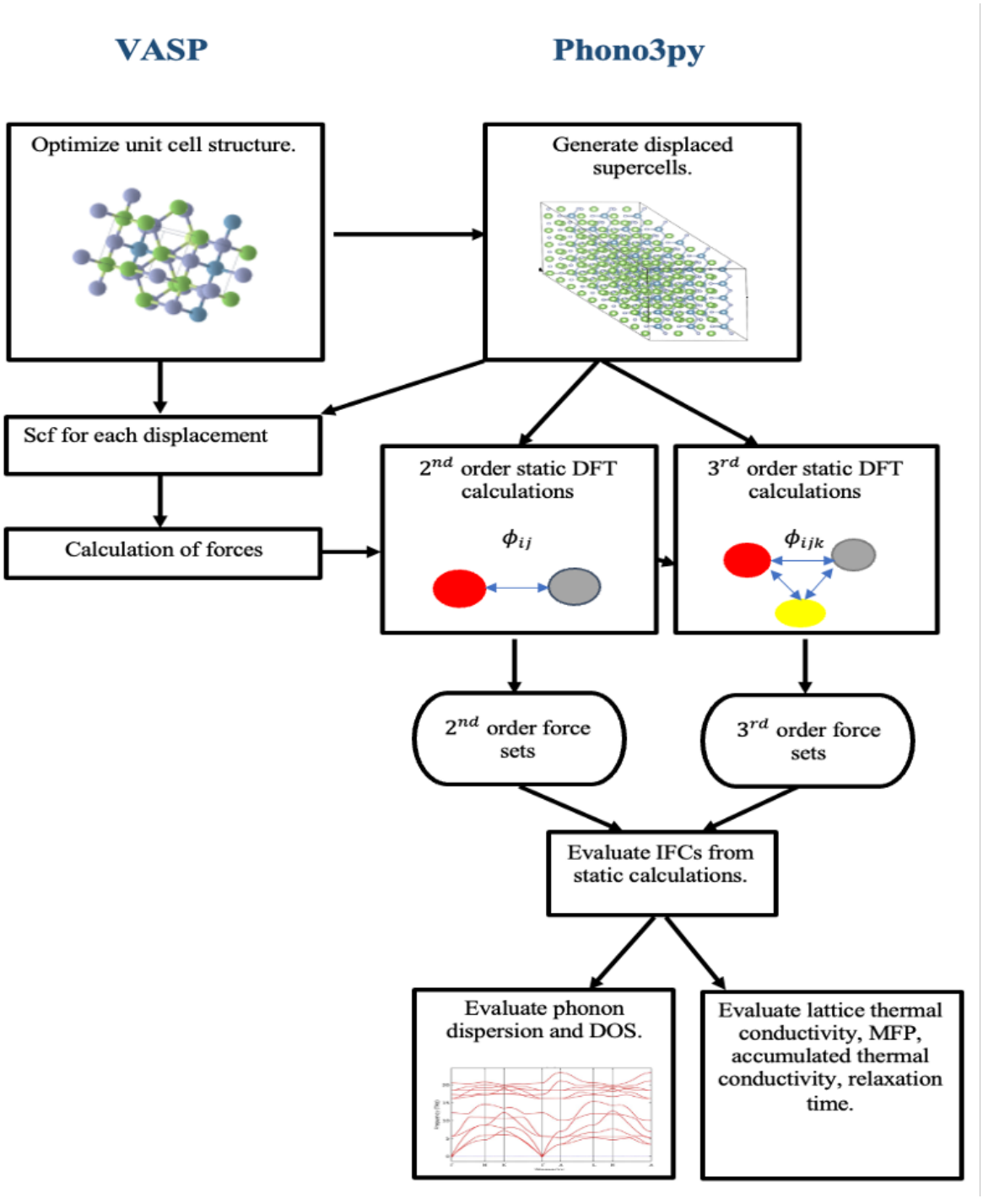

Figure 2.1. The overall workflow of calculations.

2.1. Ab-initio Calculations

Vienna Ab-Initio Simulation Package (VASP) is a software tool designed for simulating materials using first-principle techniques, which was developed by Georg Kresse and his team [73, 74]. The software is based on the Density Functional Theory (DFT) method, used to compute approximate solutions to the many-body Schrödinger equation. The Schrödinger Equation, given by:

$$-\frac{\hbar^2}{2m}\nabla^2\psi_t + U\psi_t = i\hbar\frac{\partial\psi_t}{\partial t}. \tag{2.1}$$

As illustrated by Equation (2.1), the Schrödinger Equation relates the wave function ψ_t, which describes the position of a particle such as an electron or photon, with its energy U. Although initially limited to DFT, VASP has now been augmented with more advanced methods for achieving higher accuracy in material simulations.

This equation becomes increasingly complex when multiple particles are involved. To tackle this issue, Hohenberg and Kohn proposed two fundamental assumptions: firstly, that energy can be expressed as a function of energy density, and secondly, that the ground state energy can be determined. These assumptions form the basis of the Density Functional Theory (DFT) method.Moreover, Kohn-Sham equations were introduced as follows:

$$\left[-\frac{\hbar^2}{2m}\nabla^2 + V(\mathbf{r}) + V_H(\mathbf{r}) + V_{xc}(\mathbf{r})\right]\psi(\mathbf{r}) = \epsilon_i\psi(\mathbf{r}), \tag{2.2}$$

where, V($\mathbf{r}$) represents the defined portion of the energy functional, which governs the electron-nucleus interaction. $\mathrm{V}_H(\mathbf{r})$ is the Hartree potential, which describes the Coulombic repulsion between electrons, while $\mathrm{V}_{xc}(\mathbf{r})$ is the functional derivative of the exchange-correlation energy, accounting for the effects of electron-electron correlations. Equations (2.2), describe the single-electron wavefunctions, which are expressed solely as a function of the spatial variable $\mathbf{r}$.

VASP employs a self-consistency scheme to solve the Kohn-Sham equations, where density functions are iteratively solved to ensure the convergence of the wavefunctions. This iterative process is depicted in Figure 2.2. The ultimate goal of VASP

is to define the electronic ground state by minimizing the system's free energy. This ground-state solution process plays a pivotal role in establishing the force constants used in the current study, as depicted in Figure 2.2, which visually represents this crucial aspect of the research.

To conduct calculations with VASP, four input files are necessary. First input file is called POTCAR, which contains the pseudopotential for a specific element, which approximates the effect of the ion cores on the valence electrons. The second file is called POSCAR, which sets up the basic orientations of the lattice, including the number of atoms, their positions, and the lattice spacing. This serves as the foundation for the model, and the boundary conditions are determined based on these parameters. The third file is called KPOINTS, which describes the resolution of the Brillouin zone and how the program will render it. The Brillouin zone is the region in reciprocal space containing all possible wave vectors that can represent the periodicity of a crystal lattice, and its resolution affects the accuracy of the results. Finally, the fourth file is called INCAR, which summarizes all the specifications for the model and instructs VASP on how to perform the simulation. This includes information on the type of calculation to be performed (e.g., relaxation or electronic structure), convergence criteria, and output options. Proper specification of all four input files is crucial for obtaining accurate and reliable results from VASP calculations.

In this study, VASP serves as an indispensable tool for the geometric relaxation of unit cells in both $AlGaN$ and $\beta - Ga_2O_3$ semiconductors. This initial step is pivotal as it lays the foundation for all subsequent computational analyses. VASP employs the projector-augmented wave potential (PAW) [75], a sophisticated computational approach renowned for its accuracy in capturing the intricate electronic structure of materials. With a plane-wave basis set, VASP efficiently represents the electronic wavefunctions within the system, facilitating accurate calculations. Additionally, the integration of pseudopotentials allows VASP to optimize computational resources by focusing on the chemically active valence electrons, ensuring both efficiency and accuracy in describing atomic interactions.

Working with VASP offers the advantage of employing reciprocal space over real space, a strategic choice that can significantly enhance our understanding of materials. Through the concept of k-points, VASP enables us to finely tune the resolution of the first Brillouin zone, with N^3 k-points representing a division of this zone into anNxNxN grid, where k is quantified in units of inverse length, providing researchers with a versatile tool to tailor simulations according to their precision requirements.

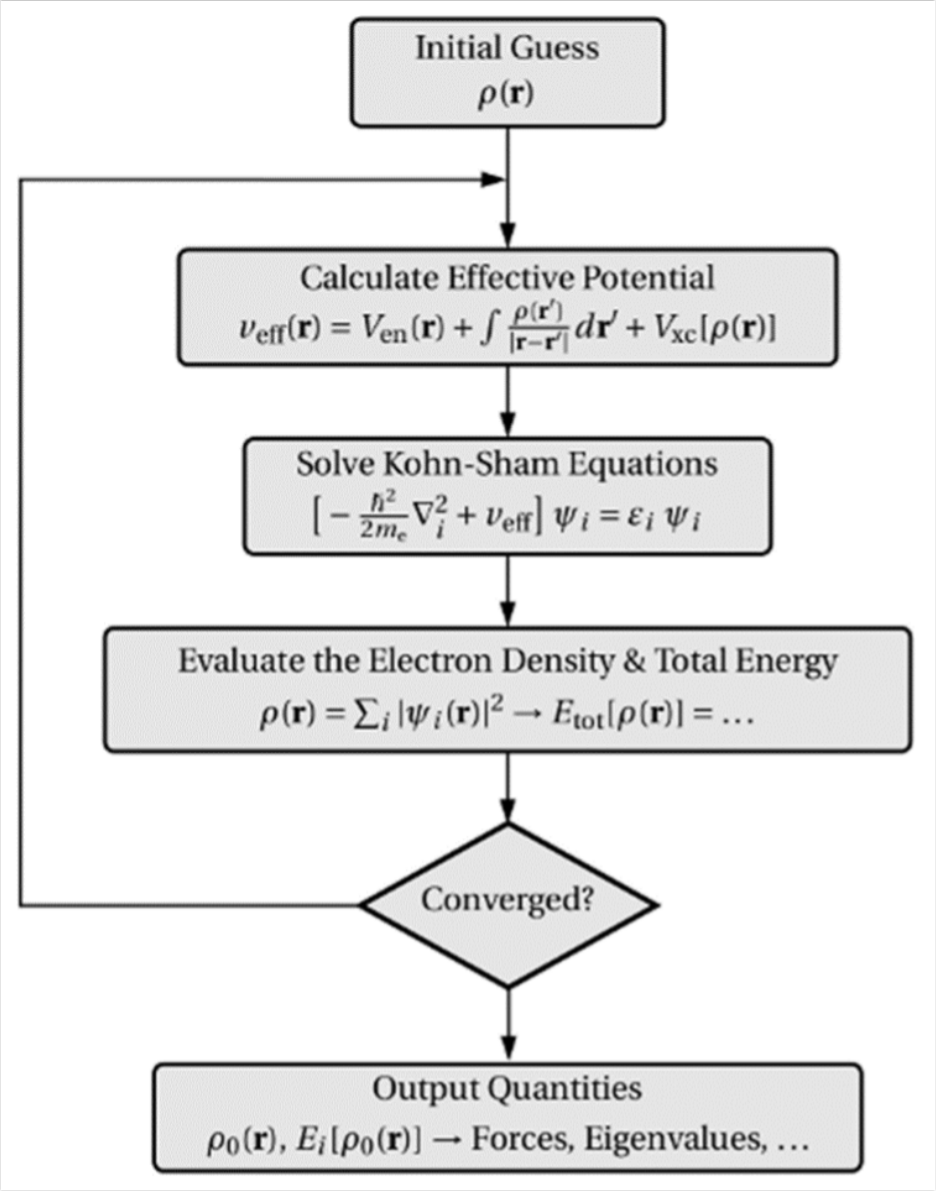

Figure 2.2. Self-consistent Field (SCF) Scheme of VASP.

2.2. Phono3py

Phono3py is a powerful computational tool developed by Atsushi Togo [46], used for studying the thermal and mechanical properties of crystals. This software uses a supercell approach to analyze phonon-phonon interactions in the crystal lattice, allowing for calculations of lattice thermal conductivity and phonon lifetime. The calculations are performed using the RTA method or a direct solution to solve the LBTE. To generate a set of displacements, Phono3py uses another independent computing program that performs DFT calculations to calculate the forces. These displacements cause anharmonicity in the lattice, which is essential for phonons and other thermodynamic phenomena to be present. Phono3py then accumulates the force calculations on the displaced supercells to determine the desired properties.

2.2.1. Phono3py Parameters

Phono3py relies on DFT calculations of the third-order force constants (FC3s) to describe phonon interactions in the system. However, these calculations are often sensitive to any perturbations in the force calculations, leading to inaccurate results. One solution is to use a larger supercell.

2.3. Phonopy

In this research, Phonopy, a software developed by Atsushi Togo [46], plays a pivotal role alongside phono3py in conducting comprehensive phonon calculations. Specifically, Phonopy is employed to discern essential phonon properties, such as the phonon band structure and density of states (DOS). The workflow for utilizing Phonopy closely resembles that of phono3py, necessitating a distinct force calculator to provide the requisite input data for accurate phonon calculations. By integrating Phonopy into the computational framework, researchers can gain deeper insights into the vibrational properties of materials, ultimately contributing to a more comprehensive understanding of their thermal and mechanical behavior.

2.4. Thermal Calculations

Thermal conductivity is calculated from phonon dispersion data and second/third-order force constants using Phono3py. It can be expressed as

$$k = \sum \kappa_{\mathbf{q}s} = \frac{1}{NV_0} \sum c_{\mathbf{q}s} v_{\mathbf{q}s} \otimes v_{\mathbf{q}s} \tau_{\mathbf{q}s}, \tag{2.3}$$

where, k refers to the bulk thermal conductivity, N represents the number of unit cells in the sample, V_0 denotes the volume of a single unit cell, $c_{\mathbf{q}s}$ refers to the specific heat, $v_{\mathbf{q}s}$ represents the group velocity, and $\tau_{\mathbf{q}s}$ corresponds to the relaxation time. Specific heat is a function of phonon frequency $\omega_{\mathbf{q}s}$ and temperature T, and is calculated as

$$c_{\mathbf{q}s} = \frac{k_b \left(\frac{\hbar\omega_{\mathbf{q}s}}{k_b T}\right)^2 \exp\left(\frac{\hbar\omega_{\mathbf{q}s}}{k_b T}\right)}{\left(\left(\frac{\hbar\omega_{\mathbf{q}s}}{k_b T}\right) - 1\right)^2}, \tag{2.4}$$

where k_b represents the Boltzmann constant, and the group velocity is expressed as

$$v_{\mathbf{q}s} = \frac{\partial \omega_{\mathbf{q}s}}{\partial \mathbf{q}}, \tag{2.5}$$

it is determined by the derivative of the dispersion relation with respect to the wavevector $\mathbf{q}$, while relaxation time approximations involve the incorporation of third-order force constants FC3 into the calculations, and the phonon line widths can be demonstrated as

$$\begin{aligned} \Gamma_{\mathbf{q}s} = \frac{18\pi}{\hbar^2} \sum_{\mathbf{q}'s'\mathbf{q}''s''} & \left|\Phi_{-\mathbf{q}s\mathbf{q}'s'\mathbf{q}''s''}\right|^2 \\ & \times \left\{ \left(n_{\mathbf{q}'s'} + n_{\mathbf{q}''s''} + 1\right) \delta\left(\omega - \omega_{\mathbf{q}'s'} - \omega_{\mathbf{q}''s''}\right) \right. \\ & \left. + \left(n_{\mathbf{q}'s'} - n_{\mathbf{q}''s''}\right) \left[\delta\left(\omega + \omega_{\mathbf{q}'s'} - \omega_{\mathbf{q}''s''}\right) - \delta\left(\omega - \omega_{\mathbf{q}'s'} - \omega_{\mathbf{q}''s''}\right)\right] \right\}. \end{aligned} \tag{2.6}$$

As seen in Equation (2.6), interaction term $\Phi_{-\mathbf{q}s\mathbf{q}'s'\mathbf{q}''s''}$ is employed in the inverse relaxation time $\Gamma_{\mathbf{q}s}$ for phonon mode $\mathbf{q}s, \mathbf{q}'s'\mathbf{q}''s''$calculations. This term is directly related to third-order interactions, and $n_{\mathbf{q}'s'}$ is determined as follows

$$n_{\mathbf{q}'s'} = \frac{1}{\exp\left(\frac{\hbar\omega_{\mathbf{q}s}}{k_b T}\right) - 1}, \tag{2.7}$$

which represents the phonon equilibrium occupation number, the phonon lifetime $\tau_{\mathbf{q}s}$ can be obtained by converting the inverse phonon line widths $\Gamma_{\mathbf{q}s}$ as

$$\tau_{\mathbf{q}s} = \frac{1}{2\Gamma_{\mathbf{q}s}(\omega_{\mathbf{q}s})}, \tag{2.8}$$

and the phonon mean free path $\Lambda_{\mathbf{q}s}$ is expressed as

$$\Lambda_{\mathbf{q}s} = v_{\mathbf{q}s}\tau_{\mathbf{q}s}, \tag{2.9}$$

it is dependent on both the phonon lifetime and group velocity. The obtained results can be incorporated into the thermal conductivity calculation, described by Equation (2.3). By defining each phonon mode $\mathbf{q}s$, we can calculate thermal conductivity in terms of the phonon mean free path (Λ) as follows

$$k_{acc}\left(\Lambda\right) = \sum_{\Lambda_{\mathbf{q}s=0}}^{\Lambda_{\mathbf{q}s}=\Lambda} k_{\mathbf{q}s}. \tag{2.10}$$

Ultimately, the thermal conductivity can be expressed as an accumulation function.

3. Results and Discussion

3.1. *AlGaN* Alloys

3.1.1. $Al_{0.25}Ga_{0.75}N$

As stated in the introduction chapter $Al_xGa_{1-x}N$ is an alloy of *AlN* and *GaN*, with *Al* impurities introduced to the *GaN* lattice. The proportions of *Al* and *Ga* atoms in *AlGaN* can be experimentally controlled, allowing for tailoring of material properties. However, calculating phonon properties for structures with large unit cells can be challenging. In the public material database, there are seven types of *AlGaN* structures, including those with space groups P3m1, P-43m, P-4m2, and others with low symmetry. Among this $Al_{0.25}Ga_{0.75}N$ possesses a cubic crystal structure with the P-43m space group, similar to $Al_{0.75}Ga_{0.25}N$. The unit cell of $AlGa_3N_4$ contains four atoms, consisting of a combination of aluminum *(Al)* and gallium *(Ga)* atoms, along with nitrogen *(N)* atoms. The composition of $AlGa_3N_4$ in the unit cell is 0.25 *Al* atoms, 0.75 *Ga* atoms, and four N atoms. The atoms within the crystal structure exhibit tetrahedral coordination, where each *Al* or *Ga* atom is bonded to four nearest-neighbor *N* atoms. This unique combination of the P-43m space group and tetrahedral coordination contributes to the distinctive structural properties of $Al_{0.25}Ga_{0.75}N$. Notably, $Al_{0.25}Ga_{0.75}N$ shares similarities with the zincblende structure, as it involves the substitution of *Al* atoms for a fraction of Ga atoms in the conventional unit cell of *GaN*. These structural characteristics influence the physical and electronic properties of $AlGa_3N_4$, making it a promising material for various technological applications.

The interatomic force constants (IFCs) were computed using density functional theory (DFT) with the generalized gradient approximation (GGA) and the projector augmented wave (PAW) [75] method implemented in VASP. Firstly, the lattice structure was optimized for the unit cell using a Gamma-centered k-mesh grid with a size of 12×12×12 and a plane wave basis with a kinetic energy cutoff of 520 eV. The harmonic

IFCs were obtained by performing self-consistent calculations through phonopy for 4 different displacements using a 3×3×3 supercell. optimized structure for $Al_{0.25}Ga_{0.75}N$, indicating agreement and consistency with literature in Figure 3.1 [76].

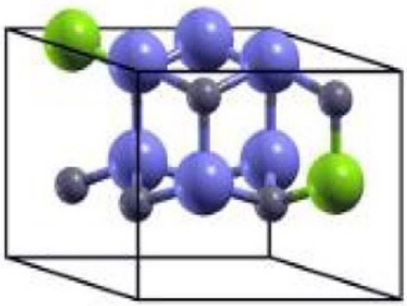

Figure 3.1. The optimized structure of $Al_{0.25}Ga_{0.75}N$ alloy [76].

According to the method by Wahyu and Stefano et al. [77] for the cubic structure *AlGaN*, the corresponding Cubic (CUB, cP)-type Brillouin zone and high symmetry k-point paths are selected. As illustrated in Figure 3.2 for the P-43m symmetry structure, the coordinates of the high symmetry paths in the first Brillouin zone are Γ-X-M-Γ-R-$X|M$-R.

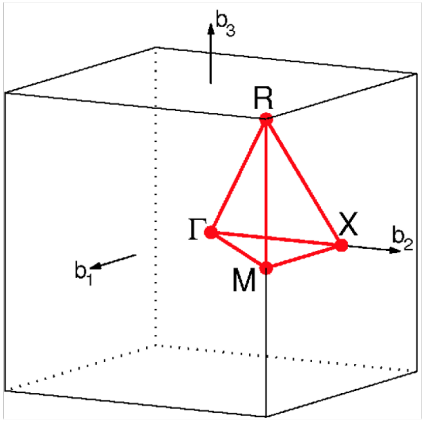

Figure 3.2. Brillouin zone of CUB lattice [77].

Figure 3.3 displays the phonon dispersion plot for $Al_{0.25}Ga_{0.75}N$, showcasing the band gaps and patterns in agreement with previous literature. The plot features 24 branches, corresponding to the 8 atoms per unit cell in $Al_{0.25}Ga_{0.75}N$, as indicated by the relation $\omega(q) = 3N$.

Thermal calculations were conducted for $Al_{0.25}Ga_{0.75}N$ following the determination of its dispersion curve. The third-order force constants (FC3s) calculations were carried out using a 2×2×2 supercell, while a 3×3×3 supercell was utilized for second-order (FC2s) calculations. To account for the intricate structure of AlGaN alloys, a cut-off distance of 3.2 Å was implemented, resulting in a larger number of interactions. The VASP software package was employed to calculate the second and third-order (FC2s), which were subsequently imported into Phono3py for thermal calculations. The relaxation time approximation was utilized, and the calculations were performed using a 13×13×9 mesh. The obtained results for the phonon thermal calculations for $Al_{0.25}Ga_{0.75}N$ will be discussed in the following section.

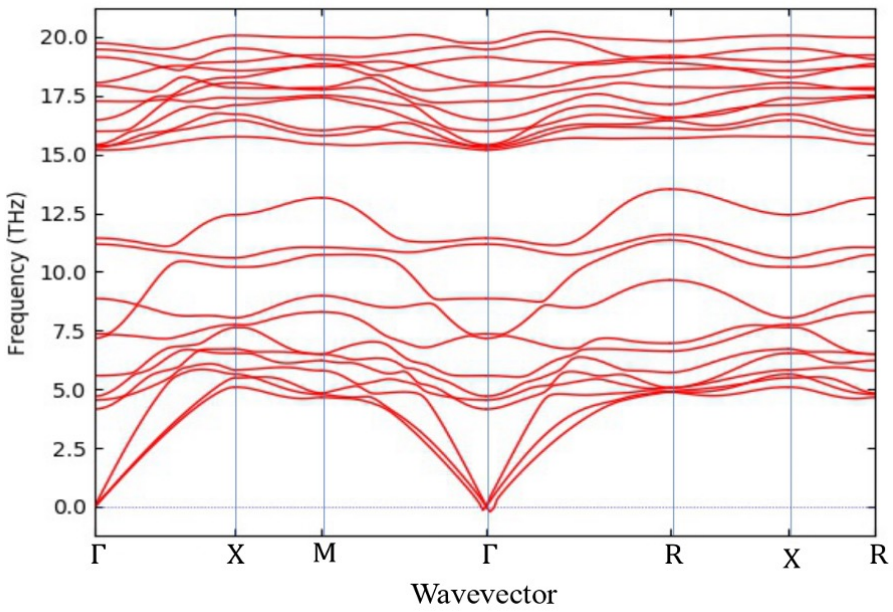

Figure 3.3. Phonon dispersion curve of $Al_{0.25}Ga_{0.75}N$.

The determined bulk conductivity values for $Al_{0.25}Ga_{0.75}N$ are as follows: 88.46 W/m.K, 47.61 W/m.K, 39.7 W/m.K, and 29.8 W/m.K at temperatures of 300 K, 500 K, 600 K, and 800 K, respectively. Notably, A. Jain et al. reported a bulk conductivity of 66.6 W/m.K at 300 K for cubic $Al_{0.25}Ga_{0.75}N$, while Liu & Balandin observed a value of 60 W/m.K at 300 K for $Al_{0.23}Ga_{0.77}N$ in the cross-sectional direction. Hence, the measured bulk conductivity of 88.46 W/m.K at 300 K aligns well with the values reported in the existing literature.

The accumulation spectra of $Al_{0.25}Ga_{0.75}N$ at 300 K, 500 K,600 k, and 800 K are presented in Figure 3.4. At 300 K, phonons with mean free paths (MFPs) smaller than 138.4 nm contribute to approximately half of the conductivity, while the MFP of thermally conductive phonons extends up to 442.2 nm. Table 3.1 provides crucial MFP values and their corresponding contributions. These observations confirm the validity of the relation between temperature and phonon spectrum; As the temperature increases, the spectrum becomes shorter, indicating that the size effects are expected to become evident at smaller scales, resulting in additional phonon entrapment.

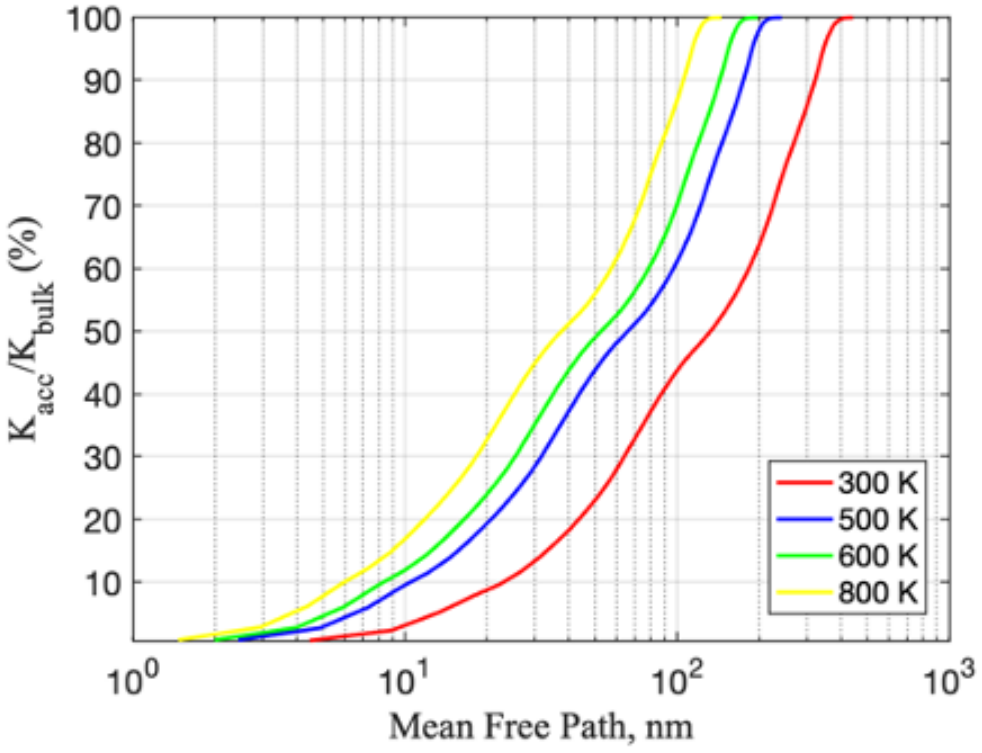

Figure 3.4. Accumulation spectra of $Al_{0.25}Ga_{0.75}N$ at T = 300 K, 500 K, 600 K, and 800 K

To comprehensively understand the effect of aluminum fraction on the relationship between phonon mean free path and thermal conductivity in $Al_xGa_{1-x}N$ alloys, we conducted a comparative analysis, as depicted in Figure 3.5. Notably, there is a lack of prior research on this specific Al composition. To address this gap, we examined existing literature results pertaining to various aluminum fractions (x) within the $Al_xGa_{1-x}N$ alloy system. This literature review provided essential insights and

reference points for our study, enabling us to explore the impact of aluminum fraction on phonon mean free path and thermal conductivity in this unique alloy context.

In examining the intricate relationship between crystal complexity and the phonon mean free path (MFP) spectrum, it is imperative to consider the valuable insights provided by Mitterhuber et al.'s TDTR (Time-Domain Thermoreflectance) research on $Al_{0.32}Ga_{0.68}N$ [42]. However, a significant challenge arises due to the divergence in the Al to Ga ratio between their study and the one under discussion, which hinders a straightforward comparison. Notably, the findings of this study present a contrasting trend with shorter MFP values when juxtaposed with Mitterhuber et al.'s work. This divergence can be attributed to the heightened intricacy of the crystal structure within our study, ultimately leading to a condensed MFP spectrum.

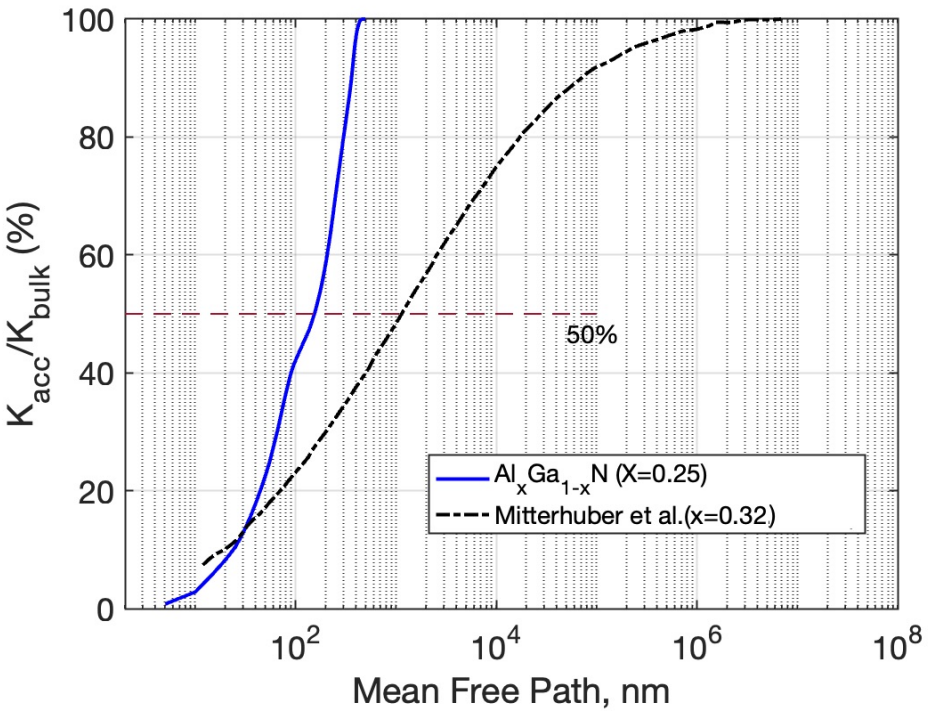

Figure 3.5. Comparison of accumulation spectra of $Al_{0.25}Ga_{0.75}N$ at T = 300 K with literature.

While Mitterhuber et al.'s theoretical framework assumes that phonons continue to contribute to thermal conductivity beyond the 0.074 m threshold, it is intriguing

that our research reports a considerably shorter total MFP spectrum of only 442.2 nm at 300 K, as outlined in Table 3.1. This stark difference prompts us to critically examine the possibility of oversimplification within their theoretical approach, potentially neglecting intricate phonon interactions that our study might have captured. In essence, this discrepancy highlights the multifaceted nature of crystal complexity's influence on phonon behavior and its implications for thermal transport in materials.

Table 3.1. Mean free path of phonons contributing to 30%, 50%, and 90% of $Al_{0.25}Ga_{0.75}N$ thermal conductivity (k) at T = 300 K, 500 K, 600 K, and 800 K.

Temperature (Kelvin)	30% of k	50% of k	90% of k	Total (100%) of k
300	>62.5 nm	>138.4 nm	>321.6 nm	<442.2 nm
500	>31.7 nm	>68.3 nm	>175.6 nm	<239 nm
600	>25.9 nm	>56 nm	>143.7 nm	<187.6 nm
800	>19.1 nm	>40 nm	>105.8 nm	<140.9 nm

3.1.2. $Al_{0.5}Ga_{0.5}N$

The crystal structure of $AlGaN_2$ with space group P3m1 is characterized by a hexagonal unit cell. The unit cell contains 4 atoms comprising two Al atoms and two nitrogen N atoms. The coordination of atoms in $AlGaN_2$ plays a crucial role in its physical and chemical properties, with the Al atoms exhibiting tetrahedral coordination and the N atoms displaying trigonal prismatic coordination. The unique arrangement of atoms gives rise to its exceptional electrical and optical properties, making it an attractive material for various technological applications.

To determine the interatomic force constants (IFCs), the computations were conducted using VASP with the local density approximation (LDA) [78] and projector augmented wave (PAW) [75] pseudopotentials. The harmonic IFCs were then extracted using the Phonopy package. A plane wave basis with a kinetic energy cutoff of

520 eV is used, and a converged 12×12×9 Gamma-centered k-mesh grid is employed to sample the Brillouin zone. The conventional unit cells are subjected to relaxation until the system reaches its minimum energy state. Obtained optimized structure for $Al_{0.5}Ga_{0.5}N$, illustrated in Figure 3.6 [76]. The lattice dimensions of the optimized structures were found to be a = b = 3.18 Å and c = 5.181 Å. The calculated results of the lattice parameters align with the findings of previous theoretical research [76]. The harmonic interatomic force constants (IFCs) were obtained by performing self-consistent calculations for eight different displacements using a 3×3×3 supercell.

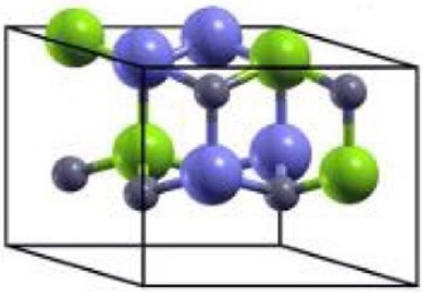

Figure 3.6. The optimized structure of $Al_{0.5}Ga_{0.5}N$ alloy [76].

This study employed the method introduced by Wahyu and Stefano et al. [77] to define the Brillouin zone (BZ) and the corresponding high symmetry directions. For the wurtzite structure *AlGaN*, the corresponding Hexagonal (HEX, hP)-type Brillouin zone, and high symmetry k-point paths are selected. For the P3m1 symmetry structure, the coordinates of the high symmetry paths in the first Brillouin zone are Γ-Y-F-L-$I|I_1$-Z-$F_1|Y$-$X_1|X$-Γ-$N|M$-Γ as illustrated in Figure 3.7.

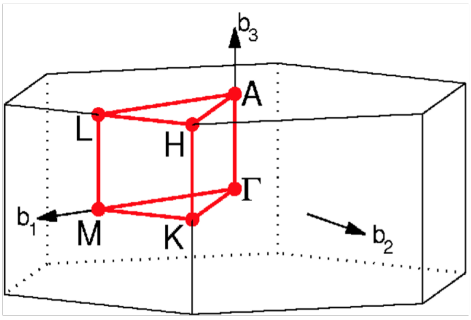

Figure 3.7. Brillouin zone of HEX lattice [77].

Figure 3.8 displays the phonon dispersion plot obtained for wurtzite $Al_{0.5}Ga_{0.5}N$ along high symmetry paths. The results are consistent with previous literature in terms of both band gaps and patterns [79]. In 3D-crystalline structures, the phonon dispersion results can be confirmed using the phonon dispersion relation equation, $\omega(q) = 3N$ (where N represents the number of atoms in the unit cell). As there are 4 atoms per unit cell in wurtzite $Al_{0.5}Ga_{0.5}N$, Figure 3.8 displays 12 branches.

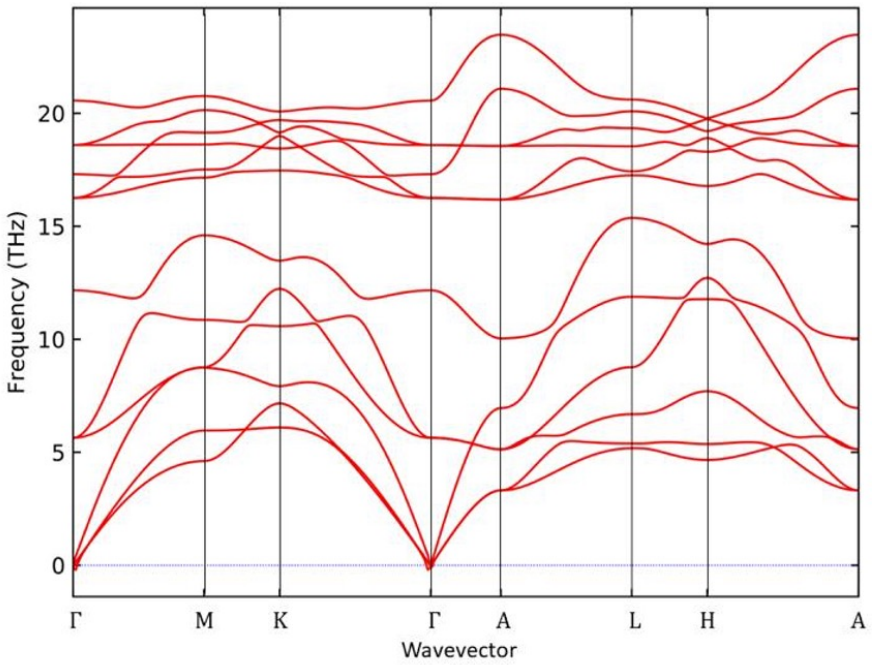

Figure 3.8. Phonon dispersion curve of $Al_{0.5}Ga_{0.5}N$.

Thermal calculations were conducted once the dispersion curve was obtained. Third-order force constants (FC3s) calculations were carried out using a 2×2×2 supercell, while a 3×3×3 supercell was used for second-order (FC2s) calculations. Due to the complex structure of *AlGaN* alloys compared to other materials, a cut-off distance of 3.2 Å was set, resulting in a larger number of interactions. The cut-off distance is a parameter that determines the range beyond which phonon interactions are neglected. By reducing the cut-off distance, the number of displacements considered in the calculations is significantly reduced. The second-and third-order FCs were obtained using VASP and imported into Phono3py for conducting thermal calculations via the relaxation time approximation over a 54×54×54 mesh.

Bulk conductivity results of $Al_{0.5}Ga_{0.5}N$ are found as follows: 81.09 W/m.K, 47.21 W/m.K, 39.23 W/m.K, 29.40 W/m.K, at 300 K, 500 K, 600 K, and 800 K, respectively. Bulk conductivity at 300 K for wurtzite $Al_{0.5}Ga_{0.5}N$ is reported as 91.0 W/m.K by A. Jain et al. [80], 151.08 W/m-K by Hiumin Wang et al., [81] and Liu & Balandin report 60 W/m.K at 300 K for $Al_{0.23}Ga_{0.77}N$ in cross-sectional direction [68]. Thus, 81.09 W/m.K at 300 K is in good agreement with the literature.

Figure 3.9 illustrates the accumulation spectra for $Al_{0.5}Ga_{0.5}N$ at temperatures of 300 K, 500 K, 600 K, and 800 K. Notably, at 300 K, phonons with mean free paths (MFPs) less than 208 nm contribute significantly, comprising half of the conductivity. At this temperature, thermally conductive phonons have impressively long MFPs, extending up to 2038 nm. Table 3.2 provides critical MFP values and their corresponding contributions. As the temperature increases, the MFP spectrum shortens due to greater phonon scattering, revealing the temperature's influence on phonon transport properties in $Al_{0.5}Ga_{0.5}N$.

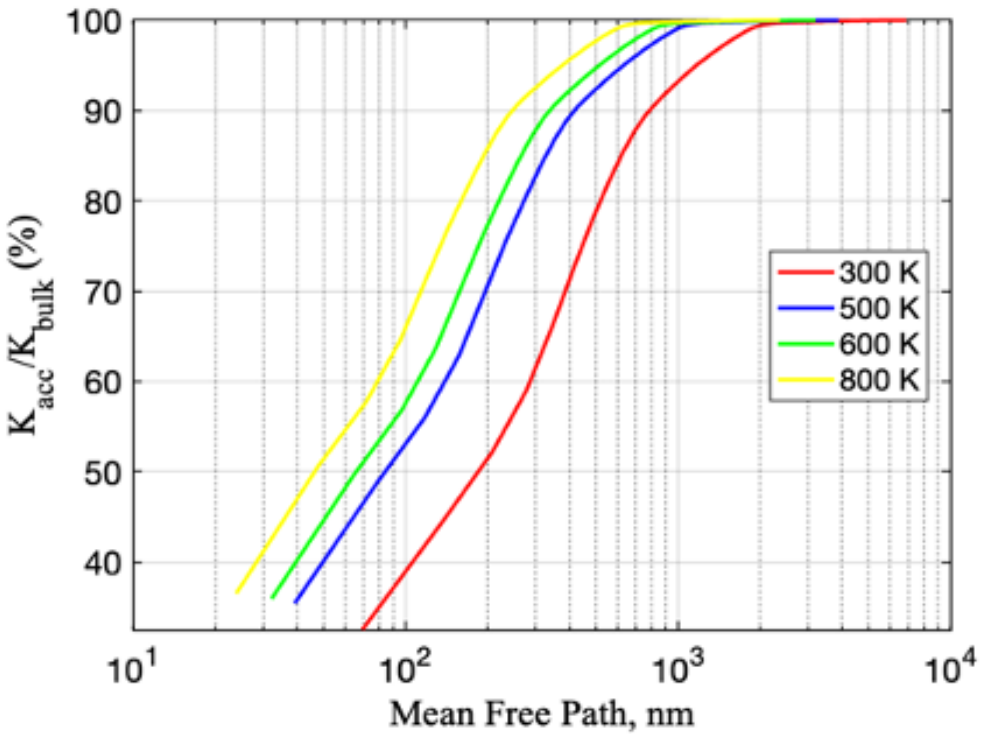

Figure 3.9. Accumulation spectra of $Al_{0.5}Ga_{0.5}N$ at T = 300 K, 500 K, 600 K, and 800 K.

Table 3.2. Mean free path of phonons contributing to 30%, 50%, and 90% of $Al_{0.5}Ga_{0.5}N$ thermal conductivity (k) at T = 300 K, 500 K, 600 K, and 800 K.

Temperature (Kelvin)	30% of k	50% of k	90% of k	Total (100%) of k
300	>70 nm	>208 nm	>763.4 nm	<2038 nm
500	>40 nm	>80.5 nm	>430 nm	<1742.5 nm
600	>32.3 nm	>64.5 nm	>354.8 nm	<1419.85 nm
800	>23.8 nm	>47.nm	>238.9 nm	<1027.56 nm

In this study, we examine the cumulative thermal conductivity of $Al_{0.5}Ga_{0.5}N$ at T=300 K, comparing it with data from the literature in Figure 3.10, where we rely on Tran Dat et al.'s experimental research using the TTR method [39]. To facilitate comparison, a 50% reference line highlights the MFP values of phonons contributing to half of the bulk thermal conductivity. Notably, our accumulation spectra cover a narrower range of phonon MFPs compared to the literature. These differences stem from various factors influencing the MFP spectrum, including crystal complexity, defects, impurities, and alloy composition.

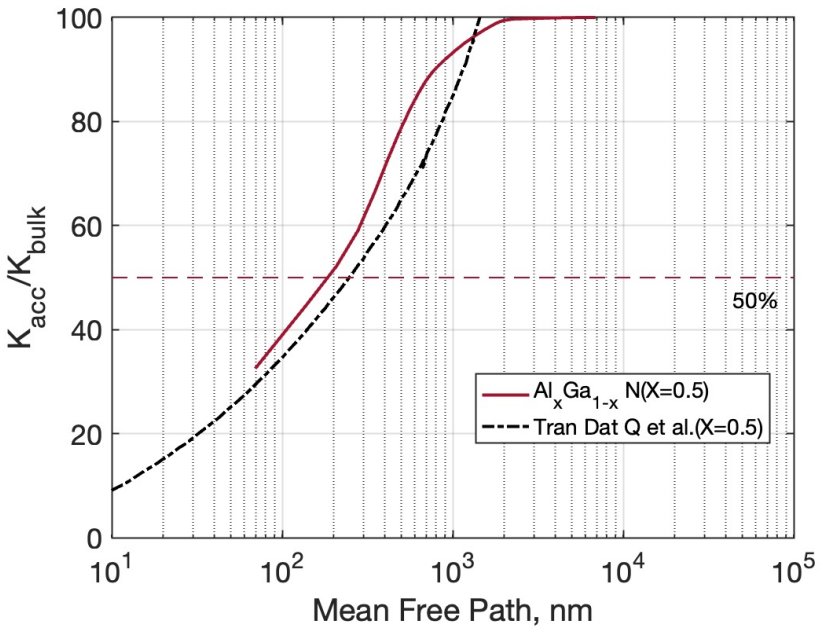

Figure 3.10. Comparison of accumulation spectra of $Al_{0.5}Ga_{0.5}N$ at T = 300 K with literature.

3.1.3. $Al_{0.75}Ga_{0.25}N$

Al_3Ga_4N has a cubic structure with space group P-43m and lattice parameters a = 4.40 Å and c = 4.40 Å. One primitive unit cell contains eight atoms, which consist of 3 *Al*, 1 *Ga*, and 4 *N*. This structure is similar to the zincblende structure, where 3 *Al* atoms replace 3 *Ga* atoms in the conventional unit cell of *GaN*. The coordination of atoms in Al_3Ga_4N is tetrahedral, with each atom bonded to 4 nearest neighbors. The Brillouin zone of Al_3Ga_4N is also cubic, reflecting its underlying crystal symmetry. These structural features of Al_3Ga_4N have important implications for its thermal properties, including the phonon mean free path spectrum and thermal conductivity.

The calculation process for $Al_{0.75}Ga_{0.25}N$ showcases certain similarities to $AlGa_3N_4$ Alloy, as both structures comprise unit cells with four atoms. Initially, the lattice structure of the $Al_{0.75}Ga_{0.25}N$ unit cell was optimized using a Gamma-centered k-mesh grid of size 12×12×12, along with a plane wave basis set and a kinetic energy cutoff of 520 eV. Determining the harmonic interatomic force constants (IFCs) involved conducting self-consistent calculations through phonopy, utilizing a 3×3×3 supercell, and employing four different displacements. The optimized structure for $Al_{0.75}Ga_{0.25}N$, is shown in Figure 3.11 [76].

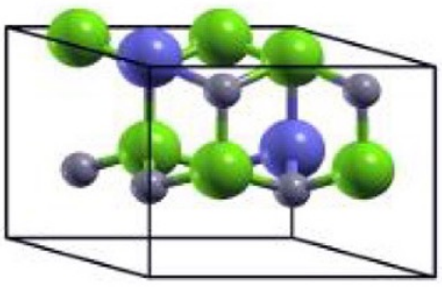

Figure 3.11. The optimized structure of $Al_{0.75}Ga_{0.25}N$ alloy [76].

Similarly to $Al_{0.25}Ga_{0.75}N$, the method by Wahyu and Stefano et al. [77] is employed to determine the Brillouin zone and high symmetry k-point paths for $Al_{0.75}Ga_{0.25}N$. as shown in Figure 3.13 the P-43m symmetry structure yields selected high symmetry paths in the first Brillouin zone, including Γ-X-M-Γ-R- $X|M$-R.

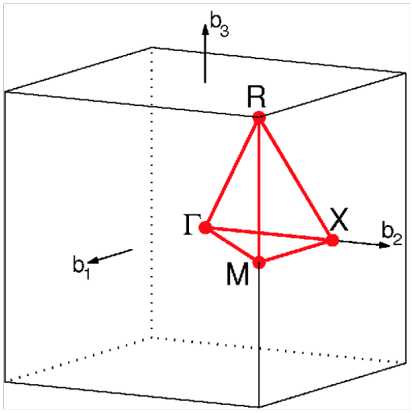

Figure 3.12. Brillouin zone of CUB lattice [77].

Figure 3.13 displays the phonon dispersion plot for $Al_{0.75}Ga_{0.25}N$ along high symmetry paths. Our findings are consistent with previously published literature on band gaps and patterns [80]. In accordance with the relation mentioned earlier, $\omega(q) = 3N$ (where N represents the number of atoms in the unit cell), the plot depicts 24 branches, reflecting the presence of 8 atoms within the unit cell of $Al_{0.75}Ga_{0.25}N$. This illustration provides valuable insights into the material's vibrational characteristics, contributing to our understanding of its structural and thermal properties.

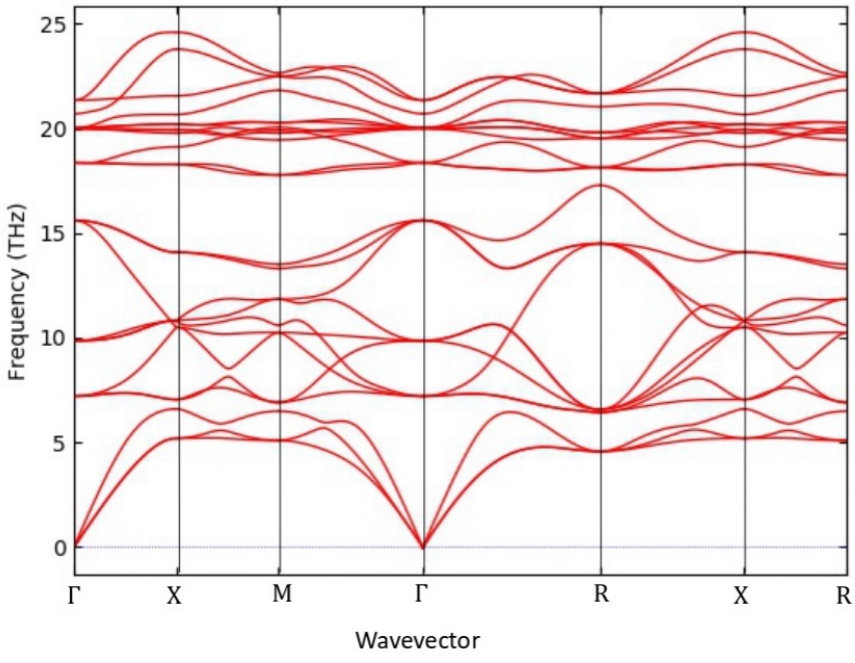

Figure 3.13. Phonon dispersion curve of $Al_{0.75}Ga_{0.25}N$.

After obtaining the dispersion curve, thermal calculations were performed. Same as the $Al_{0.5}Ga_{0.5}N$ third-order force constants (FC3s) calculations were carried out using a 2×2×2 supercell, while a 3×3×3 supercell was used for second-order force constants (FC2s) calculations for all alloys. Due to the complex structure of *AlGaN* alloys compared to other materials, a cut-off distance of 3.2 Å was set, resulting in a larger number of interactions. The VASP was employed to calculate the second and third-order force constants (FC3s), which were subsequently imported into Phono3py for thermal calculations. The relaxation time approximation was utilized for the calculations performed over a 54×54×54 mesh.

Figure 3.14 displays the accumulation spectra of ($Al_{0.75}Ga_{0.25}N$) at 300 K, 500 K, 600, and 800 K. The phonons with mean free paths (MFPs) smaller than 250 *nm* contribute to half of the conductivity at 300 K, and the MFP of thermally conductive phonons extends to 3572.5 *nm* at this temperature. Table 3.14 shows some critical MFP values and their corresponding contributions. As anticipated, the spectrum becomes shorter as the temperature increases. This indicates that as the temperature rises in the device, the size effects are expected to become apparent at smaller scales.

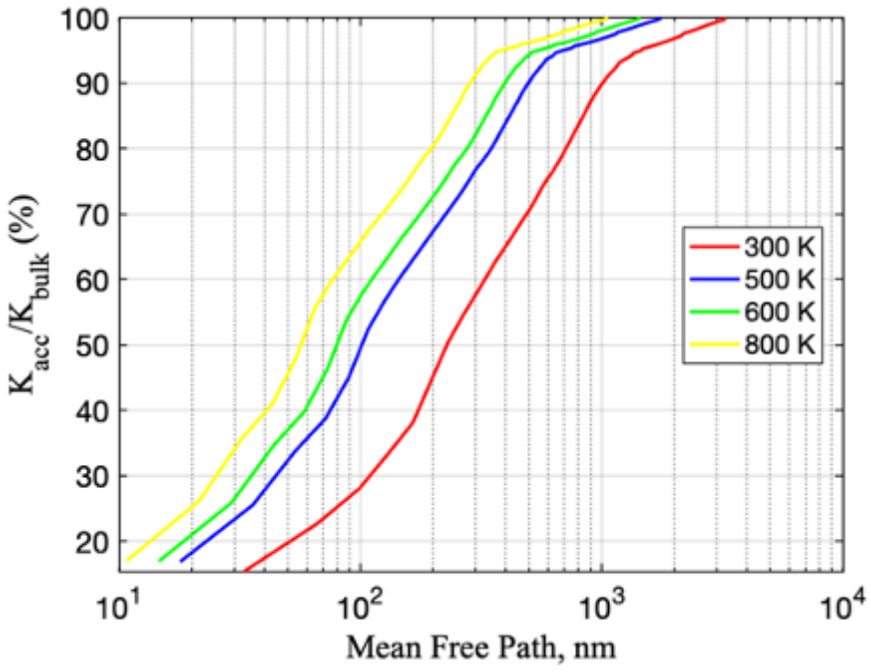

Figure 3.14. Accumulation spectra of $Al_{0.75}Ga_{0.25}N$ at T = 300 K, 500 K, 600 K, and 800 K.

The investigation into the bulk thermal conductivity of ($Al_{0.75}Ga_{0.25}N$) has yielded a comprehensive set of findings across a range of temperatures. Specifically, the values obtained are as follows: 111.7 W/m.K at 300 K, 64.74 W/m.K at 500 K, 54 W/m.K at 600 K, and 40.7 W/m.K at 800 K. These results reflect the material's thermal conductive behavior at varying temperatures, shedding light on its thermal transport properties in diverse thermal environments.

Comparing these findings to existing literature, it's noteworthy that A. Jain et al. [80] reported a bulk thermal conductivity of 77.7 W/m.K for cubic ($Al_{0.75}Ga_{0.25}N$) specifically at 300 K. This aligns closely with the observed value of 111.7 W/m.K at 300 K, indicating a consistent trend in thermal conductivity within this temperature regime. Moreover, in a different study by Liu and Balandin [68], a thermal conductivity of 60 W/m.K at 300 K was reported for ($Al_{0.23}Ga_{0.77}N$) in the cross-sectional direction, further supporting the agreement between the observed value and the existing literature. In summary, the observed thermal conductivity of 111.7 W/m.K at 300 K appears to be well-aligned with prior research, strengthening the understanding of the thermal transport characteristics of this material.Similar to $Al_{0.75}Ga_{0.25}N$, no specific theoretical and experimental studies focus on the accumulation spectra for this particular composition of Al in $Al_xGa_{1-x}N$ alloys.

Table 3.3. Mean free path of phonons contributing to 30%, 50%, and 90% of $Al_{0.75}Ga_{0.25}N$ thermal conductivity (k) at T = 300 K, 500 K, 600 K, and 800 K.

Temperature (Kelvin)	30% of k	50% of k	90% of k	Total (100%) of k
300	>120.8 nm	>231 nm	>1023.01 nm	<3135.04 nm
500	>44.3 nm	>107.6 nm	>483.7 nm	<3237.6 nm
600	>37.3 nm	>87.5 nm	>380.5 nm	<2682.2 nm
800	>29.4 nm	>60.3 nm	>279.4 nm	<1818.12 nm

3.1.4. Comparison

In Figure 3.15, obtained thermal conductivities of $Al_xGa_{1-x}N$ alloys with (x=0.25, x=0.5, x=0.75) at room temperature through simulations are depicted along with the corresponding experimental and theoretical data obtained from previous literature. By using the method explained earlier, this study found the bulk thermal conductivities at room temperature for $Al_{0.25}Ga_{0.75}N$, $Al_{0.5}Ga_{0.5}N$, and $Al_{0.75}Ga_{0.25}N$ to be 88.46 W/m.K, 81.09 W/m.K, and 111.7 W/m.K, respectively.

Figure 3.15 illustrates the thermal conductivity data obtained from the Callaway model [39] and ab-initio model [69] in the literature for $Al_xGa_{1-x}N$ alloys. The data demonstrates a significant decrease in thermal conductivity with increasing x.Notably, the thermal conductivity experiences a rapid increase for Al fractions above 0.9. Consequently, even minor alloying proportions lead to a reduction in the thermal conductivity of the alloys. Specifically, the bulk thermal conductivity of $Al_{0.5}Ga_{0.5}N$ is reduced by 64% compared to GaN [35].

According to Figure 3.15 a high level of agreement between our results and the theoretically determined room temperature thermal conductivities of $Al_xGa_{1-x}N$ by A. Jain et al. [80], and Huimin Wang et al. [81] is observed. Furthermore, the published experimental data for thermal conductivity measurements of $Al_xGa_{1-x}N$ by Liu & Balandin at T=300 K aligns well with the findings of our study [68].

While the calculated thermal conductivities in this study are lower than those of the pure materials, they are significantly higher than the data reported in previous literature. The significant discrepancy between the results of this study and the work by Jinglong Ma et al. [69] arises from the different approaches used to model the disordered lattice. In virtual crystal models, disordered lattices are replaced with ordered crystals that contain randomly distributed atoms of the constituents. According to this model, alloys consist of atoms arranged in a specific lattice, each with varying masses. The significant atomic mass differences between ions in these alloys lead to strong mass

disorder, substantially reducing thermal conductivity. In contrast, the present study employs an ordered and systematic arrangement of atoms, representing an ideal single crystalline structure.

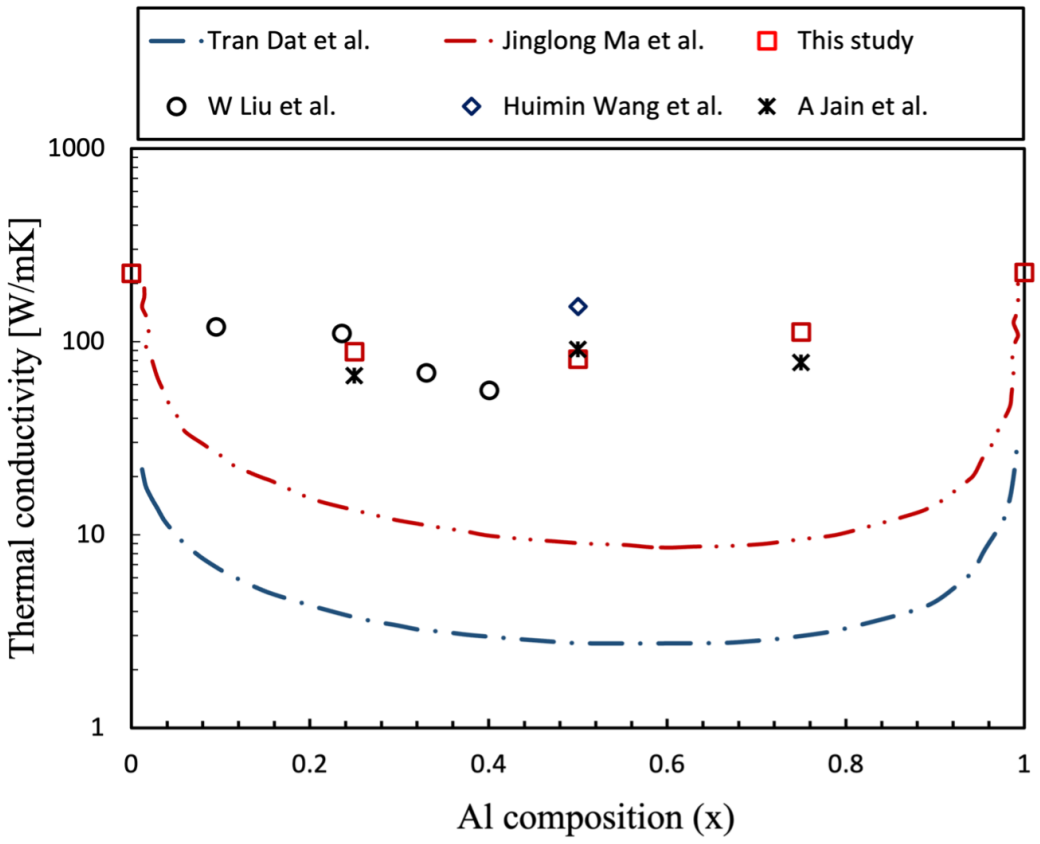

Figure 3.15. Thermal conductivities of $Al_xGa_{1-x}N$ alloy at room temperature as a function of *Al* composition. Theoretical data are from the virtual-crystal and first-principle model are shown [39, 69, 80, 81]. Experimental data from 3ω measurements is shown by the circle symbol [68].

Calculated thermal conductivity for various *Al* mass fractions (x=0.0, 0.1, 0.5, 0.9, and 1.0) in $Al_xGa_{1-x}N$ alloys is depicted in Figure 3.16. The figure illustrates a significant reduction in thermal conductivity at room temperature due to alloy scattering, encompassing a wide temperature range from approximately 10 K to 900 K, with a slight increase below 10 K. Beyond 200 K, thermal conductivity becomes more sensitive to changes in the *Al* fraction, marked by the dominance of point-defect and phonon-phonon scatterings in phonon relaxation processes. Furthermore, the most no-

table decrease in thermal conductivity occurs when there is a transition in the Al mass fraction from 0 to 0.25. This suggests that even a small amount of external atoms in the host material profoundly affect phonon scattering. Further additions of extrinsic atoms do not yield a substantial difference in the reduction of thermal conductivity.

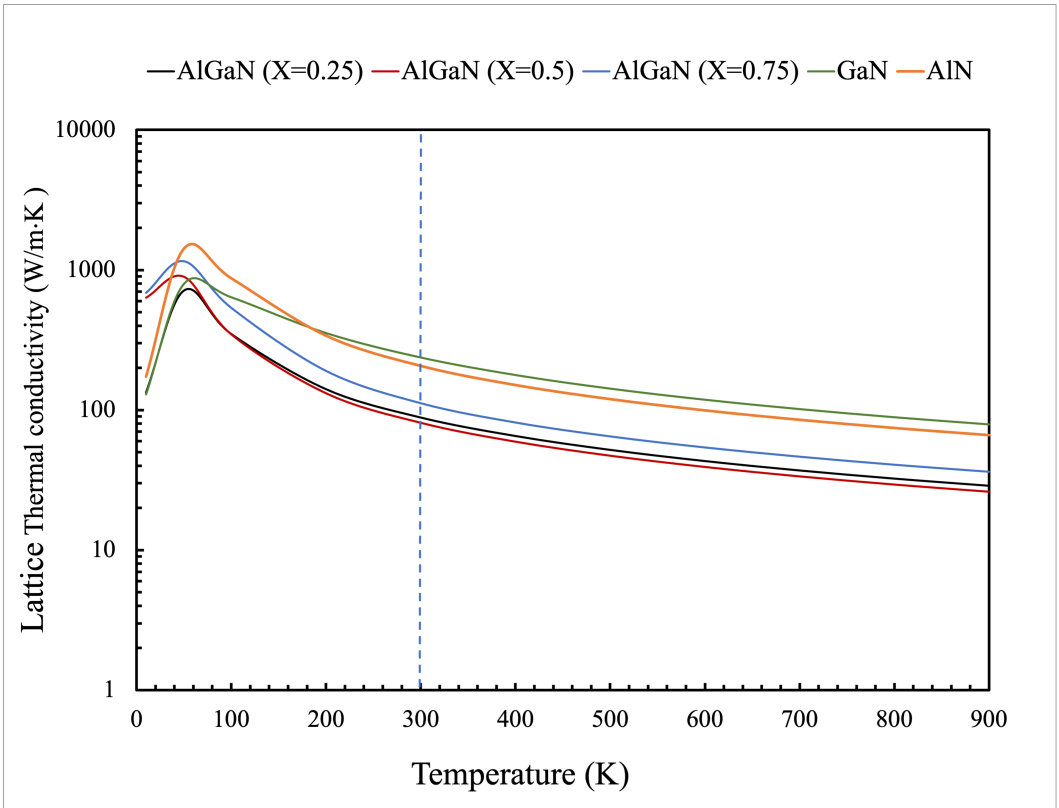

Figure 3.16. The calculated thermal conductivities of $Al_xGa_{1-x}N$ alloys with x=0.0,0.25,0.5,0.75, and 1.0 as a function of temperature.

In Figure 3.17, the cumulative thermal conductivity of $Al_xGa_{1-x}N$ alloys (x=0.25, x=0.5, x=0.75) at T=300K is plotted as a function of the phonon mean free path (MFP). These results are compared with the theoretical accumulation spectra obtained for *AlN* and *GaN* data available in the literature.The figure includes a 50% guideline, revealing the phonon mean free path (MFP) contributing to at least 50% of bulk thermal conductivity. It can be observed that 50% of the bulk thermal conductivity of the materials corresponds to phonons with MFPs of 138.4 nm, 208 nm, 231 nm, 360 nm, and 262 nm at 300K for $Al_{0.25}Ga_{0.75}N$, $Al_{0.5}Ga_{0.5}N$, $Al_{0.75}Ga_{0.25}N$, AlN, and GaN, respectively.

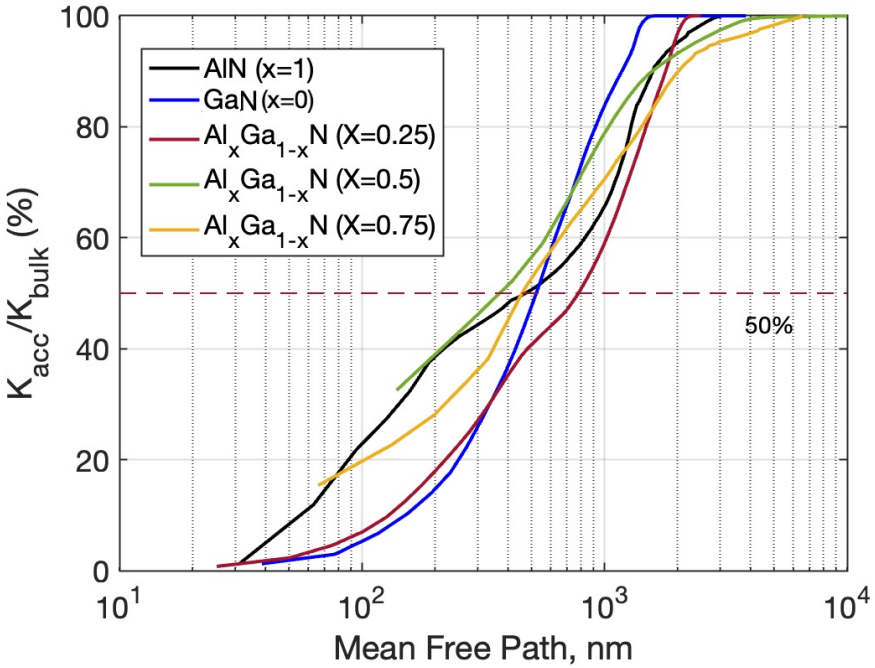

Figure 3.17. Accumulation spectrum of $Al_{0.5}Ga_{0.5}N$, $Al_{0.25}Ga_{0.75}N$, $Al_{0.75}Ga_{0.52}N$, AlN, and GaN [35].

The increased complexity of the crystal structure leads to a shorter mean free path (MFP) spectrum. In the case of *AlN* and *GaN*, which have ordered and symmetrical structures, thermal conductive phonons with MFPs larger than Λ_{max} at 300 K exhibit predominantly harmonic behavior. However, the presence of impurities, such as *AlN* atoms in $Al_xGa_{1-x}N$ disrupts phonon propagation in the lattice, resulting in a shorter MFP spectrum. Compared to the experimental and theoretical values for silicon at room temperature, the MFP values obtained for $Al_xGa_{1-x}N$ alloys are much smaller. This suggests that size effects play a significant role in the thermal transport properties of these alloys. Also, according to the figure, the accumulation spectrum of alloys is lower than that of pure systems, particularly for large MFPs.

Theoretical and experimental studies have indicated the presence of size effects in the range of tens of microns or smaller. Figure 3.17 shows that the thermally conductive *GaN* phonons predominantly have mean free paths (MFPs) ranging from 10 nm to 10000 nm, contributing to 90% of the material's thermal conductivity. In alloys, the

contribution from large MFPs is increased compared to the constituent compounds due to the stronger influence of the alloying effect on high-frequency phonons with small MFPs rather than low-frequency phonons with large MFPs.

3.2. β-form Ga_2O_3

The crystal structure of β-Ga_2O_3 is characterized by a monoclinic lattice with the space group (C2/m) and has a conventional unit cell with 20 atoms. Gallium atoms in the crystal are coordinated by 6 oxygen atoms, forming a distorted octahedral geometry, while oxygen atoms are coordinated by 4 gallium atoms, forming a tetrahedral geometry. This coordination pattern affects its electrical, and mechanical properties.

Although attempts have been made to clarify the process of transferring the conventional monoclinic unit cell to a reduced primitive cell [82], there remains some ambiguity. To mitigate the potential risk of variations in the Brillouin zone shape, researchers have opted to use the 20-atom conventional unit cell (depicted in Figure 3.18(a)) rather than the 10-atom primitive unit cell (depicted in Figure 3.18(b)) [77, 82, 83]. This choice allows for directly measuring the anisotropic thermal conductivity along the three crystallographic directions. The visualization of the conventional and primitive unit cell structures is performed in this study using VESTA software, as depicted in Figure 3.18.

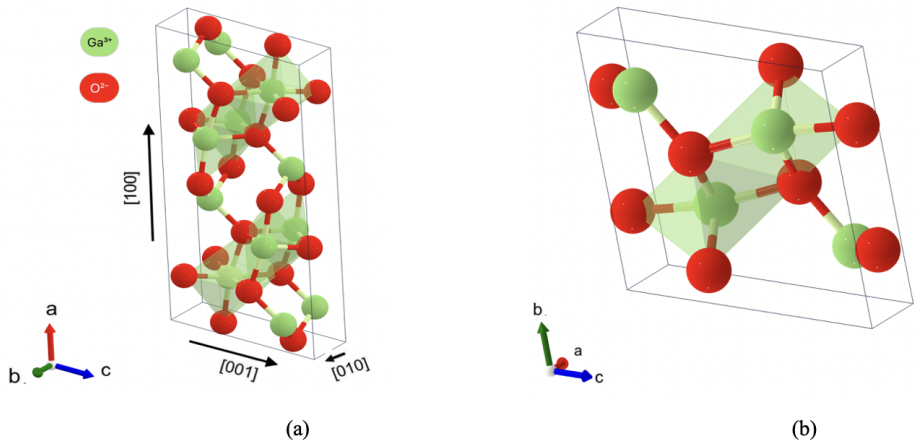

Figure 3.18. (a) Conventional unit cell of β-Ga_2O_3 (b) Primitive unit cell of β-Ga_2O_3.

The approach presented by Wahyu and Stefano et al. [77] is used to establish the Brillouin zone (BZ) and the corresponding high symmetry directions in this study. For monoclinic structure β-Ga_2O_3, the corresponding C-centered monoclinic (MCLC1, mS)-type Brillouin zone and high symmetry k-point paths are selected in this study. For the C2/m symmetry structure, the coordinates of symmetry points and the high symmetry paths in the first Brillouin zone are Γ-Y-F-L- I|I1-Z-F1|Y-X1|X-Γ-N|M-Γ as illustrated in Figure 3.19.

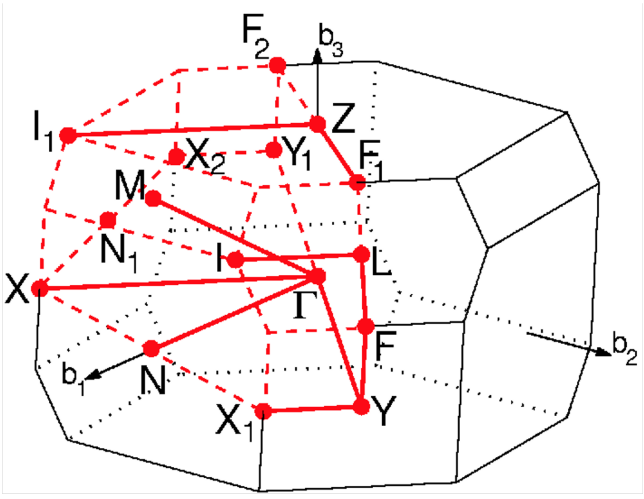

Figure 3.19. Brillouin zone of $MCLC_1$ lattice [77].

The Vienna ab initio simulation package (VASP) was employed to carry out first-principles calculations based on density functional theory (DFT) principles. The Perdew-Burke-Ernzerhof (PBE) exchange-correlation functional is employed. Before implementing the plane wave self-consistent field calculation, a structural optimization procedure is conducted using the projector-augmented wave (PAW) method along with a generalized gradient approximation (GGA). To obtain full optimization of the cell parameters for the bulk β-Ga_2O_3 with a monoclinic structure the system was relaxed using a 4×16×8 Monkhorst-Pack type k-point. The energy cutoff for the plane wave basis was set to a constant value of 520 eV, and the convergence criterion for the system energy is set to 10^{-8} eV. The optimized lattice dimensions are a = 12.50 Å, b = 3.1 Å, c = 5.74 Å and an angle of $\beta = 103.76°$, which agrees well with the computational results [71].

After optimizing the lattice parameters, a 2×2×2 supercell consisting of 160 atoms was constructed to calculate the interatomic force constants (IFCs). The harmonic IFCs were obtained by performing self-consistent calculations for 20 different displacements. Figure 3.20 displays the phonon dispersion results, and projected density of states of β-Ga_2O_3, which were obtained using Phonopy software. The phonon branches are plotted across the Brillouin zone with a 2×2×2 K-mesh described in Figure 3.20. This comprehensive representation allows us to gain valuable insights into the phonon behavior and vibrational properties of β-Ga_2O_3, shedding light on its structural and thermal characteristics.

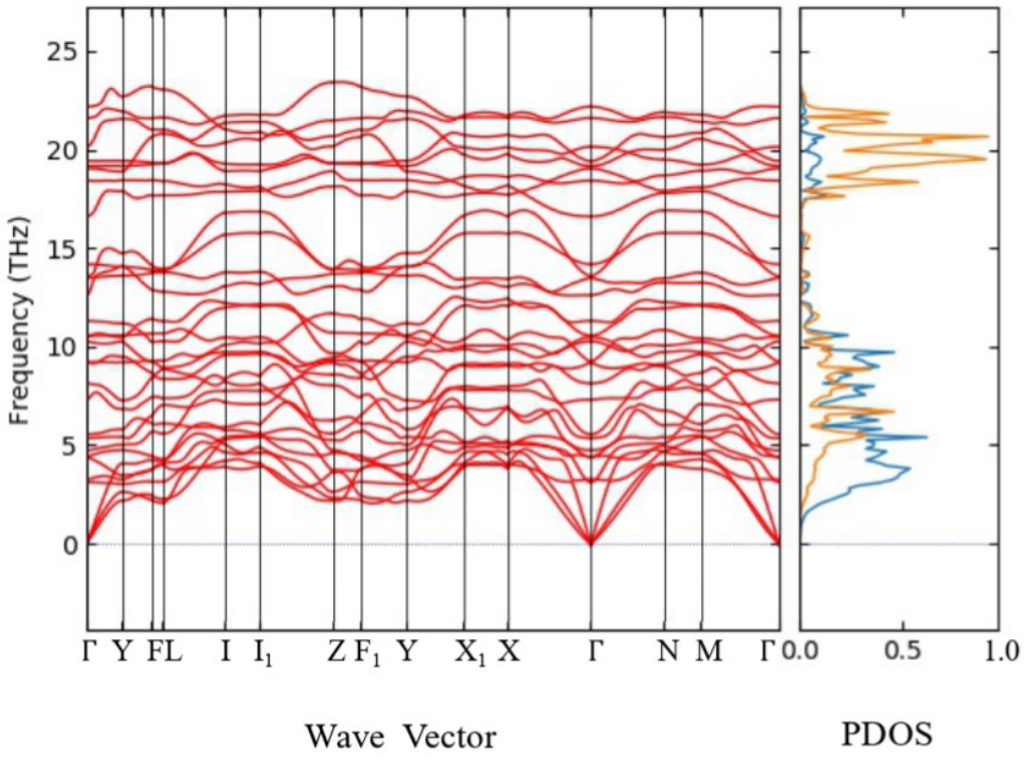

Figure 3.20. Phonon dispersion curve of β-Ga_2O_3. Orange curve corresponds to Ga atoms, while blue curve corresponds to O atoms in the projected densities of states.

The phonon frequency of β-Ga_2O_3 lies between 0 and 21 THz, as shown in Figure 3.20. The ionic crystal structure of β-Ga_2O_3 is characterized by the division of LO-TO phonons at the Γ points is also noticeable. The projected densities of states shown in Figure 3.20 reveal that lower frequency phonon modes are primarily associated with the

heavier *Ga* atoms. In comparison, higher frequency modes are predominantly linked to the lighter O atoms. The bandgap of the bulk β-Ga_2O_3 was found to be 4.8 THz, consistent with the findings of Carrete, J et al. [44].

After obtaining the dispersion curve, thermal calculations were performed. To calculate the anharmonic interatomic force constants (IFCs), a 2×2×1 supercell containing 80 atoms was used. To expedite the calculations, a cut-off distance of 2 Å was implemented in the system.

In the last step, the linearized version of the BTE is solved iteratively [44]. This approach involves solving the linearized BTE in a self-consistent manner to obtain the variation of the distribution function from equilibrium, which is caused by the perturbation of the phonon distribution. A real-space displacement approach is utilized to obtain both second- and third-order force constants. Once the second-and third-order force constants (FCs) were obtained through VASP, these force constants were transferred to Phono3py software for conducting thermal calculations through 5×17×9 mesh, where the relaxation time approximation method was utilized. This method assumes that a quasi-equilibrium distribution can describe the energy of phonons as they quickly return to a state of local equilibrium after scattering.

To maintain consistency while projecting the tensor onto the crystallographic directions of the conventional cell, the k tensor was symmetrized [84] using the point group symmetry which is as follows:

$$\kappa_{ij} = \begin{pmatrix} \kappa_{\mathcal{X}\mathcal{X}} & 0 & \kappa_{\mathcal{X}\mathcal{Z}} \\ 0 & \kappa_{\mathcal{Y}\mathcal{Y}} & 0 \\ \kappa_{\mathcal{X}\mathcal{Z}} & 0 & \kappa_{\mathcal{Z}\mathcal{Z}} \end{pmatrix}. \tag{3.1}$$

In order to obtain a steady numerical solution, various sample meshes were tested with different densities ranging from 10×10×10 to 24×24×24. A consistent convergence was achieved for all test meshes. However, as the mesh size increased, the memory

and calculation time required also increased tremendously. Finally, after considering a better convergence and computational time, the mesh density of 5×17×9 was chosen for the following lattice thermal conductivity calculation over temperatures ranging from 25 K to 1050 K. The obtained lattice thermal conductivities of β-Ga_2O_3 with different temperatures are shown in Figure 3.21.

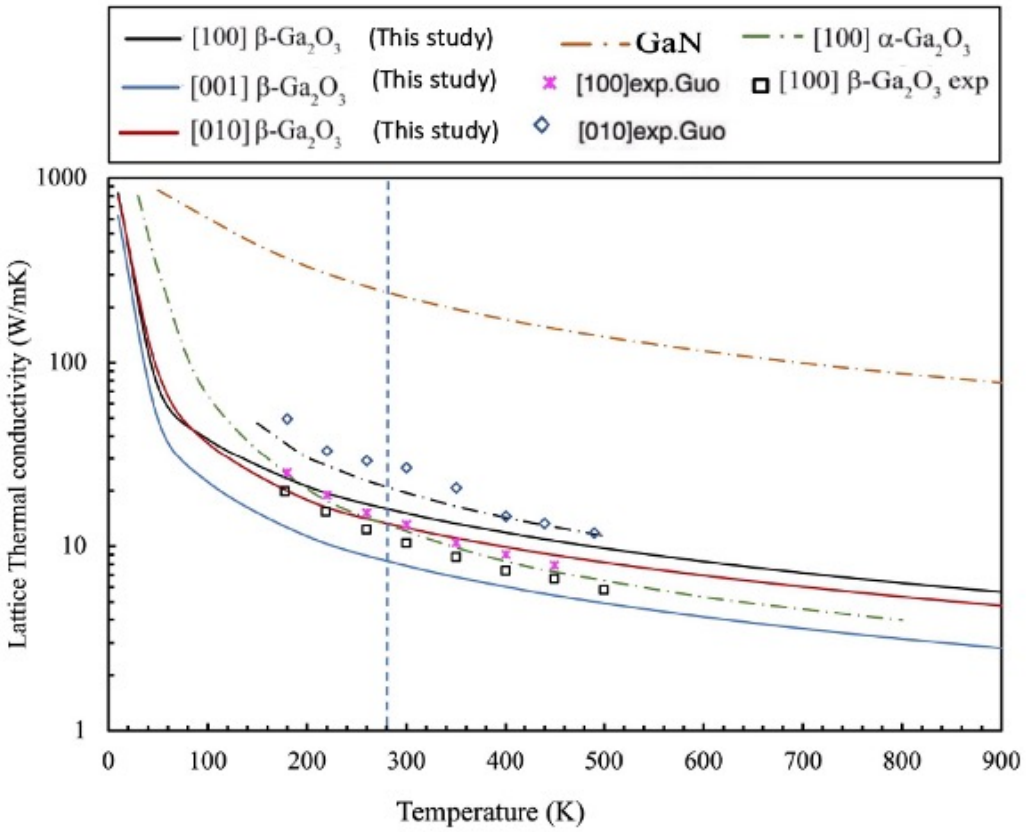

Figure 3.21. Temperature-dependency thermal conductivity of bulk β-Ga_2O_3 (this study), α-Ga_2O_3 [85], *GaN* [35], and β-Ga_2O_3 [56].

The thermal conductivity of β-Ga_2O_3 exhibits significant anisotropy along the three directions of the basis vectors of the conventional unit cell, as revealed by the results presented in Figure 3.21. The highest thermal conductivity is observed along the [100] direction with a value of 15.11 W/m.K at room temperature. In contrast, the lowest is observed along the [001] direction with a value of 7.8 W/m.K, and along the [010], the value of thermal conductivity is obtained: 12.6 W/m.K. This anisotropic behavior can be attributed to the differences in the phonon dispersion relations and

the density of states along the different directions in the crystal lattice. Also, mass and bonding strength differences between the Ga and O atoms can explain the lower thermal conductivity observed in this phase.

Bulk thermal conductivity at 300 K for the monoclinic β-Ga_2O_3 is reported experimentally as 11.9 W/m.K by Zhi Guo et al. [56], 13 $\pm$ 1 W/m.K by MHandwerg et al. [86], in [100] direction. Also, theoretical studies reported the bulk thermal conductivity of β-Ga_2O_3 along [100] 12.73 W/m.K by A. Zhequan Yan et al. [71], and in [010] direction between 20-27 W/m.K at the same temperature. As shown in Figure 3.21, the degree of anisotropy in the [100] and [001] directions of β-Ga_2O_3 indicates good agreement between our results and those obtained through previous theoretical studies and experimental data.

Comparing the thermal conductivity of β-Ga_2O_3 to that of *GaN*, which is a commonly used semiconductor in power electronic applications, is an interesting point of discussion. At room temperature, *GaN* has a thermal conductivity between 130-380 W/m.K [87, 88]; These values are significantly higher than the thermal conductivity range of β-Ga_2O_3, which falls between 10-30 W/m.K, as illustrated in Figure 3.21. It can be seen in Figure 3.21 that the thermal conductivity of β-Ga_2O_3 is higher than that of α-phase Ga_2O_3 along the [100] direction over a wide temperature range, spanning from 30 K to 800 K.

As shown in Figure 3.20, the lattice thermal conductivity of β-Ga_2O_3 exhibits a decreasing trend with increasing temperature in a wide range from 10 to 900 K. In the high-temperature region, the lattice thermal conductivity of β-Ga_2O_3 follows a T^{-1} law [89], which suggests the occurrence of the Umklapp phonon scattering process. These observations are consistent with previous studies on β-Ga_2O_3, demonstrating that the Umklapp process dominates the phonon scattering mechanism at high temperatures. The reliability of our findings is supported by the convergence of our numerical calculations on different sample meshes, as well as the agreement between our results and previous experimental and theoretical studies.

Figure 3.22 displays the accumulation spectra of β-Ga_2O_3 in [100] direction at 300 K, 500 K, 600K, and 800 K. What's strikingly evident is the progressive shortening of the mean free path (MFP) spectrum with increasing temperature, primarily due to greater phonon scattering. At 300 K, the phonon mean free path for β-Ga_2O_3 ranges from 10 to 1000 nm. At [100] direction, phonons with mean free paths (MFPs) smaller than 26.5 nm contribute to half of the conductivity at 300 K, and the MFP of thermally conductive phonons extends to 184 nm at this temperature and the same direction. Table 3.22 shows some critical MFP values and their corresponding contributions, offering valuable insights into the intricate behavior of phonons in β-Ga_2O_3 at different temperatures and directions.

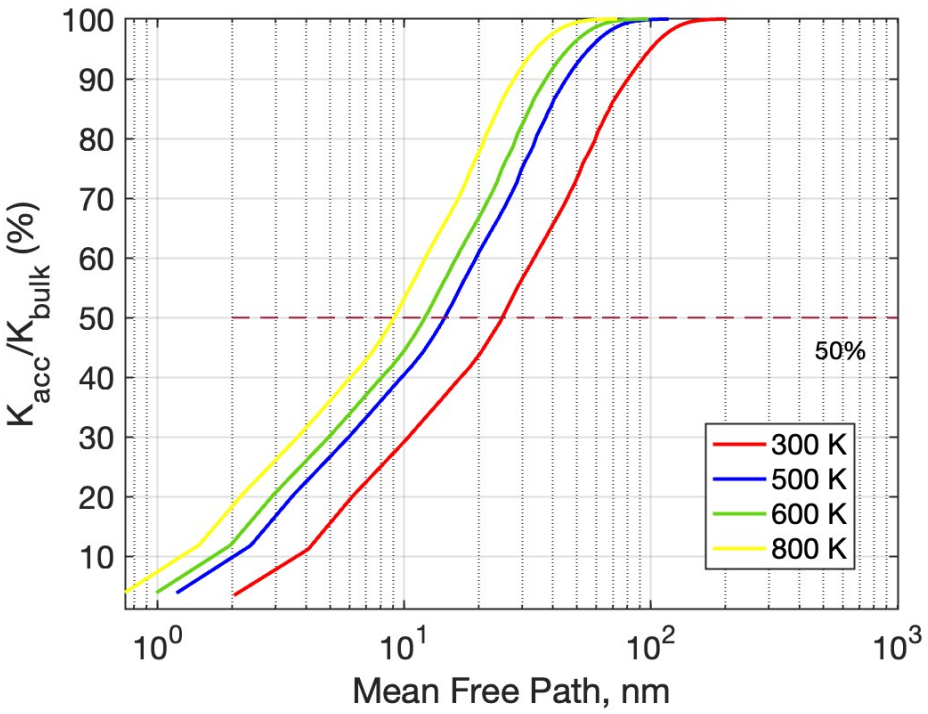

Figure 3.22. Accumulation spectra of β-Ga_2O_3 at T = 300 K, 500 K, 600 K, and 800 K.

Figure 3.23 displays the obtained accumulation spectra for β-Ga_2O_3 in [100] and [010] directions and a comparison with the accumulation spectra for GaN and α-Ga_2O_3 from the literature [35, 85]. It is evident that the phonon mean free path of β-Ga_2O_3 in both directions is slightly longer than that of α-Ga_2O_3, resulting in a higher ther-

mal conductivity for β-Ga_2O_3. Compared to GaN, β-Ga_2O_3 exhibits a shorter spectrum.The simpler and more ordered lattice structure of GaN minimizes the obstruction of phonons within the lattice, making it less likely to impede their movement so at larger scales, this material is anticipated to exhibit size effects.Therefore, these findings highlight the potentials of β-Ga_2O_3 for applications with a desired lower thermal conductivity.

Table 3.4. Mean free path of phonons contributing to 30%, 50%, and 90% of β-Ga_2O_3 thermal conductivity (k)at T = 300 K, 500 K, 600 K, and 800 K.

Temperature (Kelvin)	30% of k	50% of k	90% of k	Total (100%) of k
300	>10.2 nm	>26.5 nm	>79.5 nm	<184 nm
500	>5.9 nm	>15.47 nm	>44.04 nm	<113 nm
600	>4.9 nm	>12.82 nm	>37.5 nm	<87.83 nm
800	>3.68 nm	>9.5 nm	>27.23 nm	<54.47 nm

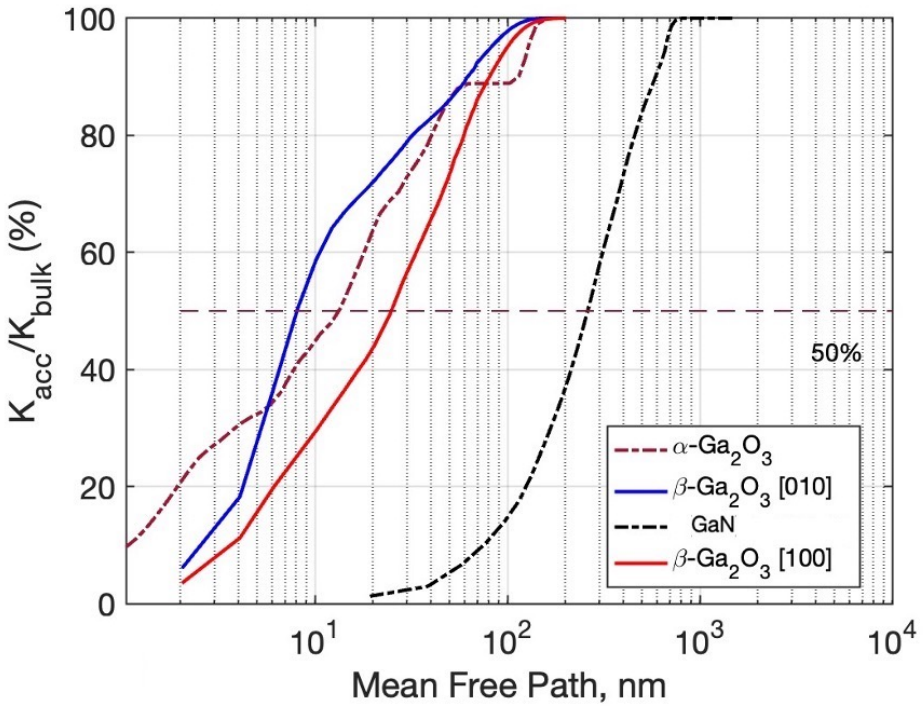

Figure 3.23. Accumulation spectra of β-Ga_2O_3 in [100] and [010] directions compared to the α-Ga_2O_3 [85], and *GaN* [35] at 300 K.

4. CONCLUSIONS AND IMPLICATIONS FOR FUTURE RESEARCH

The issue of self-heating presents a serious challenge for the ongoing development of high-power, high-frequency transistors and optoelectronic devices. Due to the superior Baliga's figure of merit surpassing that of GaN or SiC, β-Ga_2O_3, and $Al_xGa_{1-x}N$, semiconductors have emerged as highly promising materials for the next generation of high-power electronic devices. It is crucial to comprehend the thermal properties of these materials in order to enhance device performance. The phonon mean free path (MFP) is a key thermal property that plays a vital role in determining the boundaries of ballistic-diffusive thermal transport in micro and nanoscale domains. This study focuses on investigating the thermal properties of β-Ga_2O_3, and $Al_xGa_{1-x}N$ semiconductors, with a specific emphasis on understanding the phonon MFP - thermal conductivity relation for β-Ga_2O_3, and $Al_xGa_{1-x}N$ altering with the lattice temperature and the Al concentration, x. Chapter 2 introduces the methodology employed for the Ab-initio calculations in this study and the essential equations required for conducting these simulations.

The primary aim of establishing the relationship between accumulated thermal conductivity and mean free path (MFP) is to forecast the thermal characteristics of materials at small scales, such as thin films and localized hotspots. This investigation was conducted using the Vienna Ab-initio Simulation Package (VASP) with the local density approximation (LDA) and projector augmented wave (PAW) pseudopotentials. These findings were presented through tables indicating the critical MFP-thermal conductivity contributions. The results revealed that materials with simpler structures exhibit longer MFP spectra than those with asymmetric crystallographic properties.

Chapter 3 presents a detailed examination of the phonon mean free path (MFP) distribution in β-Ga_2O_3 and $Al_xGa_{1-x}N$ alloys. This analysis offers valuable insights into the thermal characteristics of these materials. A comprehensive view of the MFP

distribution is provided through the utilization of the normalized cumulative thermal conductivity" for all the materials.The calculation results demonstrate that the size effect remains significant for distances spanning several tens of micrometers. This size effect is directly linked to the distribution of mean free paths (MFPs), which is effectively represented in the normalized cumulative spectra plot [44, 90, 91].The dominant factor contributing to the reduction in thermal conductivity in alloys is anharmonic scattering for low-frequency phonon modes characterized by large mean free paths (MFPs). This reduction primarily occurs in high-frequency modes with small MFPs. Consequently, the normalized cumulative thermal conductivity of alloys is lower than that of pure systems, particularly for large MFPs. However, alloys possess a higher number of phonon modes with MFPs smaller than a specific short MFP, leading to a larger fraction of heat being carried by modes with shorter MFPs. As a result, the curves representing thermal conductivity for pure phases and alloys are anticipated to intersect at intermediate MFPs. As it can be seen in cumulative spectra plot the normalized cumulative curve of $Al_xGa_{1-x}N$ alloys intersects with that of GaN and AlN at intermediate mean free paths (MFPs).

In general, larger thermal conductivity is attributed to weaker intrinsic phonon-phonon scattering, resulting in phonons possessing larger mean free paths (MFPs). However, these longer MFPs can be more prone to being impeded by boundaries of similar dimensions. Consequently, when the intrinsic thermal conductivity is already low, further reduction becomes more challenging in nanostructures. By carefully manipulating boundary conditions, material composition, and nanostructure geometry, it is possible to enhance or suppress thermal conductivity as desired, offering opportunities for improved thermal management in nanoscale devices and systems.

Using first-principles calculations and an iterative solution of the phonon Boltzmann transport equation, we conducted an in-depth investigation into the lattice thermal conductivity of both β-Ga_2O_3 and $Al_xGa_{1-x}N$ materials. The thermal conductivity shows a decreasing trend with rising temperature as thermal scattering effects become more pronounced. Additionally, an increase in the Al mole fraction reduces

thermal conductivity for $Al_xGa_{1-x}N$ compositions with $x < 0.5$. Also, thermal conductivity exhibits a notable and rapid increase for *Al* fractions exceeding 0.9. As a result, even minor proportions of alloying elements contribute to a decrease in the thermal conductivity of the alloys. The presence of disorder within the lattice leads to an increase in phonon scattering, thereby causing a reduction in thermal conductivity *(k)*. When *Ga* is added to *AlN*, it induces a more significant reduction in thermal conductivity compared to a proportional addition of *Al* into *GaN*. This asymmetry in the reduction of thermal conductivity is attributed to the difference in atomic mass between *Ga* and *Al*. Since *Ga* is heavier than *Al* it results in a more substantial and pronounced decrease in thermal conductivity *(k)*.

In the case of β-Ga_2O_3, the thermal conductivity displays notable anisotropy in three crystallographic directions, we report room temperature values of thermal conductivity; 15.11 W/m.K, 12.6 W/m.K, 7.8 W/m.K in the direction of [100], [010], and [001] also, it is conducted that at higher temperatures, the thermal conductivity of the β-Ga_2O_3 crystal displays a distinct relationship with temperature, characterized by an approximate inverse proportionality (T^{-1}). This behavior is consistent with Umklapp phonon scattering, indicating that phonons are the primary contributors to heat transport in the crystal.

To address the challenge of heat dissipation caused by the low thermal conductivity of β-Ga_2O_3 materials, a potential solution is to directly deposit β-Ga_2O_3 on to a substrate with high thermal conductivity. One suitable option is to use diamond, which is a wide-bandgap semiconductor material known for its excellent thermal conductivity. By depositing β-Ga_2O_3 on the diamond, it is possible to enhance the overall thermal management of the system and improve heat dissipation capabilities. As a result, the interaction between phonons at the interface, whether through reflection or transmission, significantly influences the thermal transport process and is directly associated with the phonon mean free path. At higher temperatures, the maximum mean free path of phonons in β-Ga_2O_3 material falls within the range of 1-1000 nm. This suggests that the effects of interface boundary scattering are likely to influence the

thermal transport process. Consequently, when considering the utilization of β-Ga_2O_3 materials in future power device applications, it is crucial to thoroughly assess the effects of size and interface scattering.

Finally, discrepancies were analyzed, and it was observed that experimental values estimate higher MFP spectra than theoretical approaches. This has one of its roots in experimental values relying on approximations and entailing certain statistical deviations. Moreover, experimental samples have imperfections that cause discrepancies to model structure. As the anharmonicity increases due to crystal complexity, increased phonon confinement in extremely small shapes and high temperature, covering third-order force constants seems beneficial. This extensive coverage of crystal energy may also be used for explaining the thermal responses of structures with dislocations and impurities in the future. Finally, it was reached that as the anharmonicity increases, MFP spectra are shortened to both theoretical approaches and the experiments. While considering third-order force constants represents a risk of overestimating the anharmonicity, these models offer great opportunities: It becomes possible to model the materials with complex structures (for instance, $AlGaN$ and β-Ga_2O_3) and the road to predict the thermal behavior of materials at challenging conditions(extreme confinement, high temperature) is paved.

REFERENCES

1. Ding, X., Y. Zhou and J. Cheng, "A Review of Gallium Nitride Power Device and Its Applications in Motor Drive", *CES Transactions on Electrical Machines and Systems*, Vol. 3, No. 1, pp. 54–64, 2019.

2. Tian, J., C. Lai, G. Feng, D. Banerjee, W. Li and N. C. Kar, "Review of Recent Progresses on Gallium Nitride Transistor in Power Conversion Application", *International Journal of Sustainable Energy*, Vol. 39, No. 1, pp. 88–100, 2020.

3. Tsao, J., S. Chowdhury, M. Hollis, D. Jena, N. Johnson, K. Jones, R. Kaplar, S. Rajan, C. Van de Walle, E. Bellotti *et al.*, "Ultrawide-Bandgap Semiconductors: Research Opportunities and Challenges", *Advanced Electronic Materials*, Vol. 4, No. 1, p. 1600501, 2018.

4. Chu, B. H., B. S. Kang, S. C. Hung, K. H. Chen, F. Ren, A. Sciullo, B. P. Gila and S. J. Pearton, "Aluminum Gallium Nitride (GaN)/GaN High Electron Mobility Transistor-based Sensors for Glucose Detection in Exhaled Breath Condensate", *Journal of Diabetes Science and Technology*, Vol. 4, No. 1, pp. 171–179, 2010.

5. Khan, A., K. Balakrishnan and T. Katona, "Ultraviolet Light-emitting Diodes Based on Group Three Nitrides", *Nature Photonics*, Vol. 2, No. 2, pp. 77–84, 2008.

6. Wong, M. H., O. Bierwagen, R. J. Kaplar and H. Umezawa, "Ultrawide-Bandgap Semiconductors: An Overview", *Journal of Materials Research*, Vol. 36, No. 23, pp. 4601–4615, 2021.

7. Scott, M. J., L. Fu, X. Zhang, J. Li, C. Yao, M. Sievers and J. Wang, "Merits of Gallium Nitride based Power Conversion", *Semiconductor Science and Technology*, Vol. 28, No. 7, p. 074013, 2013.

8. Baldini, M., Z. Galazka and G. Wagner, "Recent Progress in the Growth of β-Ga_2O_3 for Power Electronics Applications", *Materials Science in Semiconductor Processing*, Vol. 78, pp. 132–146, 2018.

9. Stutzmann, M., O. Ambacher, H. Angerer, C. Nebel and E. Rohrer, "Electrical and Structural Properties of AlGaN: A Comparison with CVD Diamond", *Diamond and Related Materials*, Vol. 7, No. 2-5, pp. 123–128, 1998.

10. Jing, H. X., C. A. C. Abdullah, M. Z. M. Yusoff, A. Mahyuddin and Z. Hassan, "Structural and Optical Properties of AlN/GaN and AlN/AlGaN/GaN Thin Films on Silicon Substrate Prepared by Plasma Assisted Molecular Beam Epitaxy (MBE)", *Results in Physics*, Vol. 12, pp. 1177–1181, 2019.

11. Saxler, A., W. Mitchel, P. Kung and M. Razeghi, "Aluminum Gallium Nitride Short-Period SuperLattices Doped with Magnesium", *Applied Physics Letters*, Vol. 74, No. 14, pp. 2023–2025, 1999.

12. Donmezer, F., *Multiscale Electro-Thermal Modeling of AlGaN/GaN Heterostructure Field Effect Transistors*, Ph.D. Thesis, Georgia Institute of Technology, 2013.

13. Mishra, U. K., P. Parikh and Y.-F. Wu, "AlGaN/GaN HEMTs-an Overview of Device Operation and Applications", *Proceedings of the IEEE*, Vol. 90, No. 6, pp. 1022–1031, 2002.

14. Das, S., A. Panda and G. Dash, "Characterization of Electrical Properties of AlGaN/GaN Interface Using Coupled Schrödinger and Poisson Equation", *Journal of Semiconductors*, Vol. 33, No. 11, p. 113001, 2012.

15. Krishna, A., A. Raj, N. Hatui, O. Koksaldi, R. Jang, S. Keller and U. K. Mishra, "AlGaN/GaN Superlattice-Based P-Type Field-Effect Transistor with Tetramethylammonium Hydroxide Treatment", *Physica Status Solidi (a)*, Vol. 217, No. 7, p. 1900692, 2020.

16. Syaranamual, G. J., W. A. Sasangka, R. I. Made, S. Arulkumaran, G. I. Ng, S. C. Foo, C. L. Gan and C. V. Thompson, "Role of Two-Dimensional Electron Gas (2DEG) in AlGaN/GaN high Electron Mobility Transistor (HEMT) ON-state Degradation", *Microelectronics Reliability*, Vol. 64, pp. 589–593, 2016.

17. Zhang, J., Y. Gao, L. Zhou, Y.-U. Gil and K.-M. Kim, "Transparent Deep Ultraviolet Light-emitting Diodes with a p-type AlN Ohmic Contact Layer", *Light-Emitting Devices, Materials, and Applications*, Vol. 10940, p. 1094002, SPIE, 2019.

18. Shatalov, M., W. Sun, R. Jain, A. Lunev, X. Hu, A. Dobrinsky, Y. Bilenko, J. Yang, G. A. Garrett, L. E. Rodak *et al.*, "High Power AlGaN Ultraviolet Light Emitters", *Semiconductor Science and Technology*, Vol. 29, No. 8, p. 084007, 2014.

19. Tran, B. T. and H. Hirayama, "Growth and Fabrication of High External Quantum Efficiency AlGaN-based Deep Ultraviolet Light-Emitting Diode Grown on Pattern Si substrate", *Scientific Reports*, Vol. 7, No. 1, p. 12176, 2017.

20. Muhammad Navid, A. *et al.*, "High Electron Mobility Transistors: Performance Analysis, Research Trend and Applications", *INTECH Open Science*, Vol. 5, No. 772, p. 67796, 2017.

21. Li, L., Y. Zhang, S. Xu, W. Bi, Z.-H. Zhang and H.-C. Kuo, "On the Hole Injection for III-nitride Based Deep Ultraviolet Light-Emitting Diodes", *Materials*, Vol. 10, No. 10, p. 1221, 2017.

22. Stepanov, S., V. Nikolaev, V. Bougrov and A. Romanov, "Gallium Oxide: Properties and Applica 498 a Review", *Review on Advanced Material Science*, Vol. 44, pp. 63–86, 2016.

23. Lin, C.-H. and C.-T. Lee, "Ga_2O_3-Based Solar-Blind Deep Ultraviolet Light-Emitting Diodes", *Journal of Luminescence*, Vol. 224, p. 117326, 2020.

24. Sasaki, K., M. Higashiwaki, A. Kuramata, T. Masui and S. Yamakoshi, "MBE

Grown Ga2O3 and Its Power Device Applications", *Journal of Crystal Growth*, Vol. 378, pp. 591–595, 2013.

25. Higashiwaki, M., K. Sasaki, A. Kuramata, T. Masui and S. Yamakoshi, "Gallium Oxide (Ga_2O_3) Metal-Semiconductor Field-Effect Transistors on Single-crystal β-Ga_2O_3 (010) Substrates", *Applied Physics Letters*, Vol. 100, No. 1, p. 013504, 2012.

26. Chao, P.-C., K. Chu, C. Creamer, J. Diaz, T. Yurovchak, M. Shur, R. Kallaher, C. McGray, G. D. Via and J. D. Blevins, "Low-Temperature Bonded GaN-on-Diamond HEMTs with 11 W/mm Output Power at 10 GHz", *IEEE Transactions on Electron Devices*, Vol. 62, No. 11, pp. 3658–3664, 2015.

27. Mastro, M. A., A. Kuramata, J. Calkins, J. Kim, F. Ren and S. Pearton, "Perspective—Opportunities and Future Directions for Ga2O3", *ECS Journal of Solid State Science and Technology*, Vol. 6, No. 5, p. P356, 2017.

28. Oh, S., M. A. Mastro, M. J. Tadjer and J. Kim, "Solar-blind Metal-Semiconductor-Metal Photodetectors Based on an Exfoliated β-Ga_2O_3 micro-Flake", *ECS Journal of Solid State Science and Technology*, Vol. 6, No. 8, p. Q79, 2017.

29. Qin, Y., L. Li, X. Zhao, G. S. Tompa, H. Dong, G. Jian, Q. He, P. Tan, X. Hou, Z. Zhang *et al.*, "Metal–Semiconductor–Metal ε-Ga2O3 Solar-Blind Photodetectors with a Record-High Responsivity Rejection Ratio and their Gain Mechanism", *Acs Photonics*, Vol. 7, No. 3, pp. 812–820, 2020.

30. Yuan, C., R. Hanus and S. Graham, "A Review of Thermoreflectance Techniques for Characterizing Wide Bandgap Semiconductors' Thermal Properties and Devices' Temperatures", *Journal of Applied Physics*, Vol. 132, No. 22, p. 220701, 2022.

31. Wei, S. and M. Y. Chou, "Ab Initio Calculation of Force Constants and Full Phonon

Dispersions", *Physical Review Letters*, Vol. 69, No. 19, pp. 2799–2802, 1992.

32. Chen, G., *Nanoscale Energy Transport and Conversion a Parallel Treatment of Electrons, Molecules, Phonons, and Photons*, Oxford University Press, Oxford, England, 2005.

33. Chapman, J., R. Cohen, A. Kimmel and D. Duffy, "Improving the Functional Control of Aged Ferroelectrics Using Insights from Atomistic Modeling", *Physical Review Letters*, Vol. 119, No. 17, p. 177602, 2017.

34. Zhang, Z. M., Z. M. Zhang and Luby, *Nano/Microscale Heat Transfer*, Springer, New York, 2007.

35. Albar, I. and N. Donmezer, "Mean Free Path–Thermal Conductivity Accumulation Calculations for Wurtzite Gallium Nitride: Two Approaches", *Nanoscale and Microscale Thermophysical Engineering*, Vol. 24, No. 2, pp. 80–93, 2020.

36. Lindsay, L., D. Broido and N. Mingo, "Flexural Phonons and Thermal Transport in Multilayer Graphene and Graphite", *Physical Review B*, Vol. 83, No. 23, p. 235428, 2011.

37. Chen, G., "Phonon Heat Conduction in Nanostructures", *International Journal of Thermal Sciences*, Vol. 39, No. 4, pp. 471–480, 2000.

38. Szwejkowski, C. J., N. C. Creange, K. Sun, A. Giri, B. F. Donovan, C. Constantin and P. E. Hopkins, "Size Effects in the Thermal Conductivity of Gallium Oxide (β-Ga2O3) Films Grown Via Open-Atmosphere Annealing of Gallium Nitride", *Journal of Applied Physics*, Vol. 117, No. 8, p. 084308, 2015.

39. Tran, D. Q., R. Delgado-Carrascon, J. F. Muth, T. Paskova, M. Nawaz, V. Darakchieva and P. P. Paskov, "Phonon-Boundary Scattering and Thermal Transport in Al x Ga1- x N: Effect of layer Thickness", *Applied Physics Letters*, Vol. 117, No. 25, p. 252102, 2020.

40. Freedman, J. P., J. H. Leach, E. A. Preble, Z. Sitar, R. F. Davis and J. A. Malen, "Universal Phonon Mean Free Path Spectra in Crystalline Semiconductors at High Temperature", *Scientific Reports*, Vol. 3, No. 1, p. 2963, 2013.

41. Tran, D. Q., N. Blumenschein, A. Mock, P. Sukkaew, H. Zhang, J. F. Muth, T. Paskova, P. P. Paskov and V. Darakchieva, "Thermal Conductivity of Ultrawide Bandgap thin Layers–High Al-Content AlGaN and β-Ga2O3", *Physica B: Condensed Matter*, Vol. 579, p. 411810, 2020.

42. Mitterhuber, L., R. Hammer, T. Dengg and J. Spitaler, "Thermal Characterization and Modelling of AlGaN-GaN Multilayer Structures for HEMT Applications", *Energies*, Vol. 13, No. 9, p. 2363, 2020.

43. Mizokami, K., A. Togo and I. Tanaka, "Lattice Thermal Conductivities of Two SiO 2 Polymorphs by First-Principles Calculations and the Phonon Boltzmann Transport Equation", *Physical Review B*, Vol. 97, No. 22, p. 224306, 2018.

44. Li, W., J. Carrete, N. A. Katcho and N. Mingo, "ShengBTE: A Solver of the Boltzmann Transport Equation for Phonons", *Computer Physics Communications*, Vol. 185, No. 6, pp. 1747–1758, 2014.

45. Togo, A. and I. Tanaka, "First Principles Phonon Calculations in Materials Science", *Scripta Materialia*, Vol. 108, pp. 1–5, 2015.

46. Togo, A., L. Chaput and I. Tanaka, "Distributions of Phonon Lifetimes in Brillouin Zones", *Physical Review B*, Vol. 91, No. 9, p. 094306, 2015.

47. Ma, J., X. Wang, B. Huang and X. Luo, "Effects of Point Defects and Dislocations on Spectral Phonon Transport Properties of Wurtzite GaN", *Journal of Applied Physics*, Vol. 114, No. 7, p. 074311, 2013.

48. Jiang, P., X. Qian and R. Yang, "Tutorial: Time-domain Thermoreflectance (TDTR) for Thermal Property Characterization of Bulk and Thin Film Mate-

rials", *Journal of Applied Physics*, Vol. 124, No. 16, p. 161103, 2018.

49. Schmidt, A. J., R. Cheaito and M. Chiesa, "A Frequency-Domain Thermoreflectance Method for the Characterization of Thermal Properties", *Review of Scientific Instruments*, Vol. 80, No. 9, p. 094901, 2009.

50. Hu, Y., L. Zeng, A. J. Minnich, M. S. Dresselhaus and G. Chen, "Spectral Mapping of Thermal Conductivity Through Nanoscale Ballistic Transport", *Nature Nanotechnology*, Vol. 10, No. 8, pp. 701–706, 2015.

51. Killat, N., J. W. Pomeroy, J. L. Jimenez and M. Kuball, "Thermal Properties of AlGaN/GaN High Electron Mobility Transistors on 4H and 6H SiC Substrates", *Physica Status Solidi (a)*, Vol. 211, No. 12, pp. 2844–2847, 2014.

52. Kuball, M., S. Rajasingam, A. Sarua, M. Uren, T. Martin, B. Hughes, K. Hilton and R. Balmer, "Measurement of Temperature Distribution in Multifinger AlGaN/GaN Heterostructure Field-Effect Transistors Using Micro-Raman Spectroscopy", *Applied Physics Letters*, Vol. 82, No. 1, pp. 124–126, 2003.

53. Kuball, M., "Raman Spectroscopy of GaN, AlGaN and AlN for Process and Growth Monitoring/Control", *Surface and Interface Analysis: An International Journal Devoted to The Development and Application of Techniques for The Analysis of Surfaces, Interfaces and Thin Films*, Vol. 31, No. 10, pp. 987–999, 2001.

54. Killat, N., M. Montes, J. Pomeroy, T. Paskova, K. Evans, J. Leach, X. Li, Ü. Ozgur, H. Morkoc, K. Chabak *et al.*, "Thermal Properties of AlGaN/GaN HFETs on Bulk GaN Substrates", *IEEE Electron Device Letters*, Vol. 33, No. 3, pp. 366–368, 2012.

55. Liu, W. and A. A. Balandin, "Temperature Dependence of Thermal Conductivity of $Al_xGa_{1-x}N$ Thin Films Measured by the Differential 3 ω Technique", *Applied Physics Letters*, Vol. 85, No. 22, pp. 5230–5232, 2004.

56. Guo, Z., A. Verma, X. Wu, F. Sun, A. Hickman, T. Masui, A. Kuramata, M. Hi-

gashiwaki, D. Jena and T. Luo, "Anisotropic Thermal Conductivity in Single Crystal β-gallium oxide", *Applied Physics Letters*, Vol. 106, No. 11, p. 111909, 2015.

57. Varley, J. B., J. R. Weber, A. Janotti and C. G. Van de Walle, "Oxygen Vacancies and Donor Impurities in β-Ga_2O_3", *Applied Physics Letters*, Vol. 97, No. 14, p. 142106, 2010.

58. Handwerg, M., R. Mitdank, Z. Galazka and S. Fischer, "Temperature-Dependent Thermal Conductivity and Diffusivity of a Mg-Doped Insulating β-Ga_2O_3 Single Crystal Along [100],[010] and [001]", *Semiconductor Science and Technology*, Vol. 31, No. 12, p. 125006, 2016.

59. Galazka, Z., K. Irmscher, R. Uecker, R. Bertram, M. Pietsch, A. Kwasniewski, M. Naumann, T. Schulz, R. Schewski, D. Klimm *et al.*, "On the Bulk β-Ga_2O_3 Single Crystals Grown by the Czochralski Method", *Journal of Crystal Growth*, Vol. 404, pp. 184–191, 2014.

60. Zhang, Y., Q. Su, J. Zhu, S. Koirala, S. J. Koester and X. Wang, "Thickness-Dependent Thermal Conductivity of Mechanically Exfoliated β-Ga_2O_3 Thin Films", *Applied Physics Letters*, Vol. 116, No. 20, p. 202101, 2020.

61. Kaiser, J., T. Feng, J. Maassen, X. Wang, X. Ruan and M. Lundstrom, "Thermal Transport at the Nanoscale: A Fourier's Law vs. Phonon Boltzmann Equation Study", *Journal of Applied Physics*, Vol. 121, No. 4, p. 044302, 2017.

62. Miyazaki, K., T. Arashi, D. Makino and H. Tsukamoto, "Heat Conduction in Microstructured Materials", *IEEE Transactions on Components and Packaging Technologies*, Vol. 29, No. 2, pp. 247–253, 2006.

63. McGaughey, A. J., A. Jain, H.-Y. Kim and B. Fu, "Phonon Properties and Thermal Conductivity from First Principles, Lattice Dynamics, and the Boltzmann Transport Equation", *Journal of Applied Physics*, Vol. 125, No. 1, p. 011101, 2019.

64. Kotchetkov, D., J. Zou, A. Balandin, D. Florescu and F. H. Pollak, "Effect of Dislocations on Thermal Conductivity of GaN Layers", *Applied Physics Letters*, Vol. 79, No. 26, pp. 4316–4318, 2001.

65. Zhou, X., S. Aubry, R. Jones, A. Greenstein and P. Schelling, "Towards More Accurate Molecular Dynamics Calculation of Thermal Conductivity: Case Study of GaN Bulk Crystals", *Physical Review B*, Vol. 79, No. 11, p. 115201, 2009.

66. Daly, B., H. Maris, A. Nurmikko, M. Kuball and J. Han, "Optical Pump-and-Probe Measurement of the Thermal Conductivity of Nitride Thin Films", *Journal of Applied Physics*, Vol. 92, No. 7, pp. 3820–3824, 2002.

67. Koh, Y. R., M. Shirazi-HD, B. Vermeersch, A. Mohammed, J. Shao, G. Pernot, J.-H. Bahk, M. J. Manfra and A. Shakouri, "Quasi-Ballistic Thermal Transport in $Al_{0.1}Ga_{0.9}N$ Thin Film Semiconductors", *Applied Physics Letters*, Vol. 109, No. 24, 2016.

68. Liu, W. and A. A. Balandin, "Thermal Conduction in Al x Ga 1- x N Alloys and Thin Films", *Journal of Applied Physics*, Vol. 97, No. 7, p. 073710, 2005.

69. Ma, J., W. Li and X. Luo, "Intrinsic Thermal Conductivities and Size Eeffect of Alloys of Wurtzite AlN, GaN, and InN from First-Principles", *Journal of Applied Physics*, Vol. 119, No. 12, p. 125702, 2016.

70. Carrete, J., B. Vermeersch, A. Katre, A. van Roekeghem, T. Wang, G. K. Madsen and N. Mingo, "AlmaBTE: A Solver of the Space–Time Dependent Boltzmann Transport Erete, Jesús and Vermeersch, Bjorn and Katre, Ankita and Van Roekeghem, Ambroise and Wang, Tao and Madsen, Georg KH and Mingo, Natalio", *Computer Physics Communications*, Vol. 220, pp. 351–362, 2017.

71. Yan, Z. and S. Kumar, "Phonon Mode Contributions to Thermal Conductivity of Pristine and Defective β-Ga 2 O 3", *Physical Chemistry Chemical Physics*, Vol. 20,

No. 46, pp. 29236–29242, 2018.

72. Munshi, J., A. Roy, S. Hansen, C. E. Ekuma and G. Balasubramanian, "Effect of Vacancy Defects on The Thermal Transport of β-Ga2O3", *Molecular Simulation*, Vol. 47, No. 12, pp. 1017–1021, 2021.

73. Kresse, G. and J. Hafner, "Ab Initio Molecular Dynamics for Liquid Metals", *Physical Review B*, Vol. 47, No. 1, p. 558, 1993.

74. Kresse, G. and J. Furthmüller, "VASP the Guide (Universität Wien, Wien, Austria, 2007); G", *Physical Review B*, Vol. 47, p. 558, 1993.

75. Blöchl, P. E., "Projector Augmented-Wave Method", *Physical Review B*, Vol. 50, No. 24, p. 17953, 1994.

76. Fu, J., T. Song, X. Liang and G. Zhao, "Composition Dependence of Phonon and Thermodynamic Properties of the Ternary AlGaN Mixed Crystal", *Results in Physics*, Vol. 14, p. 102505, 2019.

77. Setyawan, W. and S. Curtarolo, "High-Throughput Electronic Band Structure Calculations: Challenges and Tools", *Computational Materials Science*, Vol. 49, No. 2, pp. 299–312, 2010.

78. Thomas, L. H., "The Calculation of Atomic Fields", *Mathematical Proceedings of the Cambridge Philosophical Society*, Vol. 23, pp. 542–548, Cambridge University Press, 1927.

79. Tang, D.-S. and B.-Y. Cao, "Topological Effects of Phonons in GaN and AlGaN: A Potential Perspective for Tuning Phonon Transport", *Journal of Applied Physics*, Vol. 129, No. 8, p. 085102, 2021.

80. Jain, A., H. P. Veeravenkata, S. Godse and Y. Srivastava, "High-Throughput Computational Discovery of 40 Ultralow Thermal Conductivity and 20 Highly

Anisotropic Crystalline Materials", *ArXiv Preprint ArXiv:2204.03628*, 2022.

81. Wang, H., D. Wei, J. Duan, Z. Qin, G. Qin, Y. Yao and M. Hu, "The Exceptionally High Thermal Conductivity After 'Alloying'Two-Dimensional Gallium Nitride (GaN) and Aluminum Nitride (AlN)", *Nanotechnology*, Vol. 32, No. 13, p. 135401, 2021.

82. Peelaers, H. and C. G. Van de Walle, "Brillouin Zone and Band Structure of β-Ga_2O_3", *Physica Status Solidi (b)*, Vol. 252, No. 4, pp. 828–832, 2015.

83. Mohamed, M., C. Janowitz, I. Unger, R. Manzke, Z. Galazka, R. Uecker, R. Fornari, J. Weber, J. Varley and C. Van de Walle, "The Electronic Structure of β-Ga_2O_3", *Applied Physics Letters*, Vol. 97, No. 21, p. 211903, 2010.

84. Nye, J. F., *Physical Properties of Crystals: Their Representation by Tensors and Matrices*, Oxford university press, Oxford, England, 1985.

85. Yang, G., P. R. Romeo, A. Apostoluk and B. Vilquin, "First Principles Study on the Lattice Thermal Conductivity of α-Phase Ga_2O_3", *Journal of Vacuum Science & Technology A: Vacuum, Surfaces, and Films*, Vol. 40, No. 5, p. 052801, 2022.

86. Handwerg, M., R. Mitdank, Z. Galazka and S. Fischer, "Temperature-Dependent Thermal Conductivity in Mg-Doped and Undoped β-Ga_2O_3 Bulk-Crystals", *Semiconductor Science and Technology*, Vol. 30, No. 2, p. 024006, 2015.

87. Snead, L. L., T. Nozawa, Y. Katoh, T.-S. Byun, S. Kondo and D. A. Petti, "Handbook of SiC Properties for Fuel Performance Modeling", *Journal of Nuclear Materials*, Vol. 371, No. 1-3, pp. 329–377, 2007.

88. Jeżowski, A., B. Danilchenko, M. Boćkowski, I. Grzegory, S. Krukowski, T. Suski and T. Paszkiewicz, "Thermal Conductivity of GaN Crystals in 4.2–300 K range", *Solid State Communications*, Vol. 128, No. 2-3, pp. 69–73, 2003.

89. Ziman, J. M., *Electrons and Phonons: the Theory of Transport Phenomena in Solids*, Oxford university press, Oxford, England, 2001.

90. Ward, A., D. Broido, D. A. Stewart and G. Deinzer, "Ab initio Theory of the Lattice Thermal Conductivity in Diamond", *Physical Review B*, Vol. 80, No. 12, p. 125203, 2009.

91. Li, W., L. Lindsay, D. A. Broido, D. A. Stewart and N. Mingo, "Thermal conductivity of Bulk and Nanowire $Mg_2Si_xSn_{1-x}$ alloys from First Principles", *Physical Review B*, Vol. 86, No. 17, p. 174307, 2012.

92. Venkatachalam, A., W. James and S. Graham, "Electro-Thermo-Mechanical Modeling of GaN-based HFETs and MOSHFETs", *Semiconductor Science and Technology*, Vol. 26, No. 8, p. 085027, 2011.

APPENDIX A: COPYRIGHT PERMISSIONS

This page is available in the following languages:

Creative Commons License Deed

Attribution-NonCommercial 4.0 International (CC BY-NC 4.0)

This is a human-readable summary of (and not a substitute for) the license.

You are free to:

Share — copy and redistribute the material in any medium or format

Adapt — remix, transform, and build upon the material

The licensor cannot revoke these freedoms as long as you follow the license terms.

Under the following terms:

Attribution — You must give appropriate credit, provide a link to the license, and indicate if changes were made. You may do so in any reasonable manner, but not in any way that suggests the licensor endorses you or your use.

NonCommercial — You may not use the material for commercial purposes.

No additional restrictions — You may not apply legal terms or technological measures that legally restrict others from doing anything the license permits.

Notices:

You do not have to comply with the license for elements of the material in the public domain or where your use is permitted by an applicable exception or limitation.

No warranties are given. The license may not give you all of the permissions necessary for your intended use. For example, other rights such as publicity, privacy, or moral rights may limit how you use the material.

Figure A.1. Copyright permission for Figure 1.1.

SPRINGER NATURE ORDER DETAILS

Aug 20, 2023

Order Number	501838839
Order date	Aug 20, 2023
Licensed Content Publisher	Springer Nature
Licensed Content Publication	Journal of Materials Research
Licensed Content Title	Ultrawide-bandgap semiconductors: An overview
Licensed Content Author	Man Hoi Wong et al
Licensed Content Date	Dec 28, 2021
Type of Use	I don't see my intended use
Requestor type	academic/university or research institute
Is this reuse sponsored by or associated with a pharmaceutical or a medical products company?	no
Author of this Springer Nature content	no
Requestor Location	Mrs. pegah ghanizadeh Boğaziçi Üniversitesi 34342 Bebek/İstanb istanbul, 34342 Turkey Attn: Mrs. pegah ghanizadeh

Figure A.2. Copyright permission for Figure 1.2.

ELSEVIER LICENSE
TERMS AND CONDITIONS

Aug 23, 2023

This Agreement between Mrs. pegah ghanizadeh ("You") and Elsevier ("Elsevier") consists of your license details and the terms and conditions provided by Elsevier and Copyright Clearance Center.

License Number	5614760433444
License date	Aug 23, 2023
Licensed Content Publisher	Elsevier
Licensed Content Publication	Superlattices and Microstructures
Licensed Content Title	Performance improvement of AlGaN-based deep-ultraviolet light-emitting diodes via Al-composition graded quantum wells
Licensed Content Author	Lin Lu,Yu Zhang,Fujun Xu,Gege Ding,Yuhang Liu
Licensed Content Date	Jun 1, 2018
Licensed Content Volume	118
Licensed Content Issue	n/a
Licensed Content Pages	6
Start Page	55
End Page	60

Figure A.3. Copyright permission for Figure 1.4.

Type of Use	reuse in a thesis/dissertation
Portion	figures/tables/illustrations
Number of figures/tables/illustrations	2
Format	both print and electronic
Are you the author of this Elsevier article?	No
Will you be translating?	No
Title	Phonon Mean Free Path - Thermal Conductivity Relation of AlxGa1−xN , and β-Ga2O3 semiconductors
Institution name	Bogazici University
Expected presentation date	Aug 2023
Portions	figure 1
Requestor Location	Mrs. pegah ghanizadeh Boğaziçi Üniversitesi 34342 Bebek/İstanb istanbul, 34342 Turkey Attn: Mrs. pegah ghanizadeh
Publisher Tax ID	GB 494 6272 12
Total	0.00 USD
Terms and Conditions	

INTRODUCTION

Figure A.4. Copyright permission for Figure 1.4 (cont.).

1. The publisher for this copyrighted material is Elsevier. By clicking "accept" in connection with completing this licensing transaction, you agree that the following terms and conditions apply to this transaction (along with the Billing and Payment terms and conditions established by Copyright Clearance Center, Inc. ("CCC"), at the time that you opened your RightsLink account and that are available at any time at https://myaccount.copyright.com).

GENERAL TERMS

2. Elsevier hereby grants you permission to reproduce the aforementioned material subject to the terms and conditions indicated.

3. Acknowledgement: If any part of the material to be used (for example, figures) has appeared in our publication with credit or acknowledgement to another source, permission must also be sought from that source. If such permission is not obtained then that material may not be included in your publication/copies. Suitable acknowledgement to the source must be made, either as a footnote or in a reference list at the end of your publication, as follows:

"Reprinted from Publication title, Vol /edition number, Author(s), Title of article / title of chapter, Pages No., Copyright (Year), with permission from Elsevier [OR APPLICABLE SOCIETY COPYRIGHT OWNER]." Also Lancet special credit - "Reprinted from The Lancet, Vol. number, Author(s), Title of article, Pages No., Copyright (Year), with permission from Elsevier."

4. Reproduction of this material is confined to the purpose and/or media for which permission is hereby given. The material may not be reproduced or used in any other way, including use in combination with an artificial intelligence tool (including to train an algorithm, test, process, analyse, generate output and/or develop any form of artificial intelligence tool), or to create any derivative work and/or service (including resulting from the use of artificial intelligence tools).

5. Altering/Modifying Material: Not Permitted. However figures and illustrations may be altered/adapted minimally to serve your work. Any other abbreviations, additions, deletions and/or any other alterations shall be made only with prior written authorization of Elsevier Ltd. (Please contact Elsevier's permissions helpdesk here). No modifications can be made to any Lancet figures/tables and they must be reproduced in full.

6. If the permission fee for the requested use of our material is waived in this instance, please be advised that your future requests for Elsevier materials may attract a fee.

7. Reservation of Rights: Publisher reserves all rights not specifically granted in the combination of (i) the license details provided by you and accepted in the course of this licensing transaction, (ii) these terms and conditions and (iii) CCC's Billing and Payment terms and conditions.

8. License Contingent Upon Payment: While you may exercise the rights licensed immediately upon issuance of the license at the end of the licensing process for the transaction, provided that you have disclosed complete and accurate details of your proposed use, no license is finally effective unless and until full payment is received from you (either by publisher or by CCC) as provided in CCC's Billing and Payment terms and conditions. If full payment is not received on a timely basis, then any license preliminarily granted shall be deemed automatically revoked and shall be void as if never granted. Further, in the event that you breach any of these terms and conditions or any of CCC's Billing and Payment terms and conditions, the license is automatically revoked and shall be void as if never granted. Use of materials as described in a revoked license, as well as any use of the

Figure A.5. Copyright permission for Figure 1.4 (cont.).

materials beyond the scope of an unrevoked license, may constitute copyright infringement and publisher reserves the right to take any and all action to protect its copyright in the materials.

9. Warranties: Publisher makes no representations or warranties with respect to the licensed material.

10. Indemnity: You hereby indemnify and agree to hold harmless publisher and CCC, and their respective officers, directors, employees and agents, from and against any and all claims arising out of your use of the licensed material other than as specifically authorized pursuant to this license.

11. No Transfer of License: This license is personal to you and may not be sublicensed, assigned, or transferred by you to any other person without publisher's written permission.

12. No Amendment Except in Writing: This license may not be amended except in a writing signed by both parties (or, in the case of publisher, by CCC on publisher's behalf).

13. Objection to Contrary Terms: Publisher hereby objects to any terms contained in any purchase order, acknowledgment, check endorsement or other writing prepared by you, which terms are inconsistent with these terms and conditions or CCC's Billing and Payment terms and conditions. These terms and conditions, together with CCC's Billing and Payment terms and conditions (which are incorporated herein), comprise the entire agreement between you and publisher (and CCC) concerning this licensing transaction. In the event of any conflict between your obligations established by these terms and conditions and those established by CCC's Billing and Payment terms and conditions, these terms and conditions shall control.

14. Revocation: Elsevier or Copyright Clearance Center may deny the permissions described in this License at their sole discretion, for any reason or no reason, with a full refund payable to you. Notice of such denial will be made using the contact information provided by you. Failure to receive such notice will not alter or invalidate the denial. In no event will Elsevier or Copyright Clearance Center be responsible or liable for any costs, expenses or damage incurred by you as a result of a denial of your permission request, other than a refund of the amount(s) paid by you to Elsevier and/or Copyright Clearance Center for denied permissions.

LIMITED LICENSE

The following terms and conditions apply only to specific license types:

15. **Translation**: This permission is granted for non-exclusive world **English** rights only unless your license was granted for translation rights. If you licensed translation rights you may only translate this content into the languages you requested. A professional translator must perform all translations and reproduce the content word for word preserving the integrity of the article.

16. **Posting licensed content on any Website**: The following terms and conditions apply as follows: Licensing material from an Elsevier journal: All content posted to the web site must maintain the copyright information line on the bottom of each image; A hyper-text must be included to the Homepage of the journal from which you are licensing at http://www.sciencedirect.com/science/journal/xxxxx or the Elsevier homepage for books at http://www.elsevier.com; Central Storage: This license does not include permission for a scanned version of the material to be stored in a central repository such as that provided by Heron/XanEdu.

Figure A.6. Copyright permission for Figure 1.4 (cont.).

appear more like, or to substitute for, the published journal article.

Published journal article (JPA): A published journal article (PJA) is the definitive final record of published research that appears or will appear in the journal and embodies all value-adding publishing activities including peer review co-ordination, copy-editing, formatting, (if relevant) pagination and online enrichment.

Policies for sharing publishing journal articles differ for subscription and gold open access articles:

Subscription Articles: If you are an author, please share a link to your article rather than the full-text. Millions of researchers have access to the formal publications on ScienceDirect, and so links will help your users to find, access, cite, and use the best available version.

Theses and dissertations which contain embedded PJAs as part of the formal submission can be posted publicly by the awarding institution with DOI links back to the formal publications on ScienceDirect.

If you are affiliated with a library that subscribes to ScienceDirect you have additional private sharing rights for others' research accessed under that agreement. This includes use for classroom teaching and internal training at the institution (including use in course packs and courseware programs), and inclusion of the article for grant funding purposes.

Gold Open Access Articles: May be shared according to the author-selected end-user license and should contain a CrossMark logo, the end user license, and a DOI link to the formal publication on ScienceDirect.

Please refer to Elsevier's posting policy for further information.

18. **For book authors** the following clauses are applicable in addition to the above: Authors are permitted to place a brief summary of their work online only. You are not allowed to download and post the published electronic version of your chapter, nor may you scan the printed edition to create an electronic version. **Posting to a repository:** Authors are permitted to post a summary of their chapter only in their institution's repository.

19. **Thesis/Dissertation**: If your license is for use in a thesis/dissertation your thesis may be submitted to your institution in either print or electronic form. Should your thesis be published commercially, please reapply for permission. These requirements include permission for the Library and Archives of Canada to supply single copies, on demand, of the complete thesis and include permission for Proquest/UMI to supply single copies, on demand, of the complete thesis. Should your thesis be published commercially, please reapply for permission. Theses and dissertations which contain embedded PJAs as part of the formal submission can be posted publicly by the awarding institution with DOI links back to the formal publications on ScienceDirect.

Elsevier Open Access Terms and Conditions

You can publish open access with Elsevier in hundreds of open access journals or in nearly 2000 established subscription journals that support open access publishing. Permitted third party re-use of these open access articles is defined by the author's choice of Creative Commons user license. See our open access license policy for more information.

Terms & Conditions applicable to all Open Access articles published with Elsevier:

Figure A.7. Copyright permission for Figure 1.4 (cont.).

ELSEVIER LICENSE
TERMS AND CONDITIONS

Aug 23, 2023

This Agreement between Mrs. pegah ghanizadeh ("You") and Elsevier ("Elsevier") consists of your license details and the terms and conditions provided by Elsevier and Copyright Clearance Center.

License Number	5614791217134
License date	Aug 23, 2023
Licensed Content Publisher	Elsevier
Licensed Content Publication	Chinese Journal of Physics
Licensed Content Title	Properties and perspectives of ultrawide bandgap Ga2O3 in optoelectronic applications
Licensed Content Author	Loh Kean Ping,Dilla Duryha Berhanuddin,Abhay Kumar Mondal,P. Susthitha Menon,Mohd Ambri Mohamed
Licensed Content Date	Oct 1, 2021
Licensed Content Volume	73
Licensed Content Issue	n/a
Licensed Content Pages	18
Start Page	195
End Page	212

Figure A.8. Copyright permission for Figure 1.6.

1. The publisher for this copyrighted material is Elsevier. By clicking "accept" in connection with completing this licensing transaction, you agree that the following terms and conditions apply to this transaction (along with the Billing and Payment terms and conditions established by Copyright Clearance Center, Inc. ("CCC"), at the time that you opened your RightsLink account and that are available at any time at https://myaccount.copyright.com).

GENERAL TERMS

2. Elsevier hereby grants you permission to reproduce the aforementioned material subject to the terms and conditions indicated.

3. Acknowledgement: If any part of the material to be used (for example, figures) has appeared in our publication with credit or acknowledgement to another source, permission must also be sought from that source. If such permission is not obtained then that material may not be included in your publication/copies. Suitable acknowledgement to the source must be made, either as a footnote or in a reference list at the end of your publication, as follows:

"Reprinted from Publication title, Vol /edition number, Author(s), Title of article / title of chapter, Pages No., Copyright (Year), with permission from Elsevier [OR APPLICABLE SOCIETY COPYRIGHT OWNER]." Also Lancet special credit - "Reprinted from The Lancet, Vol. number, Author(s), Title of article, Pages No., Copyright (Year), with permission from Elsevier."

4. Reproduction of this material is confined to the purpose and/or media for which permission is hereby given. The material may not be reproduced or used in any other way, including use in combination with an artificial intelligence tool (including to train an algorithm, test, process, analyse, generate output and/or develop any form of artificial intelligence tool), or to create any derivative work and/or service (including resulting from the use of artificial intelligence tools).

5. Altering/Modifying Material: Not Permitted. However figures and illustrations may be altered/adapted minimally to serve your work. Any other abbreviations, additions, deletions and/or any other alterations shall be made only with prior written authorization of Elsevier Ltd. (Please contact Elsevier's permissions helpdesk here). No modifications can be made to any Lancet figures/tables and they must be reproduced in full.

6. If the permission fee for the requested use of our material is waived in this instance, please be advised that your future requests for Elsevier materials may attract a fee.

7. Reservation of Rights: Publisher reserves all rights not specifically granted in the combination of (i) the license details provided by you and accepted in the course of this licensing transaction, (ii) these terms and conditions and (iii) CCC's Billing and Payment terms and conditions.

8. License Contingent Upon Payment: While you may exercise the rights licensed immediately upon issuance of the license at the end of the licensing process for the transaction, provided that you have disclosed complete and accurate details of your proposed use, no license is finally effective unless and until full payment is received from you (either by publisher or by CCC) as provided in CCC's Billing and Payment terms and conditions. If full payment is not received on a timely basis, then any license preliminarily granted shall be deemed automatically revoked and shall be void as if never granted. Further, in the event that you breach any of these terms and conditions or any of CCC's Billing and Payment terms and conditions, the license is automatically revoked and shall be void as if never granted. Use of materials as described in a revoked license, as well as any use of the

Figure A.9. Copyright permission for Figure 1.6 (cont.).

materials beyond the scope of an unrevoked license, may constitute copyright infringement and publisher reserves the right to take any and all action to protect its copyright in the materials.

9. Warranties: Publisher makes no representations or warranties with respect to the licensed material.

10. Indemnity: You hereby indemnify and agree to hold harmless publisher and CCC, and their respective officers, directors, employees and agents, from and against any and all claims arising out of your use of the licensed material other than as specifically authorized pursuant to this license.

11. No Transfer of License: This license is personal to you and may not be sublicensed, assigned, or transferred by you to any other person without publisher's written permission.

12. No Amendment Except in Writing: This license may not be amended except in a writing signed by both parties (or, in the case of publisher, by CCC on publisher's behalf).

13. Objection to Contrary Terms: Publisher hereby objects to any terms contained in any purchase order, acknowledgment, check endorsement or other writing prepared by you, which terms are inconsistent with these terms and conditions or CCC's Billing and Payment terms and conditions. These terms and conditions, together with CCC's Billing and Payment terms and conditions (which are incorporated herein), comprise the entire agreement between you and publisher (and CCC) concerning this licensing transaction. In the event of any conflict between your obligations established by these terms and conditions and those established by CCC's Billing and Payment terms and conditions, these terms and conditions shall control.

14. Revocation: Elsevier or Copyright Clearance Center may deny the permissions described in this License at their sole discretion, for any reason or no reason, with a full refund payable to you. Notice of such denial will be made using the contact information provided by you. Failure to receive such notice will not alter or invalidate the denial. In no event will Elsevier or Copyright Clearance Center be responsible or liable for any costs, expenses or damage incurred by you as a result of a denial of your permission request, other than a refund of the amount(s) paid by you to Elsevier and/or Copyright Clearance Center for denied permissions.

LIMITED LICENSE

The following terms and conditions apply only to specific license types:

15. **Translation**: This permission is granted for non-exclusive world **English** rights only unless your license was granted for translation rights. If you licensed translation rights you may only translate this content into the languages you requested. A professional translator must perform all translations and reproduce the content word for word preserving the integrity of the article.

16. **Posting licensed content on any Website**: The following terms and conditions apply as follows: Licensing material from an Elsevier journal: All content posted to the web site must maintain the copyright information line on the bottom of each image; A hyper-text must be included to the Homepage of the journal from which you are licensing at http://www.sciencedirect.com/science/journal/xxxxx or the Elsevier homepage for books at http://www.elsevier.com; Central Storage: This license does not include permission for a scanned version of the material to be stored in a central repository such as that provided by Heron/XanEdu.

Figure A.10. Copyright permission for Figure 1.6 (cont.).

Licensing material from an Elsevier book: A hyper-text link must be included to the Elsevier homepage at http://www.elsevier.com . All content posted to the web site must maintain the copyright information line on the bottom of each image.

Posting licensed content on Electronic reserve: In addition to the above the following clauses are applicable: The web site must be password-protected and made available only to bona fide students registered on a relevant course. This permission is granted for 1 year only. You may obtain a new license for future website posting.

17. **For journal authors:** the following clauses are applicable in addition to the above:

Preprints:

A preprint is an author's own write-up of research results and analysis, it has not been peer-reviewed, nor has it had any other value added to it by a publisher (such as formatting, copyright, technical enhancement etc.).

Authors can share their preprints anywhere at any time. Preprints should not be added to or enhanced in any way in order to appear more like, or to substitute for, the final versions of articles however authors can update their preprints on arXiv or RePEc with their Accepted Author Manuscript (see below).

If accepted for publication, we encourage authors to link from the preprint to their formal publication via its DOI. Millions of researchers have access to the formal publications on ScienceDirect, and so links will help users to find, access, cite and use the best available version. Please note that Cell Press, The Lancet and some society-owned have different preprint policies. Information on these policies is available on the journal homepage.

Accepted Author Manuscripts: An accepted author manuscript is the manuscript of an article that has been accepted for publication and which typically includes author-incorporated changes suggested during submission, peer review and editor-author communications.

Authors can share their accepted author manuscript:

- immediately
  - via their non-commercial person homepage or blog
  - by updating a preprint in arXiv or RePEc with the accepted manuscript
  - via their research institute or institutional repository for internal institutional uses or as part of an invitation-only research collaboration work-group
  - directly by providing copies to their students or to research collaborators for their personal use
  - for private scholarly sharing as part of an invitation-only work group on commercial sites with which Elsevier has an agreement
- After the embargo period
  - via non-commercial hosting platforms such as their institutional repository
  - via commercial sites with which Elsevier has an agreement

In all cases accepted manuscripts should:

- link to the formal publication via its DOI
- bear a CC-BY-NC-ND license - this is easy to do
- if aggregated with other manuscripts, for example in a repository or other site, be shared in alignment with our hosting policy not be added to or enhanced in any way to

Figure A.11. Copyright permission for Figure 1.6 (cont.).

appear more like, or to substitute for, the published journal article.

Published journal article (JPA): A published journal article (PJA) is the definitive final record of published research that appears or will appear in the journal and embodies all value-adding publishing activities including peer review co-ordination, copy-editing, formatting, (if relevant) pagination and online enrichment.

Policies for sharing publishing journal articles differ for subscription and gold open access articles:

Subscription Articles: If you are an author, please share a link to your article rather than the full-text. Millions of researchers have access to the formal publications on ScienceDirect, and so links will help your users to find, access, cite, and use the best available version.

Theses and dissertations which contain embedded PJAs as part of the formal submission can be posted publicly by the awarding institution with DOI links back to the formal publications on ScienceDirect.

If you are affiliated with a library that subscribes to ScienceDirect you have additional private sharing rights for others' research accessed under that agreement. This includes use for classroom teaching and internal training at the institution (including use in course packs and courseware programs), and inclusion of the article for grant funding purposes.

Gold Open Access Articles: May be shared according to the author-selected end-user license and should contain a CrossMark logo, the end user license, and a DOI link to the formal publication on ScienceDirect.

Please refer to Elsevier's posting policy for further information.

18. **For book authors** the following clauses are applicable in addition to the above: Authors are permitted to place a brief summary of their work online only. You are not allowed to download and post the published electronic version of your chapter, nor may you scan the printed edition to create an electronic version. **Posting to a repository:** Authors are permitted to post a summary of their chapter only in their institution's repository.

19. **Thesis/Dissertation**: If your license is for use in a thesis/dissertation your thesis may be submitted to your institution in either print or electronic form. Should your thesis be published commercially, please reapply for permission. These requirements include permission for the Library and Archives of Canada to supply single copies, on demand, of the complete thesis and include permission for Proquest/UMI to supply single copies, on demand, of the complete thesis. Should your thesis be published commercially, please reapply for permission. Theses and dissertations which contain embedded PJAs as part of the formal submission can be posted publicly by the awarding institution with DOI links back to the formal publications on ScienceDirect.

Elsevier Open Access Terms and Conditions

You can publish open access with Elsevier in hundreds of open access journals or in nearly 2000 established subscription journals that support open access publishing. Permitted third party re-use of these open access articles is defined by the author's choice of Creative Commons user license. See our open access license policy for more information.

Terms & Conditions applicable to all Open Access articles published with Elsevier:

Figure A.12. Copyright permission for Figure 1.6 (cont.).

Any reuse of the article must not represent the author as endorsing the adaptation of the article nor should the article be modified in such a way as to damage the author's honour or reputation. If any changes have been made, such changes must be clearly indicated.

The author(s) must be appropriately credited and we ask that you include the end user license and a DOI link to the formal publication on ScienceDirect.

If any part of the material to be used (for example, figures) has appeared in our publication with credit or acknowledgement to another source it is the responsibility of the user to ensure their reuse complies with the terms and conditions determined by the rights holder.

Additional Terms & Conditions applicable to each Creative Commons user license:

CC BY: The CC-BY license allows users to copy, to create extracts, abstracts and new works from the Article, to alter and revise the Article and to make commercial use of the Article (including reuse and/or resale of the Article by commercial entities), provided the user gives appropriate credit (with a link to the formal publication through the relevant DOI), provides a link to the license, indicates if changes were made and the licensor is not represented as endorsing the use made of the work. The full details of the license are available at http://creativecommons.org/licenses/by/4.0.

CC BY NC SA: The CC BY-NC-SA license allows users to copy, to create extracts, abstracts and new works from the Article, to alter and revise the Article, provided this is not done for commercial purposes, and that the user gives appropriate credit (with a link to the formal publication through the relevant DOI), provides a link to the license, indicates if changes were made and the licensor is not represented as endorsing the use made of the work. Further, any new works must be made available on the same conditions. The full details of the license are available at http://creativecommons.org/licenses/by-nc-sa/4.0.

CC BY NC ND: The CC BY-NC-ND license allows users to copy and distribute the Article, provided this is not done for commercial purposes and further does not permit distribution of the Article if it is changed or edited in any way, and provided the user gives appropriate credit (with a link to the formal publication through the relevant DOI), provides a link to the license, and that the licensor is not represented as endorsing the use made of the work. The full details of the license are available at http://creativecommons.org/licenses/by-nc-nd/4.0. Any commercial reuse of Open Access articles published with a CC BY NC SA or CC BY NC ND license requires permission from Elsevier and will be subject to a fee.

Commercial reuse includes:

- Associating advertising with the full text of the Article
- Charging fees for document delivery or access
- Article aggregation
- Systematic distribution via e-mail lists or share buttons

Posting or linking by commercial companies for use by customers of those companies.

20. **Other Conditions**:

v1.10

Figure A.13. Copyright permission for Figure 1.6 (cont.).

AIP PUBLISHING LICENSE
TERMS AND CONDITIONS

Aug 20, 2023

This Agreement between Mrs. pegah ghanizadeh ("You") and AIP Publishing ("AIP Publishing") consists of your license details and the terms and conditions provided by AIP Publishing and Copyright Clearance Center.

License Number	5613060610669
License date	Aug 20, 2023
Licensed Content Publisher	AIP Publishing
Licensed Content Publication	Journal of Applied Physics
Licensed Content Title	A review of thermoreflectance techniques for characterizing wide bandgap semiconductors' thermal properties and devices' temperatures
Licensed Content Author	Yuan, Chao; Hanus, Riley
Licensed Content Date	Dec 8, 2022
Licensed Content Volume	132
Licensed Content Issue	22
Type of Use	Thesis/Dissertation
Requestor type	Student
Format	Print and electronic

Figure A.14. Copyright permission for Figure 1.7 (a).

Portion	Photograph/Image
Number of Photographs/Images	1
Will you be translating?	No
Title	Phonon Mean Free Path - Thermal Conductivity Relation of AlxGa1–xN , and β-Ga2O3 semiconductors
Institution name	Bogazici University
Expected presentation date	Aug 2023
Portions	2
Requestor Location	Mrs. pegah ghanizadeh Boğaziçi Üniversitesi 34342 Bebek/İstanb istanbul, 34342 Turkey Attn: Mrs. pegah ghanizadeh
Total	0.00 USD

Terms and Conditions

AIP Publishing -- Terms and Conditions: Permissions Uses

AIP Publishing hereby grants to you the non-exclusive right and license to use and/or distribute the Material according to the use specified in your order, on a one-time basis, for the specified term, with a maximum distribution equal to the number that you have ordered. Any links or other content accompanying the Material are not the subject of this license.

1. You agree to include the following copyright and permission notice with the reproduction of the Material:"Reprinted from [FULL CITATION], with the permission of AIP Publishing." For an article, the credit line and permission notice must be printed on the first page of the article or book chapter. For photographs, covers, or tables, the notice may appear with the Material, in a footnote, or in the reference list.
2. If you have licensed reuse of a figure, photograph, cover, or table, it is your responsibility to ensure that the material is original to AIP Publishing and does not contain the copyright of another entity, and that the copyright notice of the figure,

Figure A.15. Copyright permission for Figure 1.7 (a) (cont.).

photograph, cover, or table does not indicate that it was reprinted by AIP Publishing, with permission, from another source. Under no circumstances does AIP Publishing purport or intend to grant permission to reuse material to which it does not hold appropriate rights.
You may not alter or modify the Material in any manner. You may translate the Material into another language only if you have licensed translation rights. You may not use the Material for promotional purposes.

3. The foregoing license shall not take effect unless and until AIP Publishing or its agent, Copyright Clearance Center, receives the Payment in accordance with Copyright Clearance Center Billing and Payment Terms and Conditions, which are incorporated herein by reference.
4. AIP Publishing or Copyright Clearance Center may, within two business days of granting this license, revoke the license for any reason whatsoever, with a full refund payable to you. Should you violate the terms of this license at any time, AIP Publishing, or Copyright Clearance Center may revoke the license with no refund to you. Notice of such revocation will be made using the contact information provided by you. Failure to receive such notice will not nullify the revocation.
5. AIP Publishing makes no representations or warranties with respect to the Material. You agree to indemnify and hold harmless AIP Publishing, and their officers, directors, employees or agents from and against any and all claims arising out of your use of the Material other than as specifically authorized herein.
6. The permission granted herein is personal to you and is not transferable or assignable without the prior written permission of AIP Publishing. This license may not be amended except in a writing signed by the party to be charged.
7. If purchase orders, acknowledgments or check endorsements are issued on any forms containing terms and conditions which are inconsistent with these provisions, such inconsistent terms and conditions shall be of no force and effect. This document, including the CCC Billing and Payment Terms and Conditions, shall be the entire agreement between the parties relating to the subject matter hereof.

This Agreement shall be governed by and construed in accordance with the laws of the State of New York. Both parties hereby submit to the jurisdiction of the courts of New York County for purposes of resolving any disputes that may arise hereunder.

V1.2

Questions? customercare@copyright.com.

Figure A.16. Copyright permission for Figure 1.7 (a) (cont.).

American Physical Society
Reuse and Permissions License

20-Aug-2023

This license agreement between the American Physical Society ("APS") and pegah ghanizadeh ("You") consists of your license details and the terms and conditions provided by the American Physical Society and SciPris.

Licensed Content Information

License Number:	**RNP/23/AUG/069526**
License date:	20-Aug-2023
DOI:	10.1103/PhysRevLett.69.2799
Title:	Ab initio calculation of force constants and full phonon dispersions
Author:	Siqing Wei and M. Y. Chou
Publication:	Physical Review Letters
Publisher:	American Physical Society
Cost:	USD $ 0.00

Request Details

Does your reuse require significant modifications: No

Specify intended distribution locations:	United States
Reuse Category:	Reuse in a thesis/dissertation
Requestor Type:	Student
Items for Reuse:	Figures/Tables
Number of Figure/Tables:	2
Figure/Tables Details:	ross-sectional schematics illustrating the localized heating of the structure of and β − Ga2O3 MOSFET
Format for Reuse:	Electronic and Print
Total number of print copies:	Up to 1000

Information about New Publication:

University/Publisher:	Bogazici university
Title of dissertation/thesis:	Phonon Mean Free Path - Thermal Conductivity Relation of AlxGa1−xN , andβ-Ga2O3 semiconductors
Author(s):	pegah ghanizadeh
Expected completion date:	Aug. 2023

License Requestor Information

Name:	pegah ghanizadeh
Affiliation:	Individual
Email Id:	pegah.ghanizadeh@boun.edu.tr
Country:	Turkey

Figure A.17. Copyright permission for Figure 1.7 (b)

American Physical Society
Reuse and Permissions License

TERMS AND CONDITIONS

The American Physical Society (APS) is pleased to grant the Requestor of this license a non-exclusive, non-transferable permission, limited to Electronic and Print format, provided all criteria outlined below are followed.

1. You must also obtain permission from at least one of the lead authors for each separate work, if you haven't done so already. The author's name and affiliation can be found on the first page of the published Article.
2. For electronic format permissions, Requestor agrees to provide a hyperlink from the reprinted APS material using the source material's DOI on the web page where the work appears. The hyperlink should use the standard DOI resolution URL, http://dx.doi.org/{DOI}. The hyperlink may be embedded in the copyright credit line.
3. For print format permissions, Requestor agrees to print the required copyright credit line on the first page where the material appears: "Reprinted (abstract/excerpt/figure) with permission from [(FULL REFERENCE CITATION) as follows: Author's Names, APS Journal Title, Volume Number, Page Number and Year of Publication.] Copyright (YEAR) by the American Physical Society."
4. Permission granted in this license is for a one-time use and does not include permission for any future editions, updates, databases, formats or other matters. Permission must be sought for any additional use.
5. Use of the material does not and must not imply any endorsement by APS.
6. APS does not imply, purport or intend to grant permission to reuse materials to which it does not hold copyright. It is the requestor's sole responsibility to ensure the licensed material is original to APS and does not contain the copyright of another entity, and that the copyright notice of the figure, photograph, cover or table does not indicate it was reprinted by APS with permission from another source.
7. The permission granted herein is personal to the Requestor for the use specified and is not transferable or assignable without express written permission of APS. This license may not be amended except in writing by APS.
8. You may not alter, edit or modify the material in any manner.
9. You may translate the materials only when translation rights have been granted.
10. APS is not responsible for any errors or omissions due to translation.
11. You may not use the material for promotional, sales, advertising or marketing purposes.
12. The foregoing license shall not take effect unless and until APS or its agent, Aptara, receives payment in full in accordance with Aptara Billing and Payment Terms and Conditions, which are incorporated herein by reference.
13. Should the terms of this license be violated at any time, APS or Aptara may revoke the license with no refund to you and seek relief to the fullest extent of the laws of the USA. Official written notice will be made using the contact information provided with the permission request. Failure to receive such notice will not nullify revocation of the permission.
14. APS reserves all rights not specifically granted herein.
15. This document, including the Aptara Billing and Payment Terms and Conditions, shall be the entire agreement between the parties relating to the subject matter hereof.

Figure A.18. Copyright permission for Figure 1.7 (b) (cont.).

AIP PUBLISHING LICENSE
TERMS AND CONDITIONS

Aug 23, 2023

This Agreement between Mrs. pegah ghanizadeh ("You") and AIP Publishing ("AIP Publishing") consists of your license details and the terms and conditions provided by AIP Publishing and Copyright Clearance Center.

License Number	5615041104150
License date	Aug 23, 2023
Licensed Content Publisher	AIP Publishing
Licensed Content Publication	Applied Physics Letters
Licensed Content Title	Phonon-boundary scattering and thermal transport in $Al_xGa_{1-x}N$: Effect of layer thickness
Licensed Content Author	Tran, Dat Q.; Delgado-Carrascon, Rosalia
Licensed Content Date	Dec 21, 2020
Licensed Content Volume	117
Licensed Content Issue	25
Type of Use	Thesis/Dissertation
Requestor type	Student
Format	Print and electronic

Figure A.19. Copyright permission for Figure 1.12.

Portion	Figure/Table
Number of figures/tables	2
Will you be translating?	No
Title	Phonon Mean Free Path - Thermal Conductivity Relation of AlxGa1−xN , and β-Ga2O3 semiconductors
Institution name	Bogazici University
Expected presentation date	Aug 2023
Portions	figure 1
Requestor Location	Mrs. pegah ghanizadeh Boğaziçi Üniversitesi 34342 Bebek/İstanb istanbul, 34342 Turkey Attn: Mrs. pegah ghanizadeh
Total	0.00 USD

Terms and Conditions

AIP Publishing -- Terms and Conditions: Permissions Uses

AIP Publishing hereby grants to you the non-exclusive right and license to use and/or distribute the Material according to the use specified in your order, on a one-time basis, for the specified term, with a maximum distribution equal to the number that you have ordered. Any links or other content accompanying the Material are not the subject of this license.

1. You agree to include the following copyright and permission notice with the reproduction of the Material:"Reprinted from [FULL CITATION], with the permission of AIP Publishing." For an article, the credit line and permission notice must be printed on the first page of the article or book chapter. For photographs, covers, or tables, the notice may appear with the Material, in a footnote, or in the reference list.
2. If you have licensed reuse of a figure, photograph, cover, or table, it is your responsibility to ensure that the material is original to AIP Publishing and does not contain the copyright of another entity, and that the copyright notice of the figure,

Figure A.20. Copyright permission for Figure 1.12 (cont.).

photograph, cover, or table does not indicate that it was reprinted by AIP Publishing, with permission, from another source. Under no circumstances does AIP Publishing purport or intend to grant permission to reuse material to which it does not hold appropriate rights.
You may not alter or modify the Material in any manner. You may translate the Material into another language only if you have licensed translation rights. You may not use the Material for promotional purposes.

3. The foregoing license shall not take effect unless and until AIP Publishing or its agent, Copyright Clearance Center, receives the Payment in accordance with Copyright Clearance Center Billing and Payment Terms and Conditions, which are incorporated herein by reference.
4. AIP Publishing or Copyright Clearance Center may, within two business days of granting this license, revoke the license for any reason whatsoever, with a full refund payable to you. Should you violate the terms of this license at any time, AIP Publishing, or Copyright Clearance Center may revoke the license with no refund to you. Notice of such revocation will be made using the contact information provided by you. Failure to receive such notice will not nullify the revocation.
5. AIP Publishing makes no representations or warranties with respect to the Material. You agree to indemnify and hold harmless AIP Publishing, and their officers, directors, employees or agents from and against any and all claims arising out of your use of the Material other than as specifically authorized herein.
6. The permission granted herein is personal to you and is not transferable or assignable without the prior written permission of AIP Publishing. This license may not be amended except in a writing signed by the party to be charged.
7. If purchase orders, acknowledgments or check endorsements are issued on any forms containing terms and conditions which are inconsistent with these provisions, such inconsistent terms and conditions shall be of no force and effect. This document, including the CCC Billing and Payment Terms and Conditions, shall be the entire agreement between the parties relating to the subject matter hereof.

This Agreement shall be governed by and construed in accordance with the laws of the State of New York. Both parties hereby submit to the jurisdiction of the courts of New York County for purposes of resolving any disputes that may arise hereunder.

V1.2

Questions? customercare@copyright.com.

Figure A.21. Copyright permission for Figure 1.12 (cont.).

AIP PUBLISHING LICENSE
TERMS AND CONDITIONS

Aug 20, 2023

This Agreement between Mrs. pegah ghanizadeh ("You") and AIP Publishing ("AIP Publishing") consists of your license details and the terms and conditions provided by AIP Publishing and Copyright Clearance Center.

License Number	5613030822833
License date	Aug 20, 2023
Licensed Content Publisher	AIP Publishing
Licensed Content Publication	Journal of Applied Physics
Licensed Content Title	Size effects in the thermal conductivity of gallium oxide (β-Ga_2O_3) films grown via open-atmosphere annealing of gallium nitride
Licensed Content Author	Szwejkowski, Chester J.; Creange, Nicole C.
Licensed Content Date	Feb 25, 2015
Licensed Content Volume	117
Licensed Content Issue	8
Type of Use	Thesis/Dissertation
Requestor type	Student
Format	Print and electronic

Figure A.22. Copyright permission for Figure 1.13.

Portion	Photograph/Image
Number of Photographs/Images	1
Will you be translating?	No
Title	Phonon Mean Free Path - Thermal Conductivity Relation of AlxGa1−xN , and β-Ga2O3 semiconductors
Institution name	Bogazici University
Expected presentation date	Aug 2023
Portions	6
Requestor Location	Mrs. pegah ghanizadeh Boğaziçi Üniversitesi 34342 Bebek/İstanb istanbul, 34342 Turkey Attn: Mrs. pegah ghanizadeh
Total	0.00 USD

Terms and Conditions

AIP Publishing -- Terms and Conditions: Permissions Uses

AIP Publishing hereby grants to you the non-exclusive right and license to use and/or distribute the Material according to the use specified in your order, on a one-time basis, for the specified term, with a maximum distribution equal to the number that you have ordered. Any links or other content accompanying the Material are not the subject of this license.

1. You agree to include the following copyright and permission notice with the reproduction of the Material:"Reprinted from [FULL CITATION], with the permission of AIP Publishing." For an article, the credit line and permission notice must be printed on the first page of the article or book chapter. For photographs, covers, or tables, the notice may appear with the Material, in a footnote, or in the reference list.
2. If you have licensed reuse of a figure, photograph, cover, or table, it is your responsibility to ensure that the material is original to AIP Publishing and does not contain the copyright of another entity, and that the copyright notice of the figure,

Figure A.23. Copyright permission for Figure 1.13 (cont.).

photograph, cover, or table does not indicate that it was reprinted by AIP Publishing, with permission, from another source. Under no circumstances does AIP Publishing purport or intend to grant permission to reuse material to which it does not hold appropriate rights.
You may not alter or modify the Material in any manner. You may translate the Material into another language only if you have licensed translation rights. You may not use the Material for promotional purposes.

3. The foregoing license shall not take effect unless and until AIP Publishing or its agent, Copyright Clearance Center, receives the Payment in accordance with Copyright Clearance Center Billing and Payment Terms and Conditions, which are incorporated herein by reference.
4. AIP Publishing or Copyright Clearance Center may, within two business days of granting this license, revoke the license for any reason whatsoever, with a full refund payable to you. Should you violate the terms of this license at any time, AIP Publishing, or Copyright Clearance Center may revoke the license with no refund to you. Notice of such revocation will be made using the contact information provided by you. Failure to receive such notice will not nullify the revocation.
5. AIP Publishing makes no representations or warranties with respect to the Material. You agree to indemnify and hold harmless AIP Publishing, and their officers, directors, employees or agents from and against any and all claims arising out of your use of the Material other than as specifically authorized herein.
6. The permission granted herein is personal to you and is not transferable or assignable without the prior written permission of AIP Publishing. This license may not be amended except in a writing signed by the party to be charged.
7. If purchase orders, acknowledgments or check endorsements are issued on any forms containing terms and conditions which are inconsistent with these provisions, such inconsistent terms and conditions shall be of no force and effect. This document, including the CCC Billing and Payment Terms and Conditions, shall be the entire agreement between the parties relating to the subject matter hereof.

This Agreement shall be governed by and construed in accordance with the laws of the State of New York. Both parties hereby submit to the jurisdiction of the courts of New York County for purposes of resolving any disputes that may arise hereunder.

V1.2

Questions? customercare@copyright.com.

Figure A.24. Copyright permission for Figure 1.13 (cont.).

This page is available in the following languages:

Creative Commons License Deed

Attribution-NonCommercial-NoDerivatives 4.0 International (CC BY-NC-ND 4.0)

This is a human-readable summary of (and not a substitute for) the license.

You are free to:

Share — copy and redistribute the material in any medium or format

The licensor cannot revoke these freedoms as long as you follow the license terms.

Under the following terms:

Attribution — You must give appropriate credit, provide a link to the license, and indicate if changes were made. You may do so in any reasonable manner, but not in any way that suggests the licensor endorses you or your use.

NonCommercial — You may not use the material for commercial purposes.

NoDerivatives — If you remix, transform, or build upon the material, you may not distribute the modified material.

No additional restrictions — You may not apply legal terms or technological measures that legally restrict others from doing anything the license permits.

Notices:

You do not have to comply with the license for elements of the material in the public domain or where your use is permitted by an applicable exception or limitation.

No warranties are given. The license may not give you all of the permissions necessary for your intended use. For example, other rights such as publicity, privacy, or moral rights may limit how you use the material.

Figure A.25. Copyright permission for Figure Figure 3.1, 3.6, 3.11.

AIP PUBLISHING LICENSE
TERMS AND CONDITIONS

Aug 20, 2023

This Agreement between Mrs. pegah ghanizadeh ("You") and AIP Publishing ("AIP Publishing") consists of your license details and the terms and conditions provided by AIP Publishing and Copyright Clearance Center.

License Number	5613030822833
License date	Aug 20, 2023
Licensed Content Publisher	AIP Publishing
Licensed Content Publication	Journal of Applied Physics
Licensed Content Title	Size effects in the thermal conductivity of gallium oxide (β-Ga_2O_3) films grown via open-atmosphere annealing of gallium nitride
Licensed Content Author	Szwejkowski, Chester J.; Creange, Nicole C.
Licensed Content Date	Feb 25, 2015
Licensed Content Volume	117
Licensed Content Issue	8
Type of Use	Thesis/Dissertation
Requestor type	Student
Format	Print and electronic

Figure A.26. Copyright permission for Figure 1.13.

ELSEVIER LICENSE
TERMS AND CONDITIONS

Aug 20, 2023

This Agreement between Mrs. pegah ghanizadeh ("You") and Elsevier ("Elsevier") consists of your license details and the terms and conditions provided by Elsevier and Copyright Clearance Center.

License Number	5613021134266
License date	Aug 20, 2023
Licensed Content Publisher	Elsevier
Licensed Content Publication	Computational Materials Science
Licensed Content Title	High-throughput electronic band structure calculations: Challenges and tools
Licensed Content Author	Wahyu Setyawan,Stefano Curtarolo
Licensed Content Date	Aug 1, 2010
Licensed Content Volume	49
Licensed Content Issue	2
Licensed Content Pages	14
Start Page	299
End Page	312

Figure A.27. Copyright permission for Figure Figure 3.2, 3.7, 3.12.

Type of Use	reuse in a thesis/dissertation
Portion	figures/tables/illustrations
Number of figures/tables/illustrations	4
Format	both print and electronic
Are you the author of this Elsevier article?	No
Will you be translating?	No
Title	Phonon Mean Free Path - Thermal Conductivity Relation of AlxGa1−xN , and β-Ga2O3 semiconductors
Institution name	Bogazici University
Expected presentation date	Aug 2023
Portions	figure 1, 13,17
Requestor Location	Mrs. pegah ghanizadeh Boğaziçi Üniversitesi 34342 Bebek/İstanb istanbul, 34342 Turkey Attn: Mrs. pegah ghanizadeh
Publisher Tax ID	GB 494 6272 12
Total	0.00 USD
Terms and Conditions	

INTRODUCTION

Figure A.28. Copyright permission for Figure Figure 3.2, 3.7, 3.12 (cont.).

1. The publisher for this copyrighted material is Elsevier. By clicking "accept" in connection with completing this licensing transaction, you agree that the following terms and conditions apply to this transaction (along with the Billing and Payment terms and conditions established by Copyright Clearance Center, Inc. ("CCC"), at the time that you opened your RightsLink account and that are available at any time at https://myaccount.copyright.com).

GENERAL TERMS

2. Elsevier hereby grants you permission to reproduce the aforementioned material subject to the terms and conditions indicated.

3. Acknowledgement: If any part of the material to be used (for example, figures) has appeared in our publication with credit or acknowledgement to another source, permission must also be sought from that source. If such permission is not obtained then that material may not be included in your publication/copies. Suitable acknowledgement to the source must be made, either as a footnote or in a reference list at the end of your publication, as follows:

"Reprinted from Publication title, Vol /edition number, Author(s), Title of article / title of chapter, Pages No., Copyright (Year), with permission from Elsevier [OR APPLICABLE SOCIETY COPYRIGHT OWNER]." Also Lancet special credit - "Reprinted from The Lancet, Vol. number, Author(s), Title of article, Pages No., Copyright (Year), with permission from Elsevier."

4. Reproduction of this material is confined to the purpose and/or media for which permission is hereby given. The material may not be reproduced or used in any other way, including use in combination with an artificial intelligence tool (including to train an algorithm, test, process, analyse, generate output and/or develop any form of artificial intelligence tool), or to create any derivative work and/or service (including resulting from the use of artificial intelligence tools).

5. Altering/Modifying Material: Not Permitted. However figures and illustrations may be altered/adapted minimally to serve your work. Any other abbreviations, additions, deletions and/or any other alterations shall be made only with prior written authorization of Elsevier Ltd. (Please contact Elsevier's permissions helpdesk here). No modifications can be made to any Lancet figures/tables and they must be reproduced in full.

6. If the permission fee for the requested use of our material is waived in this instance, please be advised that your future requests for Elsevier materials may attract a fee.

7. Reservation of Rights: Publisher reserves all rights not specifically granted in the combination of (i) the license details provided by you and accepted in the course of this licensing transaction, (ii) these terms and conditions and (iii) CCC's Billing and Payment terms and conditions.

8. License Contingent Upon Payment: While you may exercise the rights licensed immediately upon issuance of the license at the end of the licensing process for the transaction, provided that you have disclosed complete and accurate details of your proposed use, no license is finally effective unless and until full payment is received from you (either by publisher or by CCC) as provided in CCC's Billing and Payment terms and conditions. If full payment is not received on a timely basis, then any license preliminarily granted shall be deemed automatically revoked and shall be void as if never granted. Further, in the event that you breach any of these terms and conditions or any of CCC's Billing and Payment terms and conditions, the license is automatically revoked and shall be void as if never granted. Use of materials as described in a revoked license, as well as any use of the

Figure A.29. Copyright permission for Figure Figure 3.2, 3.7, 3.12 (cont.).

materials beyond the scope of an unrevoked license, may constitute copyright infringement and publisher reserves the right to take any and all action to protect its copyright in the materials.

9. Warranties: Publisher makes no representations or warranties with respect to the licensed material.

10. Indemnity: You hereby indemnify and agree to hold harmless publisher and CCC, and their respective officers, directors, employees and agents, from and against any and all claims arising out of your use of the licensed material other than as specifically authorized pursuant to this license.

11. No Transfer of License: This license is personal to you and may not be sublicensed, assigned, or transferred by you to any other person without publisher's written permission.

12. No Amendment Except in Writing: This license may not be amended except in a writing signed by both parties (or, in the case of publisher, by CCC on publisher's behalf).

13. Objection to Contrary Terms: Publisher hereby objects to any terms contained in any purchase order, acknowledgment, check endorsement or other writing prepared by you, which terms are inconsistent with these terms and conditions or CCC's Billing and Payment terms and conditions. These terms and conditions, together with CCC's Billing and Payment terms and conditions (which are incorporated herein), comprise the entire agreement between you and publisher (and CCC) concerning this licensing transaction. In the event of any conflict between your obligations established by these terms and conditions and those established by CCC's Billing and Payment terms and conditions, these terms and conditions shall control.

14. Revocation: Elsevier or Copyright Clearance Center may deny the permissions described in this License at their sole discretion, for any reason or no reason, with a full refund payable to you. Notice of such denial will be made using the contact information provided by you. Failure to receive such notice will not alter or invalidate the denial. In no event will Elsevier or Copyright Clearance Center be responsible or liable for any costs, expenses or damage incurred by you as a result of a denial of your permission request, other than a refund of the amount(s) paid by you to Elsevier and/or Copyright Clearance Center for denied permissions.

LIMITED LICENSE

The following terms and conditions apply only to specific license types:

15. **Translation**: This permission is granted for non-exclusive world **English** rights only unless your license was granted for translation rights. If you licensed translation rights you may only translate this content into the languages you requested. A professional translator must perform all translations and reproduce the content word for word preserving the integrity of the article.

16. **Posting licensed content on any Website**: The following terms and conditions apply as follows: Licensing material from an Elsevier journal: All content posted to the web site must maintain the copyright information line on the bottom of each image; A hyper-text must be included to the Homepage of the journal from which you are licensing at http://www.sciencedirect.com/science/journal/xxxxx or the Elsevier homepage for books at http://www.elsevier.com; Central Storage: This license does not include permission for a scanned version of the material to be stored in a central repository such as that provided by Heron/XanEdu.

Figure A.30. Copyright permission for Figure Figure 3.2, 3.7, 3.12 (cont.).

Licensing material from an Elsevier book: A hyper-text link must be included to the Elsevier homepage at http://www.elsevier.com . All content posted to the web site must maintain the copyright information line on the bottom of each image.

Posting licensed content on Electronic reserve: In addition to the above the following clauses are applicable: The web site must be password-protected and made available only to bona fide students registered on a relevant course. This permission is granted for 1 year only. You may obtain a new license for future website posting.

17. **For journal authors:** the following clauses are applicable in addition to the above:

Preprints:

A preprint is an author's own write-up of research results and analysis, it has not been peer-reviewed, nor has it had any other value added to it by a publisher (such as formatting, copyright, technical enhancement etc.).

Authors can share their preprints anywhere at any time. Preprints should not be added to or enhanced in any way in order to appear more like, or to substitute for, the final versions of articles however authors can update their preprints on arXiv or RePEc with their Accepted Author Manuscript (see below).

If accepted for publication, we encourage authors to link from the preprint to their formal publication via its DOI. Millions of researchers have access to the formal publications on ScienceDirect, and so links will help users to find, access, cite and use the best available version. Please note that Cell Press, The Lancet and some society-owned have different preprint policies. Information on these policies is available on the journal homepage.

Accepted Author Manuscripts: An accepted author manuscript is the manuscript of an article that has been accepted for publication and which typically includes author-incorporated changes suggested during submission, peer review and editor-author communications.

Authors can share their accepted author manuscript:

- immediately
  - via their non-commercial person homepage or blog
  - by updating a preprint in arXiv or RePEc with the accepted manuscript
  - via their research institute or institutional repository for internal institutional uses or as part of an invitation-only research collaboration work-group
  - directly by providing copies to their students or to research collaborators for their personal use
  - for private scholarly sharing as part of an invitation-only work group on commercial sites with which Elsevier has an agreement
- After the embargo period
  - via non-commercial hosting platforms such as their institutional repository
  - via commercial sites with which Elsevier has an agreement

In all cases accepted manuscripts should:

- link to the formal publication via its DOI
- bear a CC-BY-NC-ND license - this is easy to do
- if aggregated with other manuscripts, for example in a repository or other site, be shared in alignment with our hosting policy not be added to or enhanced in any way to

Figure A.31. Copyright permission for Figure Figure 3.2, 3.7, 3.12 (cont.).

appear more like, or to substitute for, the published journal article.

Published journal article (JPA): A published journal article (PJA) is the definitive final record of published research that appears or will appear in the journal and embodies all value-adding publishing activities including peer review co-ordination, copy-editing, formatting, (if relevant) pagination and online enrichment.

Policies for sharing publishing journal articles differ for subscription and gold open access articles:

Subscription Articles: If you are an author, please share a link to your article rather than the full-text. Millions of researchers have access to the formal publications on ScienceDirect, and so links will help your users to find, access, cite, and use the best available version.

Theses and dissertations which contain embedded PJAs as part of the formal submission can be posted publicly by the awarding institution with DOI links back to the formal publications on ScienceDirect.

If you are affiliated with a library that subscribes to ScienceDirect you have additional private sharing rights for others' research accessed under that agreement. This includes use for classroom teaching and internal training at the institution (including use in course packs and courseware programs), and inclusion of the article for grant funding purposes.

Gold Open Access Articles: May be shared according to the author-selected end-user license and should contain a CrossMark logo, the end user license, and a DOI link to the formal publication on ScienceDirect.

Please refer to Elsevier's posting policy for further information.

18. **For book authors** the following clauses are applicable in addition to the above: Authors are permitted to place a brief summary of their work online only. You are not allowed to download and post the published electronic version of your chapter, nor may you scan the printed edition to create an electronic version. **Posting to a repository:** Authors are permitted to post a summary of their chapter only in their institution's repository.

19. **Thesis/Dissertation**: If your license is for use in a thesis/dissertation your thesis may be submitted to your institution in either print or electronic form. Should your thesis be published commercially, please reapply for permission. These requirements include permission for the Library and Archives of Canada to supply single copies, on demand, of the complete thesis and include permission for Proquest/UMI to supply single copies, on demand, of the complete thesis. Should your thesis be published commercially, please reapply for permission. Theses and dissertations which contain embedded PJAs as part of the formal submission can be posted publicly by the awarding institution with DOI links back to the formal publications on ScienceDirect.

Elsevier Open Access Terms and Conditions

You can publish open access with Elsevier in hundreds of open access journals or in nearly 2000 established subscription journals that support open access publishing. Permitted third party re-use of these open access articles is defined by the author's choice of Creative Commons user license. See our open access license policy for more information.

Terms & Conditions applicable to all Open Access articles published with Elsevier:

Figure A.32. Copyright permission for Figure Figure 3.2, 3.7, 3.12 (cont.).

Any reuse of the article must not represent the author as endorsing the adaptation of the article nor should the article be modified in such a way as to damage the author's honour or reputation. If any changes have been made, such changes must be clearly indicated.

The author(s) must be appropriately credited and we ask that you include the end user license and a DOI link to the formal publication on ScienceDirect.

If any part of the material to be used (for example, figures) has appeared in our publication with credit or acknowledgement to another source it is the responsibility of the user to ensure their reuse complies with the terms and conditions determined by the rights holder.

Additional Terms & Conditions applicable to each Creative Commons user license:

CC BY: The CC-BY license allows users to copy, to create extracts, abstracts and new works from the Article, to alter and revise the Article and to make commercial use of the Article (including reuse and/or resale of the Article by commercial entities), provided the user gives appropriate credit (with a link to the formal publication through the relevant DOI), provides a link to the license, indicates if changes were made and the licensor is not represented as endorsing the use made of the work. The full details of the license are available at http://creativecommons.org/licenses/by/4.0.

CC BY NC SA: The CC BY-NC-SA license allows users to copy, to create extracts, abstracts and new works from the Article, to alter and revise the Article, provided this is not done for commercial purposes, and that the user gives appropriate credit (with a link to the formal publication through the relevant DOI), provides a link to the license, indicates if changes were made and the licensor is not represented as endorsing the use made of the work. Further, any new works must be made available on the same conditions. The full details of the license are available at http://creativecommons.org/licenses/by-nc-sa/4.0.

CC BY NC ND: The CC BY-NC-ND license allows users to copy and distribute the Article, provided this is not done for commercial purposes and further does not permit distribution of the Article if it is changed or edited in any way, and provided the user gives appropriate credit (with a link to the formal publication through the relevant DOI), provides a link to the license, and that the licensor is not represented as endorsing the use made of the work. The full details of the license are available at http://creativecommons.org/licenses/by-nc-nd/4.0. Any commercial reuse of Open Access articles published with a CC BY NC SA or CC BY NC ND license requires permission from Elsevier and will be subject to a fee.

Commercial reuse includes:

- Associating advertising with the full text of the Article
- Charging fees for document delivery or access
- Article aggregation
- Systematic distribution via e-mail lists or share buttons

Posting or linking by commercial companies for use by customers of those companies.

20. **Other Conditions**:

v1.10

Figure A.33. Copyright permission for Figure Figure 3.2, 3.7, 3.12 (cont.).

Questions? customercare@copyright.com.

Figure A.34. Copyright permission for Figure Figure 3.2, 3.7, 3.12 (cont.).